C2

NACA TN 2445

NATIONAL ADVISORY COMMITTEE FOR AERONAUTICS

TECHNICAL NOTE 2445

WIND-TUNNEL TESTS AT LOW SPEED OF SWEPT AND YAWED WINGS HAVING VARIOUS PLAN FORMS

By Paul E. Purser and M. Leroy Spearman

Langley Aeronautical Laboratory
Langley Field, Va.

Washington

December 1951

1H

NATIONAL ADVISORY COMMITTEE FOR AERONAUTICS

TECHNICAL NOTE 2445

WIND-TUNNEL TESTS AT LOW SPEED OF SWEPT AND YAWED WINGS HAVING VARIOUS PLAN FORMS[1]

By Paul E. Purser and M. Leroy Spearman

SUMMARY

Wind-tunnel tests of an exploratory nature have been made at low speed of various small-scale models of sweptback, sweptforward, and yawed wings. The tests covered changes in aspect ratio, taper ratio, and tip shape. Some data were obtained with high-lift devices on sweptback wings and with ailerons on sweptforward wings. The data have been briefly analyzed and some comparisons have been made with the available theory.

The results of the tests and the analyses indicated that the values of lift-curve slope and effective dihedral of swept wings can be computed with a reasonable degree of accuracy in the low-lift-coefficient range by means of existing theories.

In general, reducing the aspect ratio and the ratio of root chord to tip chord resulted in increases in drag and effective dihedral and increased the longitudinal stability near the stall. Cutting off the tip of a sweptback wing normal to the leading edge reduced the effective dihedral at low lift coefficients and gave a slight reduction in the drag at high lift coefficients. Sweeping forward a part of the outer panel of a sweptback wing improved the longitudinal stability and decreased the effective dihedral but also slightly decreased the maximum lift coefficient and increased the drag at high lift coefficients. The use of high-lift devices at either the leading edge or the trailing edge of sweptback wings increased the lift-drag ratio and the effective dihedral at high lift coefficients. An increase in the ratio of root chord to tip chord for sweptforward wings resulted in decreases in aileron rolling-moment effectiveness that were greater than the values computed for unswept wings.

---

[1]Supersedes NACA RM L7D23 entitled "Wind-Tunnel Tests at Low Speed of Swept and Yawed Wings Having Various Plan Forms" by Paul E. Purser and M. Leroy Spearman.

INTRODUCTION

Much interest in the use of highly swept wings has arisen since the theory of reference 1 indicated the increases in flight critical Mach number that could be obtained by the use of sweep. The effects of sweep on the low-speed characteristics of wings have long been recognized and theory (reference 2) indicates that the effects may be rather large. Some experimental data on untapered sweptback wings are provided in reference 3. The present paper reports tests made on various swept and yawed wings as an extension of the work of reference 3 to include the additional effects of taper ratio and sweepforward and to provide data for comparison with the theory of reference 2.

COEFFICIENTS AND SYMBOLS

The results of the tests are presented as standard NACA coefficients of forces and moments which are referred in all cases to the quarter-chord point of the mean aerodynamic chord of the model tested. The data for the swept-wing tests are referred to the stability axes (fig. 1(a)), and the data for the yawed-wing tests are referred to the stability axes and to the wind axes (fig. 1(b)).

For the stability axes the coefficients and symbols are defined as follows:

C_L lift coefficient $\left(\frac{\text{Lift}}{qS} \text{ where } \text{Lift} = -Z\right)$

$C_{L_{max}}$ maximum lift coefficient

C_n yawing-moment coefficient $\left(\frac{N}{qSb}\right)$

C_X longitudinal-force coefficient $\left(\frac{X}{qS}\right)$

C_Y lateral-force coefficient $\left(\frac{Y}{qS}\right)$

C_l rolling-moment coefficient $\left(\frac{L}{qSb}\right)$

C_m pitching-moment coefficient $\left(\frac{M}{qSc'}\right)$

X force along X-axis, pounds

Y force along Y-axis, pounds

Z force along Z-axis, pounds

L rolling moment about X-axis, pound-feet

M pitching moment about Y-axis, pound-feet

N yawing moment about Z-axis, pound-feet

For the wind axes the coefficients and symbols are defined as follows:

C_D drag coefficient $\left(\frac{\text{Drag}}{qS} \text{ where } \text{Drag} = -X'\right)$

X' force along X-axis, pounds

Y' force along Y-axis, pounds

Z force along Z-axis, pounds

L' rolling moment about X-axis, pound-feet

M' pitching moment about Y-axis, pound-feet

N yawing moment about Z-axis, pound-feet

Other symbols are defined as follows:

A apsect ratio $\left(\frac{b^2}{S}\right)$

q free-stream dynamic pressure, pounds per square foot $\left(\frac{\rho V^2}{2}\right)$

S wing area

c airfoil section chord, measured in flight direction

c' wing mean aerodynamic chord $\left(\frac{2}{S}\int_0^{b/2} c^2 dy\right)$

b wing span

y distance along wing span

V air velocity, feet per second

ρ mass density of air, slugs per cubic foot

α angle of attack of chord line in stability-axis XZ-plane, degrees

α' angle of attack of chord line in wind-axis X'Z-plane, degrees

ψ angle of yaw, degrees

Λ angle of sweep of airfoil leading edge, positive for sweepback, degrees

$\Lambda_{\frac{c}{4}}$ angle of sweep of quarter-chord line, positive for sweepback, degrees

Γ angle of dihedral, degrees

λ taper ratio $\left(\frac{\text{Root chord}}{\text{Tip chord}}\right)$

δ_f flap deflection, measured in flight direction, degrees

δ_a aileron deflection, measured in flight direction, degrees

n_o aerodynamic-center location, percent mean aerodynamic chord

Subscripts:

L_0 conditions for zero lift

Symbols used as subscripts denote partial derivatives of coefficients with respect to angle of yaw, angle of attack, flap deflection, aileron deflection, and lift coefficient. For example,

$$\left(C_{l_\psi}\right)_{C_L} = \frac{\partial}{\partial C_L}\left(\frac{\partial C_l}{\partial \psi}\right)$$

MODELS

The models, which were mahogany wings used in previous investigations in the Langley 7- by 10-foot tunnel, are illustrated in figures 2 and 3. The models having conventional taper were of NACA 23012 airfoil section in planes parallel to the original planes of symmetry. The untapered models were of NACA 0012 and NACA 0015 airfoil section in planes normal to the leading edges. The model having inverse taper had low-drag-type airfoil sections, the ordinates of which are given in table I. The wing tips were faired on only the inverse-taper model. The full-span split flap tested on one of the untapered sweptback models was of $\frac{1}{16}$- inch steel and had a chord equal to 25 percent of the wing chord. The nose spoiler tested on one of the untapered sweptback models was of $\frac{1}{32}$- inch steel, had a chord equal to 2.5 percent of the wing chord, and was mounted at the leading edge as an extension to the wing-chord line. The half-span split flap tested on the inverse-taper model was of $\frac{1}{8}$- inch Masonite and had chords equal to 20 percent of the airfoil section chord. The nose flap (or slat) tested on the inverse-taper model was of NACA 22 airfoil section (reference 4) in a plane normal to its leading edge and had a constant chord equal to $8\frac{1}{2}$ percent of the average chord of the part of the wing $\left(0.36\frac{b}{2}\text{ to }0.95\frac{b}{2}\right)$ over which the flap (or slat) was located.

TESTS AND RESULTS

Test Conditions

The tests were made in the Langley 7- by 10-foot tunnel at dynamic pressures of 16.37 and 9.21 pounds per square foot, which correspond to airspeeds of about 80 and 60 miles per hour, respectively. The test Reynolds numbers (fig. 4) ranged from 620,000 to 1,250,000, the value depending on the dynamic pressure and on the mean aerodynamic chord of the model tested. Because of the turbulence factor of 1.6 for the tunnel, the effective Reynolds numbers (for maximum lift coefficients) ranged from 992,000 to 2,000,000 (fig. 4).

Corrections

Data for only the inverse-taper model have been corrected for tares caused by the model support strut. No tare data were obtained for the

other wing models because experience has shown that, for the type of support used (fig. 3), appreciable tares occur only in the values of drag, angle of attack, and pitching moment at zero lift. These items were not considered significant for the present investigation.

For all data except the yawed-wing tests, jet-boundary corrections were applied to the angles of attack and to the longitudinal-force coefficients. The corrections were computed as follows by use of reference 5:

$$\Delta\alpha = 57.3\delta_w \frac{S}{C} C_L$$

$$\Delta C_X = -\delta_w \frac{S}{C} C_L^2$$

where

δ_w jet-boundary-correction factor at wing

S wing area, square feet

C tunnel cross-sectional area, square feet

All jet-boundary corrections were added to the test data, and the values used for each model can be determined from figure 5.

Test Procedure and Presentation of Data

The various swept wings were, in general, tested through the angle-of-attack range at angles of yaw of 0° and $\pm 5^\circ$ from below zero lift to above maximum lift at increments of angle of attack of 2° except near maximum lift where increments of 1° were used. Sketches or photographs were made of the action of small silk or wool tufts attached to the wing upper surface for some arrangements; no force-test data were taken with the tufts in place. The slopes C_{l_ψ}, C_{n_ψ}, and C_{Y_ψ} were obtained by assuming straight-line variations of C_l, C_n, and C_Y between angles of yaw of 5° and -5°.

The yawed wings were tested through the angle-of-attack range from below zero lift either to above maximum lift or to an angle of attack of about 55° measured in a plane normal to the leading edge, whichever was smaller.

The data are presented in figures 6 to 43 in three general groups — force-test data, tuft sketches, and comparison plots — and are indexed in table II.

THEORETICAL RELATIONSHIPS

The basic theory for swept and yawed wings as developed by Betz (reference 2) is based on the concept that only the component of velocity normal to the wing leading edge determines the chordwise pressure distribution. Among the simplifying assumptions made by Betz are: The spanwise load distribution is rectangular, the two semispans of a swept wing may be considered independently as yawed wings, and the wing is swept by first setting the panels at an angle of attack and then sweeping the wing in such a manner that the leading edges of the panels remain in a horizontal plane. The last assumption, since it introduces a geometric dihedral, primarily affects the rolling moments, and, since maintaining the panel leading edges in a plane is not a practical arrangement, a series of equations was developed from Betz's work without such an assumption.

The normal-component-of-velocity concept and the assumptions of independent semispans and rectangular span loading, however, were retained in the development of the following equations, which are not all used in the present paper but are presented for future reference:

Yawed wings:

$$C_{L_\alpha} = \left(C_{L_\alpha}\right)_{\psi=0} \cos^2\psi \tag{1}$$

$$C_{L_{\alpha'}} = \left(C_{L_{\alpha'}}\right)_{\psi=0} \cos\ \psi = \left(C_{L_\alpha}\right)_{\psi=0} \cos\ \psi \tag{2}$$

$$C_{L_{\delta_f}} = \left(C_{L_{\delta_f}}\right)_{\psi=0} \cos^2\psi \tag{3}$$

Swept wings without flaps or camber:

$$C_{L_\alpha} = \left(C_{L_\alpha}\right)_{\Lambda=\psi=0} \cos \Lambda \cos^2\psi \tag{4}$$

$$C_{L_{\alpha'}} = \left(C_{L_\alpha}\right)_{\Lambda=\psi=0} \cos \Lambda \cos \psi \tag{5}$$

$$C_l = \frac{1}{4} C_L \tan \Lambda \tan \psi + \frac{57.3}{4} C_{L_\alpha} \tan \Gamma \tan \psi \tag{6}$$

$$C_{l_\psi} \approx 0.0044 \left(C_L \tan \Lambda + 57.3\, C_{L_\alpha} \tan \Gamma\right) \tag{7}$$

$$C_{l_{\delta_a}} = \left(C_{l_{\delta_a}}\right)_{\Lambda=\psi=0} \cos \Lambda \cos^2\psi \tag{8}$$

Swept wings with full-span flaps or camber:

$$C_{L_{\delta_f}} = \left(C_{L_{\delta_f}}\right)_{\Lambda=\psi=0} \cos \Lambda \cos^2\psi \quad \text{(flaps)} \tag{9}$$

$$\left(C_L\right)_{\alpha=0} = \left(C_L\right)_{\alpha=\Lambda=\psi=0} \cos^2\Lambda \cos^2\psi \quad \text{(camber)} \tag{10}$$

$$\alpha_{L_0} = \left(\alpha_{L_0}\right)_{\Lambda=\psi=0} \cos \Lambda \tag{11}$$

$$C_l = \frac{1}{2}\left(C_L\right)_{\alpha=0} \tan \Lambda \tan \psi + \frac{57.3}{4} C_{L_\alpha} \tan \Gamma \tan \psi + \frac{1}{4}\left[C_L - \left(C_L\right)_{\alpha=0}\right] \tan \Lambda \tan \psi \tag{12}$$

$$C_{l_\psi} \approx \frac{\frac{1}{2}\left(C_L\right)_{\alpha=0} \tan \Lambda}{57.3} + \frac{1}{4} C_{L_\alpha} \tan \Gamma + \frac{\frac{1}{4}\left[C_L - \left(C_L\right)_{\alpha=0}\right] \tan \Lambda}{57.3} \qquad (13)$$

or since

$$C_{l_\psi} \approx 0.0087\left(C_L\right)_{\alpha=0} \tan \Lambda + \frac{1}{4} C_{L_\alpha} \tan \Gamma + 0.0044 C_L \tan \Lambda - 0.0044\left(C_L\right)_{\alpha=0} \tan \Lambda \qquad (14)$$

$$C_{l_\psi} \approx 0.0044\left[\left(C_L\right)_{\alpha=0} \tan \Lambda + 57.3 C_{L_\alpha} \tan \Gamma + C_L \tan \Lambda\right] \qquad (15)$$

Equations (1) to (15) take no account of aspect ratio and taper ratio. For lift and aileron effectiveness these factors may be accounted for approximately in several ways as follows: (1) by use of standard corrections with the aspect ratio and taper ratio based on an unswept wing having the same panels as the swept wing (reference 3); (2) by use of charts developed by Mutterperl (reference 6) which give the span loading and total lift of sweptback wings calculated by a method based on Weighardt's extension to lifting-line theory (reference 7); (3) by use of lifting-surface-theory computations (reference 8). For effective dihedral, in order to account for aspect ratio and taper ratio, the following items may be noted: (1) equations (7), (13), and (15) actually provide only increments in C_{l_ψ} caused by sweep and dihedral; (2) the basic values of C_{l_ψ} may be obtained from Weissinger (reference 9) by using the values of aspect ratio and taper ratio actually existing on the swept wings.

DISCUSSION

Longitudinal Stability of Swept Wings

Effect of aspect ratio.- As has been shown in references 3 and 10, the pitching-moment curves become increasingly nonlinear as the sweep angle is increased and tend to become unstable near the stall. Decreasing

the aspect ratio generally reduces the nonlinearity and tends to make the pitching-moment curve stable near the stall. (See figs. 6, 7, 9, and 36 for example.) The data for all the wings included in the present investigation, both sweptback and sweptforward, agree very well with the summary chart of reference 10 as to the effects of sweep angle and aspect ratio on the pitching-moment characteristics near the stall. As shown in figure 36, increases in aspect ratio moved the aerodynamic center at low lift coefficients slightly back for the unswept and sweptforward wings and slightly forward for the sweptback wings.

Effect of taper ratio.- In agreement with the data of reference 10, the present investigation showed little or no effect of taper on the pitching-moment characteristics near the stall for sweptback wings. (See figs. 13 and 14.) For sweptforward wings, however, increasing the ratio of root chord to tip chord provided a slight stabilizing effect on the pitching-moment curve near the stall. (See figs. 26 to 28.) Increases in the ratio of root chord to tip chord moved the aerodynamic center at low lift coefficients back for sweptback wings, very little for unswept wings, and forward for sweptforward wings. (See fig. 37.)

Effect of high-lift devices.- The use of a full-span split flap at the trailing edge or of a spoiler extending from the nose on an untapered 60° sweptback wing (figs. 7, 8, and 38) had little effect on the pitching-moment curve except for a change in trim produced by the trailing-edge flap. For the inverse-taper sweptback wing (figs. 14 and 38) the use of a half-span center-section split flap at the trailing edge and a half-span tip slat or flap at the leading edge — either separately or in combination — delayed the excessive stability at high lift coefficients and had little effect on the stability at low lift coefficients. All combinations produced some change in trim, and in the order of increasing the negative value of C_m at $C_L = 0$ the devices are: leading-edge slat, trailing-edge flap, trailing-edge flap and leading-edge slat, trailing-edge flap and leading-edge flap, and leading-edge flap.

Effect of tip modification.- Cutting off the tip normal to the leading edge on an untapered 60° sweptback wing had little effect on the nonlinearity of the pitching-moment curve or on the stability near the stall (figs. 6 and 10) but did move the aerodynamic center back at low lift coefficients (fig. 39). When the outer 40 percent of the wing panels was swept forward, however, the pitching-moment curve became nearly linear and indicated stability near the stall. (See figs. 6, 11, and 39.)

Effective Dihedral of Swept Wings

Effect of aspect ratio.- For unswept wings the slope of the curve of C_{l_ψ} against C_L is increased positively as the aspect ratio is decreased. (See fig. 36.) The same effect is shown in figure 36 for untapered sweptback wings. Although insufficient data are available to show directly the effect of aspect ratio on $\left(C_{l_\psi}\right)_{C_L}$ for sweptforward wings, the agreement between experiment and calculation shown in the section entitled "Comparison with Theory" supports the argument that aspect-ratio effects on $\left(C_{l_\psi}\right)_{C_L}$ are independent of sweep. The maximum value of C_{l_ψ} for the sweptback wings (fig. 36) was increased slightly as the aspect ratio was reduced.

Effect of taper ratio.- According to the calculations of Weissinger (reference 9) an increase in the ratio of root chord to tip chord should give a reduction in the positive value of $\left(C_{l_\psi}\right)_{C_L}$. That this result is true is indicated by the data of figure 37 for both sweptback and sweptforward wings. The apparent discrepancy for the unswept and for the approximately unswept wings (fig. 37) is attributable to the fact that the tapered wing built with a straight trailing edge had enough sweepback to counteract the small taper-ratio effect. For sweptback wings, increases in the ratio of root chord to tip chord apparently increased the maximum positive value of C_{l_ψ} and the lift coefficient at which this maximum value occurred.

Effect of high-lift devices.- The data of figure 38 show that the use of high-lift devices can greatly increase the maximum values of C_{l_ψ} obtained with sweptback wings. The use of a full-span split flap at the trailing edge of an untapered wing having a 60° sweepback gave an increment in the value of C_{l_ψ} at $C_L = 0$, an increment in the maximum value of C_{l_ψ}, and an increment in the value of C_L at which the maximum value of C_{l_ψ} occurred. For the inverse-taper sweptback wing, a half-span center-section split flap at the trailing edge produced practically no change in the value of C_{l_ψ} at $C_L = 0$, probably because at $C_L = 0$ the wing tips were carrying a negative load; this load in in turn produced a negative value of C_{l_ψ} to counteract the positive

increment provided by the flap. The use of the flap did, however, extend the curve of C_{l_ψ} enough to produce an appreciable increase in the maximum value of C_{l_ψ} and in the lift coefficient at which the maximum value of C_{l_ψ} occurred. For the inverse-taper sweptback wing the use of the half-span tip-section leading-edge slat (or flap) — either alone or in combination with the trailing-edge flap — resulted in little change in the value of C_{l_ψ} at $C_L = 0$ but did increase the maximum value of C_{l_ψ} and the lift coefficient at which the maximum value occurred, probably because the leading-edge devices improved the flow over the tips at high lift coefficients. The use of full-span and half-span tip-section nose spoilers extending forward from the chord plane on the 60° sweptback wing apparently improved the flow conditions over the wing outer panel and slightly increased the maximum value of C_{l_ψ}.

Effect of tip modification.- Cutting off the tip normal to the leading edge on an untapered 60° sweptback wing reduced the slope of the curve of C_{l_ψ} against C_L at low lift coefficients but did not change the maximum value of C_{l_ψ}. Sweeping forward the outer 40 percent of the span, however, markedly reduced both $\left(C_{l_\psi}\right)_{C_L}$ and the maximum value of C_{l_ψ}. (See fig. 39.)

Induced Drag, Maximum Lift, and Stalling of Swept Wings

Effect of aspect ratio.- Curves in figures 19 and 36 indicate the effect of aspect ratio on the induced drag, the maximum lift, and the stalling characteristics for unswept straight wings. Reducing the aspect ratio from 6 to 3 increases the drag, since the induced drag varies inversely to the aspect ratio. A reduction in $C_{L_{max}}$ occurs as the aspect ratio is decreased although the stall angle is higher for the lower aspect ratio.

Wings swept back 30° (fig. 15) show generally the same effect as unswept straight wings. When the aspect ratio is reduced from 5.2 to 4.5, an increase in drag and a reduction in $C_{L_{max}}$ occur. Wings swept back 60° (figs. 6, 7, 9, and 36) also show an increase in drag as the aspect ratio is reduced in the lower lift-coefficient range, but at higher lift coefficients the drag of the wing with the smaller aspect ratio is less than that of the wing with the higher aspect ratio. The same effect was obtained in tests of 60° sweptback wings in the

Langley 300 MPH 7- by 10-foot tunnel (reference 11). The higher drag of the wing with the larger aspect ratio is probably caused by the spanwise flow toward the tips of sweptback wings; this flow results in a thickening of the boundary layer and causes separated flow over the wing. This condition apparently becomes more aggravated at the higher sweep angles as the span is increased and results in a drag increment large enough to offset any decrease in induced drag caused by increasing the aspect ratio.

Aspect-ratio changes have a normal effect on sweptforward wings, as seen in figures 25 and 34. The effect is similar to that for unswept and for 30° sweptback wings, but the increase in drag and the loss in $C_{L_{max}}$ with decreases in aspect ratio appear larger for the sweptforward wings.

Effect of taper ratio.- For unswept wings figure 37 shows that an increase of taper reduced the induced drag, but the apparent increase in $C_{L_{max}}$ for the wing with taper ratio of 3.0 is probably a false effect since the tapered wings are cambered (NACA 23012) airfoil sections whereas the untapered wing is uncambered. Comparison of the tapered-wing data with data on a rectangular NACA 23012 airfoil section (reference 12) shows no effect of taper on $C_{L_{max}}$. As the wings are swept either forward or back the favorable effect of increased ratio of root chord to tip chord in reducing the induced drag becomes quite large.

Tuft studies of the sweptback wings (fig. 35) indicate that the stall pattern is similar to that observed on other sweptback wings at low Reynolds numbers. At moderate lift coefficients a region of disturbed flow occurs on the leading edge; then the tip stalls and the stall moves progressively toward the center section. Changes in taper did not appreciably affect the general pattern of the stall.

Effect of high-lift devices.- The use of full-span split flaps on the trailing edge of an untapered 60° sweptback wing (fig. 7) increased $C_{L_{max}}$ only slightly but did reduce the angle of attack for $C_{L_{max}}$. The drag was increased over most of the lift-coefficient range and became less than for the plain wing only slightly below $C_{L_{max}}$. The full-span nose spoiler tested on the 60° sweptback wing (fig. 8) gave a slightly larger increment of $C_{L_{max}}$ than did the split flap but indicated no change in the stall angle. The drag was increased up to a lift coefficient of about 0.6 but was less than the drag of the plain wing above $C_L = 0.6$.

Deflecting a half-span split flap on the trailing edge of a 37.5° sweptback wing (fig. 14) or adding either a leading-edge slat or flap

on the tip increased $C_{L_{max}}$. Deflecting the flap increased the drag up to a lift coefficient of 0.65 and then gave less drag than the plain wing up to $C_{L_{max}}$. The addition of either the leading-edge slat or flap further reduced the drag from a lift coefficient of 0.65 up to $C_{L_{max}}$. The addition of either the leading-edge slat or flap with the trailing-edge flap undeflected reduced the drag in the higher lift range by an amount about equal to that caused by deflecting the trailing-edge flap alone. Deflecting the split flap had little effect on the stall pattern but use of the tip slat considerably delayed the stall at the wing tip (figs. 35(c) and 35(d)).

Estimates based on aileron data (fig. 30) were made to determine the effectiveness of a split flap on the tip of sweptforward wings. The increment of lift at $\alpha = 0$ for the half-span split flap on the tip of a 45° sweptforward wing was slightly greater than that for an inboard half-span split flap on a 45° sweptback wing (reference 3) and almost twice as great as that for an outboard half-span split flap on a 45° sweptback wing (references 3 and 13). Little difference was noted in the increment of $C_{L_{max}}$ provided by the split flap on sweptforward and sweptback wings.

Effect of tip modification.- Cutting off the tip of a sweptback wing normal to the leading edge caused a reduction in drag from a lift coefficient of 0.50 up to maximum lift since the taper ratio was effectively increased (fig. 39). Sweeping the outer 40 percent of the wing forward increased the drag from a lift coefficient of 0.80 to $C_{L_{max}}$ and slightly reduced $C_{L_{max}}$, probably because of the increased interference between the sweptforward and the sweptback panels.

Aileron Effectiveness for Sweptforward Wings

Data for two 45° sweptforward wings of taper ratio 1.0 and 4.0 equipped with half-span split-flap-type 0.20c ailerons deflected on the left wing only are presented in figures 30 and 33.

Comparisons which accounted for the relative effectiveness of plain and split flaps (reference 13) indicate that the aileron effectiveness $C_{l_{\delta_a}}$ at a lift coefficient of 0.2 for the 45° untapered sweptforward wing was about 10 percent greater than the value that would be obtained for the 45° untapered sweptback wing of reference 3. This result is probably caused by the thinner boundary layer and the less turbulent flow existing on the tips of sweptforward wings.

The data showed that the loss in aileron rolling-moment effectiveness resulting from increased taper was greater for the sweptforward wing than the loss indicated for unswept wings in reference 14.

COMPARISON WITH THEORY

Yawed-Wing Lift-Curve Slope

The tests of the yawed wings were made primarily to provide a relatively quick preliminary check on Betz's concept of the effect of yaw on the lift-curve slope (reference 2). As shown by figure 40 the data for the NACA 0012 wing of aspect ratio 6 agreed almost exactly with the cosine law. Tests of an NACA 0012 wing of aspect ratio 3, however, showed less effect of yaw on C_{L_α} than is indicated by the cosine law. In an effort to explain the discrepancy, tests were made of two flat plates having aspect ratios of 3, one rectangular and one of infinite taper. As shown by figure 40 the infinite-taper model showed more effect of yaw than the cosine law and the rectangular plate showed less effect. Additional tests of a flat plate having an aspect ratio of 1.27 showed an increase rather than a decrease in C_{L_α}, as the model was yawed. These results may be partly explained by the fact that as a rectangle is yawed the span normal to the air-stream direction - and thus the aspect ratio - increases for part of the yaw range. The amount of increase and the angles of yaw over which this increase appears are functions of the aspect ratio and the taper of the basic model. Corrections applied on this basis indicate that all the data would group about the curve for the infinite-taper plate having an aspect ratio of 3. The resulting curve showed a slightly greater effect of yaw than is indicated by the cosine law.

Swept-Wing Lift-Curve Slope

The data of reference 3 indicate that in the computation of the lift-curve slope of swept wings the cosine law is valid provided the aspect ratio used is that of an unswept wing having the same panels as the swept wing. On this basis and by use of the lifting-surface-theory equation for the lift-curve slope (reference 15) figure 41 was derived. By use of figure 41 and a value of 0.099 for the section lift-curve slope the values of C_{L_α} were computed for all the swept-wing tests. The measured and the computed values of C_{L_α} are shown in figure 42. The agreement is reasonably good but indicates, as did the yawed-wing data, that the cosine law does not indicate quite enough drop in C_{L_α} as Λ is increased.

Swept-Wing Effective Dihedral

In the calculation of the effective dihedral the same procedure was followed as in reference 3 except that the aspect ratio and taper ratio as well as the sweep were accounted for by obtaining $\left(C_{l_\psi C_L}\right)_{\Lambda=0}$ from the following formula of Weissinger (reference 9):

$$57.3\frac{\partial^2 C_l}{\partial\psi\,\partial C_L} = 57.3\left(C_{l_\psi}\right)_{C_L} = 0.5\left\{\frac{2K}{A}\left[\frac{1 + 0.15(\lambda - 1)}{\lambda + 1}\right] - 0.10\right\} \qquad (16)$$

Reference 9 states that the constant K is indeterminate but depends on the wing-tip shape and is probably of the order of magnitude of unity for square-cut tips. The data for the NACA 0012 airfoils having aspect ratios of 3 and 6 were used to evaluate K and a value of 1.51 was obtained.

The values of $\left(C_{l_\psi}\right)_{C_L}$ for the models tested in the present investigation were computed by using $K = 1.51$ and equations (15) and (16). Figure 43 shows the remarkably close agreement obtained between the measured and the computed values.

CONCLUSIONS

The results of low-speed tests in the Langley 7- by 10-foot tunnel of several small-scale models of yawed and swept wings indicated the following conclusions:

1. The lift-curve slope and the effective dihedral for swept wings can be computed with a reasonable degree of accuracy in the low lift-coefficient range by means of existing theories.

2. In general, reducing the aspect ratio and the ratio of root chord to tip chord produced increases in drag and effective dihedral and slightly increased the longitudinal stability near the stall.

3. Cutting off the tip of a sweptback wing normal to the leading edge reduced the effective dihedral at low lift coefficients and gave a slight reduction in the drag at high lift coefficients.

4. Sweeping forward a part of the outer panel of a sweptback wing improved the longitudinal stability and decreased the effective dihedral but also increased the drag at high lift coefficients and slightly decreased the maximum lift coefficient.

5. The use of either leading-edge or trailing-edge high-lift devices on sweptback wings increased the lift-drag ratio and the effective dihedral at high lift coefficients.

6. An increase in the ratio of root chord to tip chord on a swept-forward wing caused decreases in aileron rolling-moment effectiveness that were greater than the losses computed for unswept wings.

Langley Aeronautical Laboratory
National Advisory Committee for Aeronautics
Langley Field, Va., May 22, 1947

REFERENCES

1. Jones, Robert T.: Wing Plan Forms for High-Speed Flight. NACA Rep. 863, 1947. (Formerly NACA TN 1033.)

2. Betz, A.: Applied Airfoil Theory. Unsymmetrical and Non-Steady Types of Motion. Vol. IV of Aerodynamic Theory, div. J, ch. IV, sec. 4, W. F. Durand, ed., Julius Springer (Berlin), 1935, pp. 97-107.

3. Letko, William, and Goodman, Alex: Preliminary Wind-Tunnel Investigation at Low Speed of Stability and Control Characteristics of Swept-Back Wings. NACA TN 1046, 1946.

4. Weick, Fred E., and Noyes, Richard W.: Wind-Tunnel Research Comparing Lateral Control Devices Particularly at High Angles of Attack. XIII - Auxiliary Airfoils Used as External Ailerons. NACA Rep. 510, 1935.

5. Gillis, Clarence L., Polhamus, Edward C., and Gray, Joseph L., Jr.: Charts for Determining Jet-Boundary Corrections for Complete Models in 7- by 10-Foot Closed Rectangular Wind Tunnels. NACA ARR L5G31, 1945.

6. Mutterperl, William: The Calculation of Span Load Distributions on Swept-Back Wings. NACA TN 834, 1941.

7. Wieghardt, Karl: Chordwise Load Distribution of a Simple Rectangular Wing. NACA TM 963, 1940.

8. Cohen, Doris: A Method for Determining the Camber and Twist of a Surface to Support a Given Distribution of Lift, with Applications to the Load over a Sweptback Wing. NACA Rep. 826, 1945. (Formerly NACA TN 855.)

9. Weissinger, J.: Ergänzungen und Berichtigungen zur Theorie der schiebenden Flügels. Jahrb. 1943 der DVL, E.V. (Berlin-Adlershof), IA021, pp. 1-6.

10. Shortal, Joseph A., and Maggin, Bernard: Effect of Sweepback and Aspect Ratio on Longitudinal Stability Characteristics of Wings at Low Speeds. NACA TN 1093, 1946.

11. Lowry, John G., and Schneiter, Leslie E.: Investigation at Low Speed of the Longitudinal Stability Characteristics of a 60° Swept-Back Tapered Low-Drag Wing. NACA TN 1284, 1947.

12. Purser, Paul E., and Turner, Thomas R.: Wind-Tunnel Investigation of Perforated Split Flaps for Use as Dive Brakes on a Rectangular NACA 23012 Airfoil. NACA ACR, July 1941.

13. Wenzinger, Carl J., and Harris, Thomas A.: Wind-Tunnel Investigation of an N.A.C.A. 23012 Airfoil with Various Arrangements of Slotted Flaps. NACA Rep. 664, 1939.

14. Weick, Fred E., and Jones, Robert T.: Résumé and Analysis of N.A.C.A. Lateral Control Research. NACA Rep. 605, 1937.

15. Swanson, Robert S., and Crandall, Stewart M.: Lifting-Surface-Theory Aspect-Ratio Corrections to the Lift and Hinge-Moment Parameters for Full-Span Elevators on Horizontal Tail Surfaces. NACA Rep. 911, 1948. (Formerly NACA TN 1175.)

TABLE I

AIRFOIL ORDINATES MEASURED ON INVERSE-TAPER MODEL

[Chordwise stations and ordinates given in percent of airfoil-section chord]

Chordwise station	Spanwise station					
	Center line		21.25 in. right of center line		21.25 in. left of center line	
	Upper surface	Lower surface	Upper surface	Lower surface	Upper surface	Lower surface
0	0	0	0	0	0	0
.75	.90	.82	.72	.65	.79	.65
1.25	1.12	.98	.94	.82	.98	.84
2.5	1.55	1.28	1.32	1.10	1.40	1.15
5.0	2.21	1.73	1.94	1.55	1.99	1.65
7.5	2.65	2.06	2.40	1.90	2.45	2.05
10	3.03	2.30	2.77	2.20	2.83	2.35
20	4.00	2.83	3.70	2.90	3.89	2.93
30	4.55	2.95	4.13	3.21	4.40	3.21
40	4.68	2.92	4.26	3.15	4.46	3.17
50	4.53	2.73	4.25	2.99	4.35	3.01
60	3.98	2.48	3.80	2.66	3.90	2.66
70	3.07	1.85	3.08	2.16	3.17	2.02
80	2.07	1.32	2.15	1.50	2.19	1.42
90	1.05	.77	1.10	.80	1.12	.75
100	0	0	0	0	0	0

TABLE II

INDEX OF FIGURES

Model	$\Lambda_{\frac{c}{4}}$ (deg)	Aspect ratio, A	Taper ratio, λ	Airfoil section	Model configuration and test conditions	Figure
Force-test data						
1	60	2.6	1	NACA 0012	$\psi = 0^\circ, \pm 5^\circ$	6
2	60	1.5	1	NACA 0012	$\psi = 0^\circ, \pm 5^\circ$; wing + split flap	7
2	60	1.5	1	NACA 0012	$\psi = 0^\circ, \pm 5^\circ$; wing + nose spoiler	8
3, 4	60	3, 1.5	1	NACA 0015	$\psi = 0^\circ$	9
5	60	3.1	1	NACA 0012	$\psi = 0^\circ, \pm 5^\circ$; cut-off tips	10
6	±60	2.6	1	NACA 0012	$\psi = 0^\circ, \pm 5^\circ$; sweptforward outer panels	11
7	56	2.1	2.5	NACA 23012	$\psi = 0^\circ, \pm 5^\circ$	12
8	37.5	3	2.04	NACA 23012	$\psi = 0^\circ, \pm 5^\circ$	13
9	37.5	3	0.617	Low-drag-type	$\psi = 0^\circ, \pm 5^\circ$; faired tip; split flap; nose slat and flap	14
10, 11	30	5.2, 4.5	1	NACA 0015	$\psi = 0^\circ$	15
12	14	6	3	NACA 23012	$\psi = 0^\circ, \pm 5^\circ$	16
13	6	6	5	NACA 23012	$\psi = 0^\circ$	17
14	0	6	1	NACA 0012	$\psi = 0^\circ$	18
15, 16	0	6, 3	1	NACA 0015	$\psi = 0^\circ$	19
14	0	6	1	NACA 0012	Yaw range; stability and wind axes	20
17	0	3	1	NACA 0012	Yaw range; stability and wind axes	21
18	0	3	1	Flat plate	Yaw range; stability and wind axes	22
19	0	3	∞	Flat plate	Yaw range; stability and wind axes	23
20	0	1.27	1	Flat Plate	Yaw range; stability and wind axes	24
21, 22	-30	5.2, 4.5	1	NACA 0015	$\psi = 0^\circ$	25
23	-30	3.6	1	NACA 0012	$\psi = 0^\circ, \pm 5^\circ$	26
24	-32	3.6	2.85	NACA 23012	$\psi = 0^\circ, \pm 5^\circ$	27
25	-30	3.6	4.24	NACA 23012	$\psi = 0^\circ, \pm 5^\circ$	28
26	-45	2.1	1	NACA 0012	$\psi = 0^\circ, \pm 5^\circ$	29
26	-45	2.1	1	NACA 0012	$\psi = 0^\circ, \pm 5^\circ$; wing + aileron	30
27	-46.6	2.1	2.5	NACA 23012	$\psi = 0^\circ$	31
28	-45	2.1	4	NACA 23012	$\psi = 0^\circ, \pm 5^\circ$	32
28	-45	2.1	4	NACA 23012	$\psi = 0^\circ, \pm 5^\circ$; wing + aileron	33
29, 30	-60	3, 1.5	1	NACA 0015	$\psi = 0^\circ$	34
Tuft sketches						
2	60	1.5	1	NACA 0012		35a
7	56	2.1	2.5	NACA 23012		35b
9	37.5	3	0.617	Low-drag-type	Plain wing	35c
9	37.5	3	0.617	Low-drag-type	Wing + tip slat	35d
13	6	6	5	NACA 23012		35e
27	-45	2.1	2.5	NACA 23012		35f
Comparison figures						
Effect of aspect ratio						36
Effect of taper ratio						37
Effect of high-lift devices						38
Effect of tip modification						39
Yawed-wing lift-curve slope						40
Lift-curve slope for swept wings						41
Comparison of measured and computed lift-curve slopes for swept wings						42
Comparison of measured and computed values of effective dihedral for swept wings						43

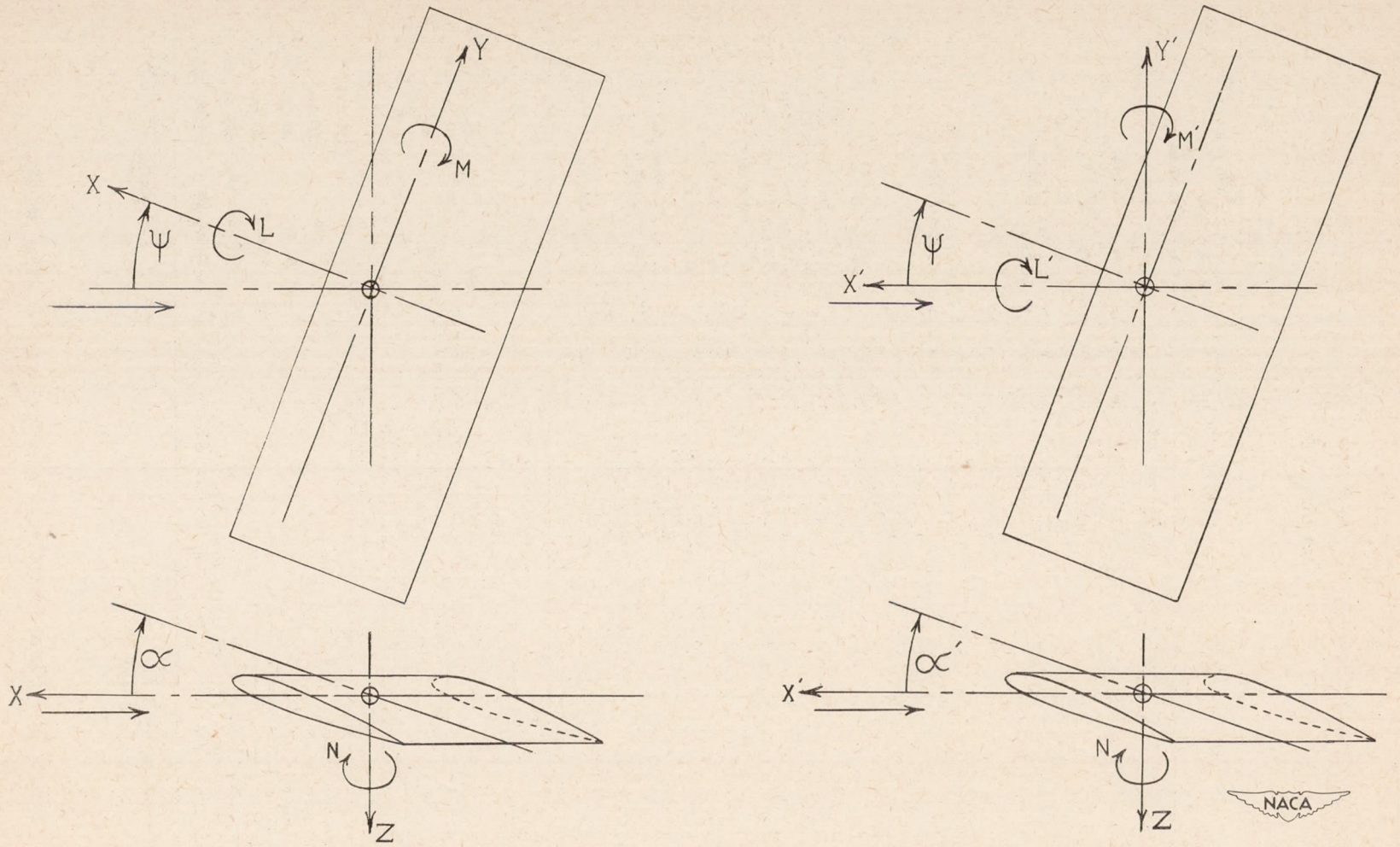

(a) Stability axes.

(b) Wind axes.

Figure 1.- Systems of axes used. Positive values of forces, moments, and angles are indicated by arrows.

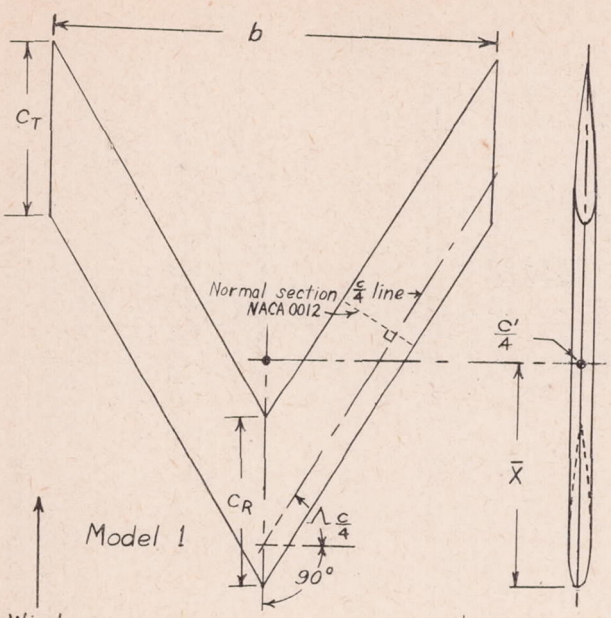

$\Lambda_{c/4}$	60°
A	2.62
λ	1
b	51.81 in.
c'	19.8 in.
c_R	19.8 in.
c_T	19.8 in.
S	1026.5 sq. in.
$\bar{x}$	27.33 in.

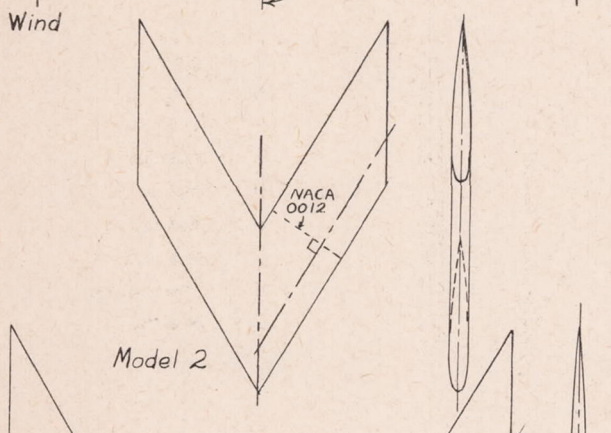

$\Lambda_{c/4}$	60°
A	1.49
λ	1
b	29.6 in.
c'	19.8 in.
c_R	19.8 in.
c_T	19.8 in.
S	586.08 sq. in.
$\bar{x}$	17.79 in.

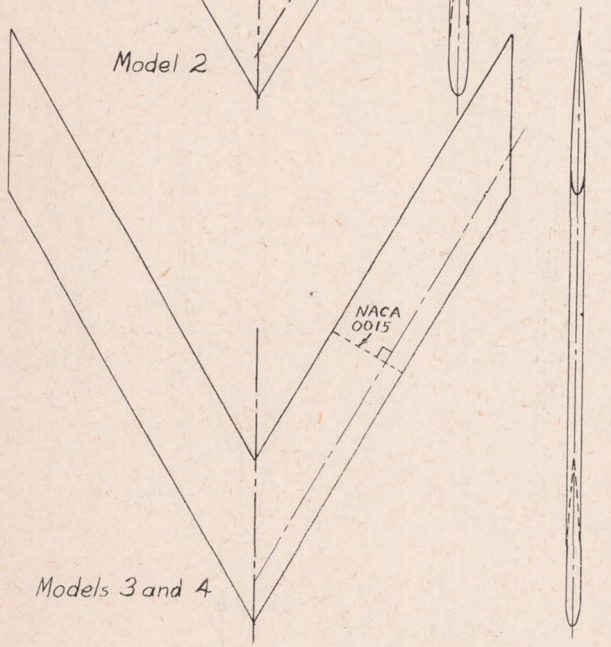

	Model 3	Model 4
$\Lambda_{c/4}$	60°	60°
A	3	1.5
λ	1	1
b	60 in.	30 in.
c'	20 in.	20 in.
c_R	20 in.	20 in.
c_T	20 in.	20 in.
S	1200 sq. in.	600 sq. in.
$\bar{x}$	30.965 in.	17.989 in.

Figure 2.- Plan forms and dimensions of wing models.

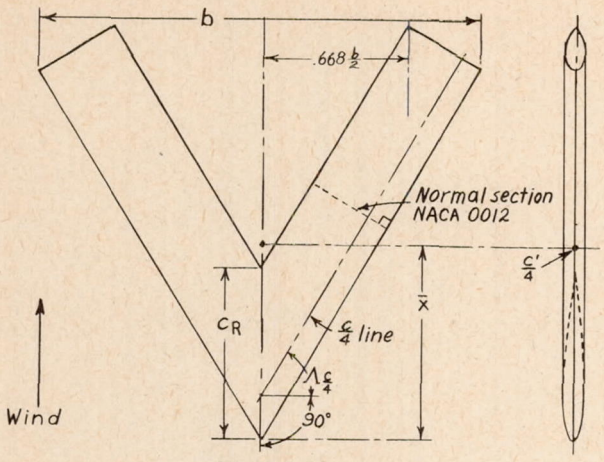

Model 5

$\Lambda_{c/4}$	60°
A	3.14
λ	1
b	51.81 in.
c'	18.26 in.
c_R	19.8 in.
c_T	0
S	856.5 sq. in.
$\bar{x}$	23.92 in.

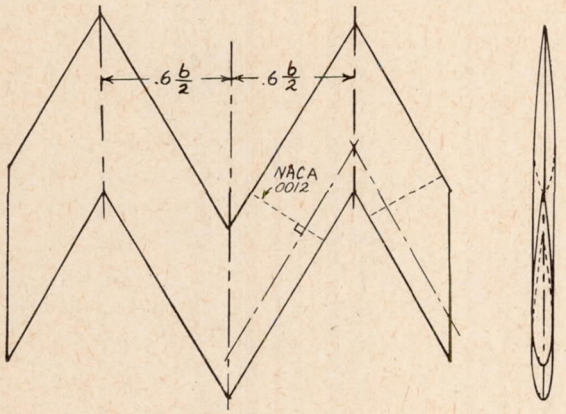

Model 6

$\Lambda_{c/4}$	± 60°
A	2.62
λ	1
b	51.81 in.
c'	19.8 in.
c_R	19.8 in.
c_T	19.8 in.
S	1026.5 sq. in.
$\bar{x}$	19.28 in.

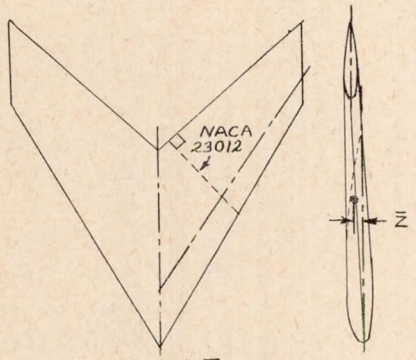

Model 7

$\Lambda_{c/4}$	55.8°	c_R	23.91 in.
A	2.08	c_T	9.76 in.
λ	2.45	S	589.73 sq. in.
b	35.05 in.	$\bar{x}$	17.03 in.
c'	17.83 in.	$\bar{z}$	0.269 in.

Figure 2.- Continued.

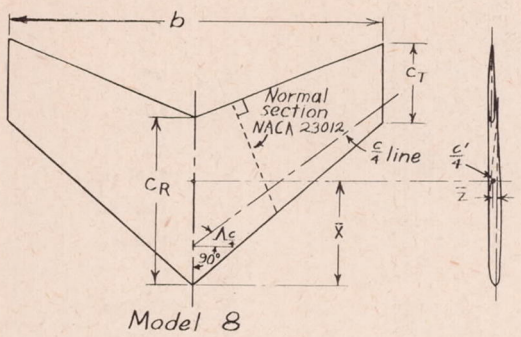

Model 8

$\Lambda_{c/4}$	37.5°
A	3
λ	2.04
b	38.84 in.
c'	13.17 in.
c_R	17.07 in.
c_T	8.35 in.
S	494 sq. in.
$\bar{x}$	10.85 in.
$\bar{z}$	0.25 in.

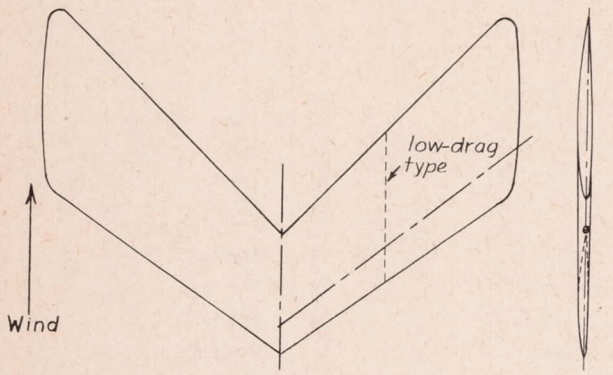

Model 9

$\Lambda_{c/4}$	37.5°
A	3
λ	0.617
b	47 in.
c'	15.61 in.
c_R	11.875 in.
c_T	19.33 in.
S	721.44 sq. in.
$\bar{x}$	12.41

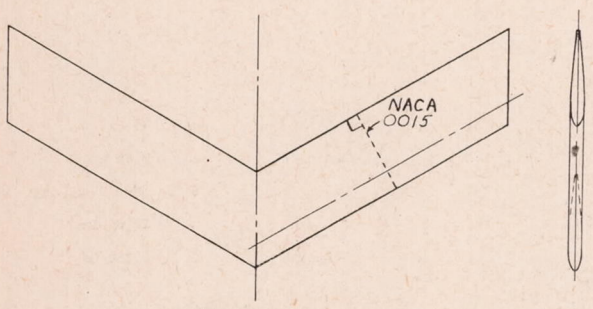

Models 10 and 11

	Model 10	Model 11
$\Lambda_{c/4}$	30°	30°
A	5.2	4.5
λ	1	1
b	60 in.	52 in.
c'	11.54 in.	11.54 in.
c_R	11.54 in.	11.54 in.
c_T	11.54 in.	11.54 in.
S	692.84 sq. in.	600 sq. in.
$\bar{x}$	11.548 in.	10.393 in.

Figure 2.- Continued.

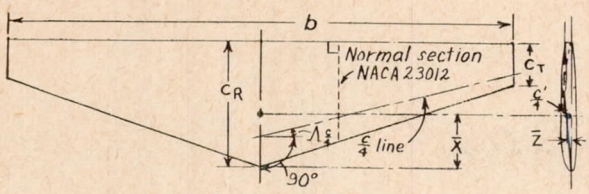

Model 12

$\Lambda_{c/4}$	14.04°
A	6
λ	3
b	60 in.
c'	10.833 in.
c_R	15 in.
c_T	5 in.
S	600 sq. in.
$\bar{x}$	6.875 in.
$\bar{z}$	0.317 in.

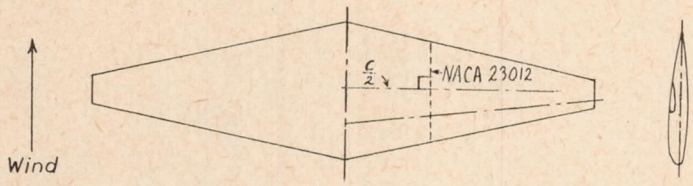

Model 13

$\Lambda_{c/4}$	6.34°
A	6
λ	5
b	60 in.
c'	11.48 in.
c_R	16.667 in.
c_T	3.333 in.
S	600 sq. in.
$\bar{x}$	5.46 in.
$\bar{z}$	0.394 in.

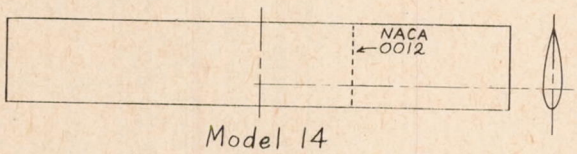

Model 14

$\Lambda_{c/4}$	0°
A	6
λ	1
b	60 in.
c'	10 in.
c_R	10 in.
c_T	10 in.
S	600 sq. in.
$\bar{x}$	2.5 in.

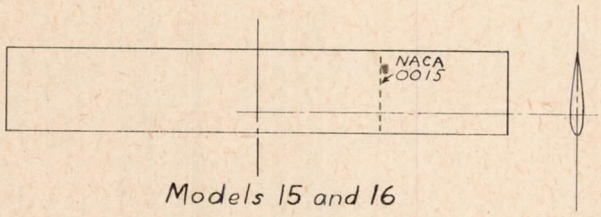

Models 15 and 16

	Model 15	Model 16
$\Lambda_{c/4}$	0°	0°
A	6	3
λ	1	1
b	60 in.	30 in.
c	10 in.	10 in.
c_R	10 in.	10 in.
c_T	10 in.	10 in.
S	600 sq. in.	300 sq. in.
$\bar{x}$	2.5 in.	2.5 in.

Figure 2.- Continued.

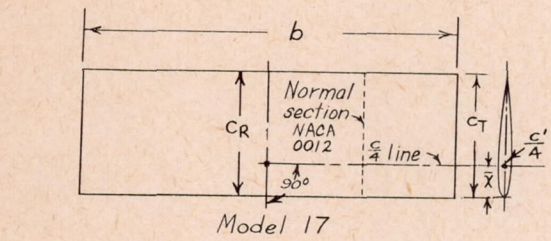

Model 17

$\Lambda_{c/4}$	0°	c_R	10 in.
A	3	c_T	10 in.
λ	1	S	300 sq in.
b	30 in.	$\bar{x}$	2.5 in.
c′	10 in.		

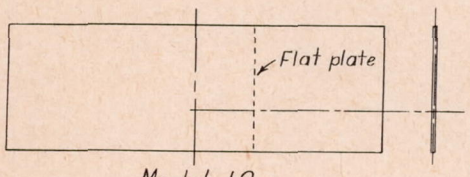

Model 18

$\Lambda_{c/4}$	0°	c_R	10 in.
A	3	c_T	10 in.
λ	1	S	300 sq in.
b	30 in.	$\bar{x}$	2.5 in.
c′	10 in.		

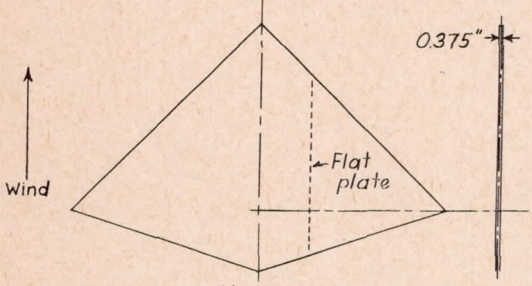

Model 19

$\Lambda_{c/4}$	0°	c_R	20 in.
A	3	c_T	0
λ	∞	S	150 sq in.
b	30 in.	$\bar{x}$	4.99 in.
c′	13.335 in.		

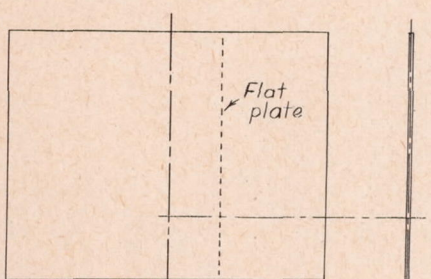

Model 20

$\Lambda_{c/4}$	0°	c_R	20 in.
A	1.27	c_T	20 in.
λ	1	S	510 sq in.
b	25.5 in	$\bar{x}$	5 in.
c′	20 in.		

Figure 2.- Continued.

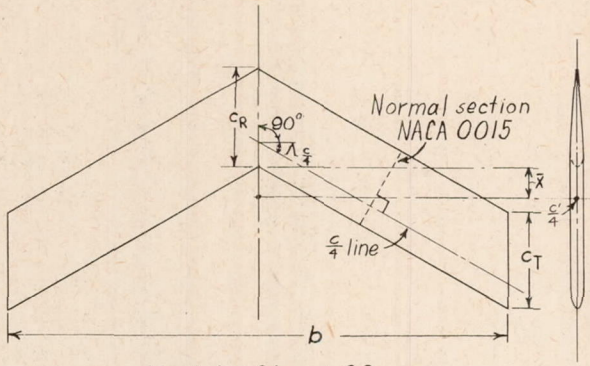

Models 21 and 22

	Model 21	Model 22
$\Lambda_{c/4}$	-30°	-30°
A	5.2	4.5
λ	1	1
b	60 in.	52 in.
c'	11.54 in.	11.54 in.
c_R	11.54 in.	11.54 in.
c_T	11.54 in.	11.54 in.
S	692.84 sq. in.	600 sq. in.
$-\bar{x}$	5.774 in.	4.619 in.

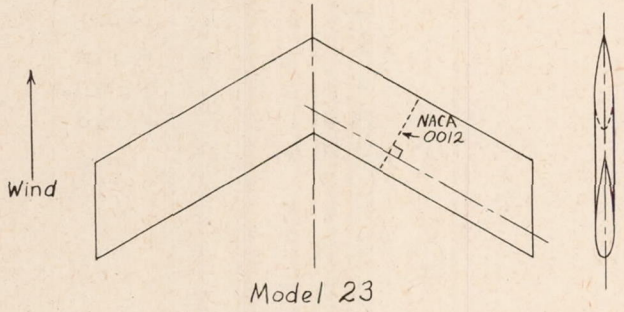

Model 23

$\Lambda_{c/4}$	-30°
A	3.59
λ	1
b	41.5 in.
c'	11.54 in.
c_R	11.54 in.
c_T	11.54 in.
S	482 sq. in.
$-\bar{x}$	5.61 in.

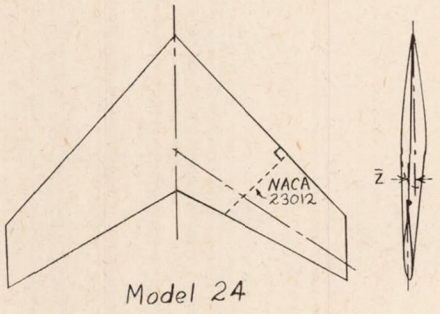

Model 24

$\Lambda_{c/4}$	-32°	c_R	19.1 in.
A	3.61	c_T	6.69 in.
λ	2.85	S	600.9 sq. in.
b	46.6 in.	$-\bar{x}$	1.27 in.
c'	13.9 in.	$\bar{z}$	0.3 in.

NACA

Figure 2.- Continued.

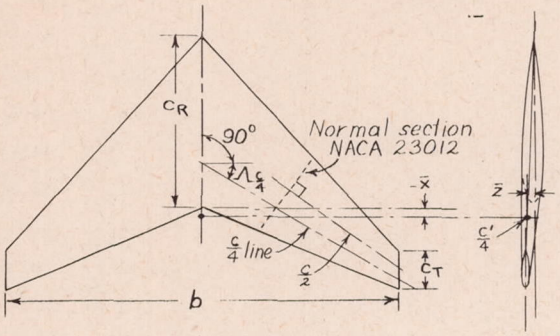

Model 25

$\Lambda_{c/4}$	30°
A	3.55
λ	4.24
b	46.5 in.
c'	14.8 in.
c_R	21.25 in.
c_T	5 in.
S	610 sq. in.
$-\bar{x}$	0.46 in.
$\bar{z}$	0.68 in.

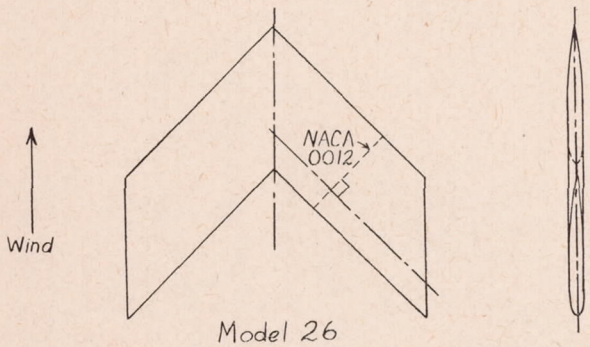

Model 26

$\Lambda_{c/4}$	45°
A	2.1
λ	1
b	29.7 in.
c'	14.14 in.
c_R	14.14 in.
c_T	14.14 in.
S	420 sq. in.
$-\bar{x}$	3.89 in.

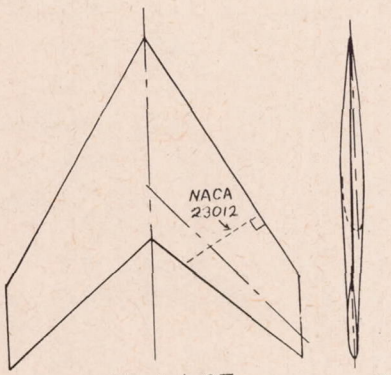

Model 27

$\Lambda_{c/4}$	46.6°
A	2.09
λ	2.47
b	35.19 in.
c'	17.85 in.
c_R	23.98 in.
c_T	9.71 in.
S	592.74 sq. in.
$\bar{x}$	2.02 in.
$\bar{z}$	0.225 in.

NACA

Figure 2.- Continued.

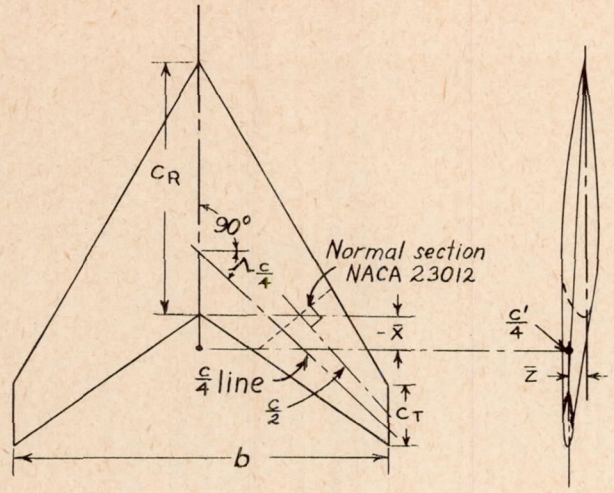

Model 28

$\Lambda_{c/4}$	-45°
A	2.1
λ	3.88
b	36.62 in.
c'	18.51 in.
c_R	26.38 in.
c_T	6.78 in.
S	607 sq. in.
$-\bar{x}$	0.97 in.
$\bar{z}$	0.31 in.

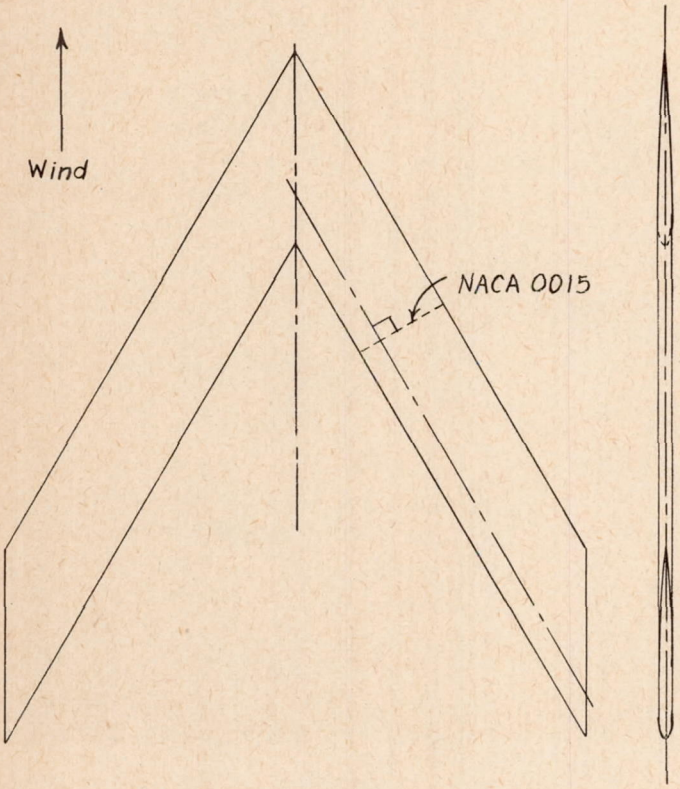

Models 29 and 30

	Model 29	Model 30
$\Lambda_{c/4}$	-60°	-60°
A	3	1.5
λ	1	1
b	60 in.	30 in.
c'	20 in.	20 in.
c_R	20 in.	20 in.
c_T	20 in.	20 in.
S	1200 sq. in.	600 sq. in.
$-\bar{x}$	20.965 in.	7.99 in.

Figure 2.- Concluded.

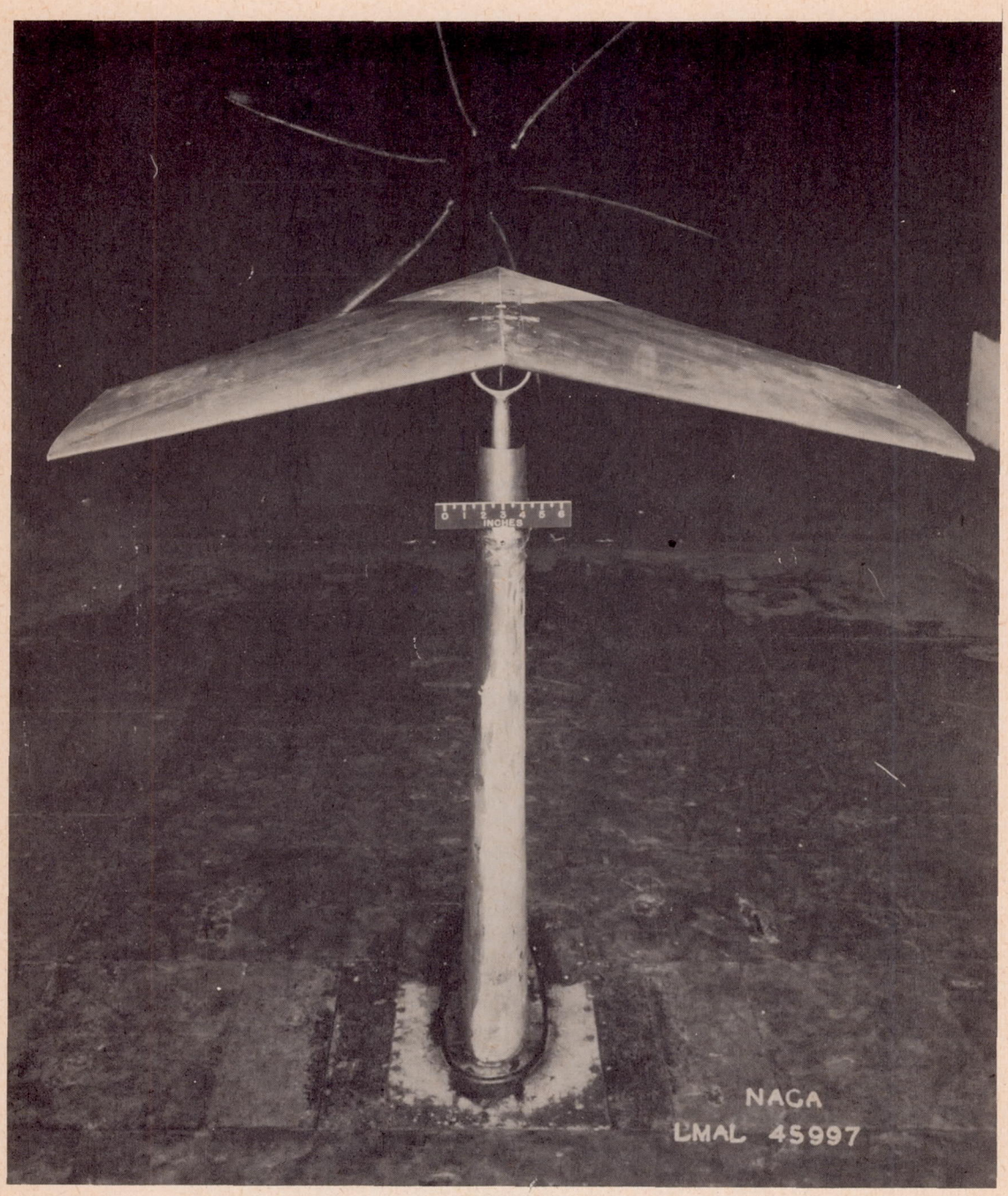

(a) 45° sweptforward wing.

Figure 3.- Swept wings mounted in test section of Langley 7- by 10-foot tunnel. Front view.

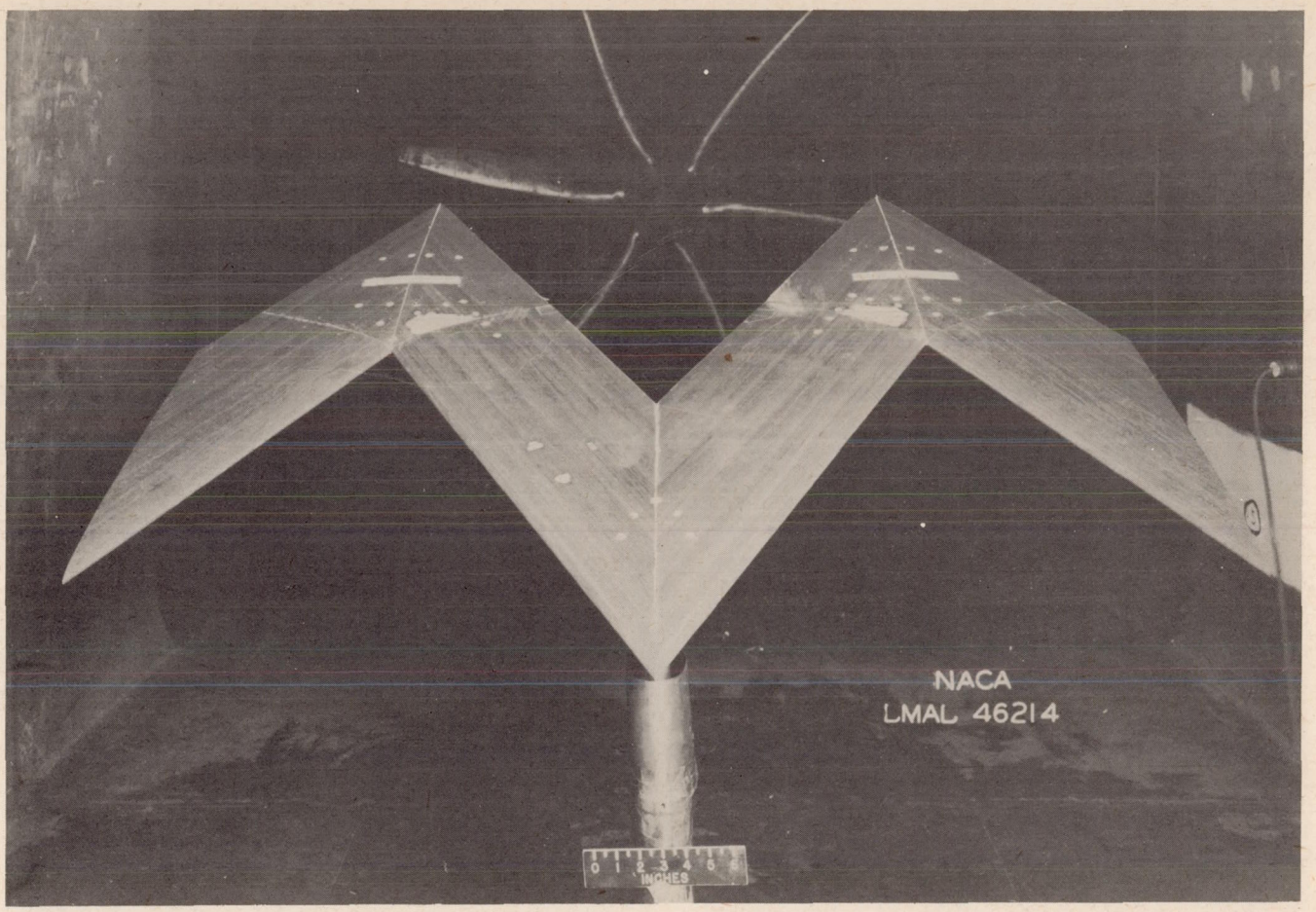

(b) 60° sweptback wing with 60° sweptforward outer panels.

Figure 3.- Concluded.

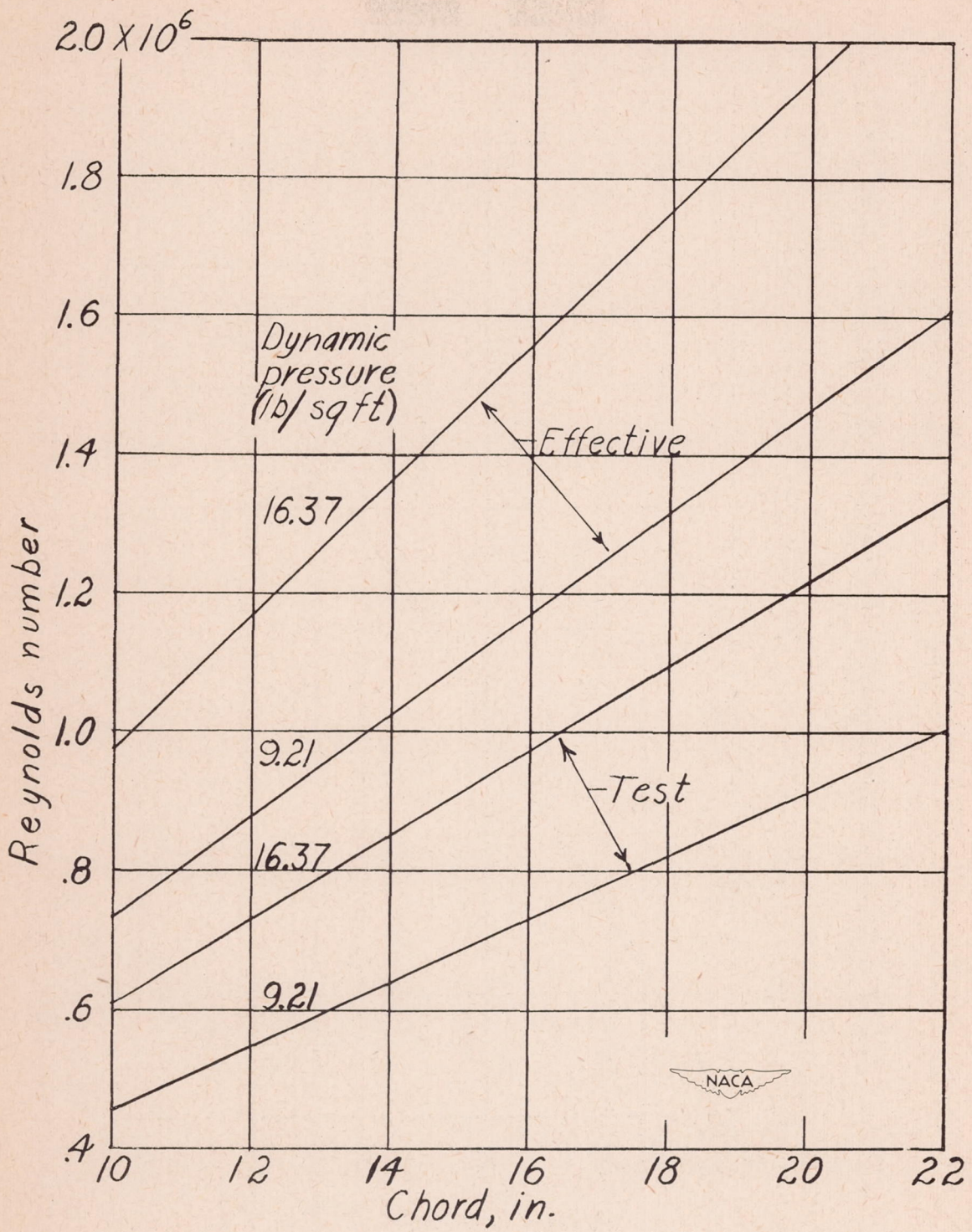

Figure 4.- Variation of test and effective Reynolds number with dynamic pressure and model chord for Langley 7- by 10-foot tunnel.

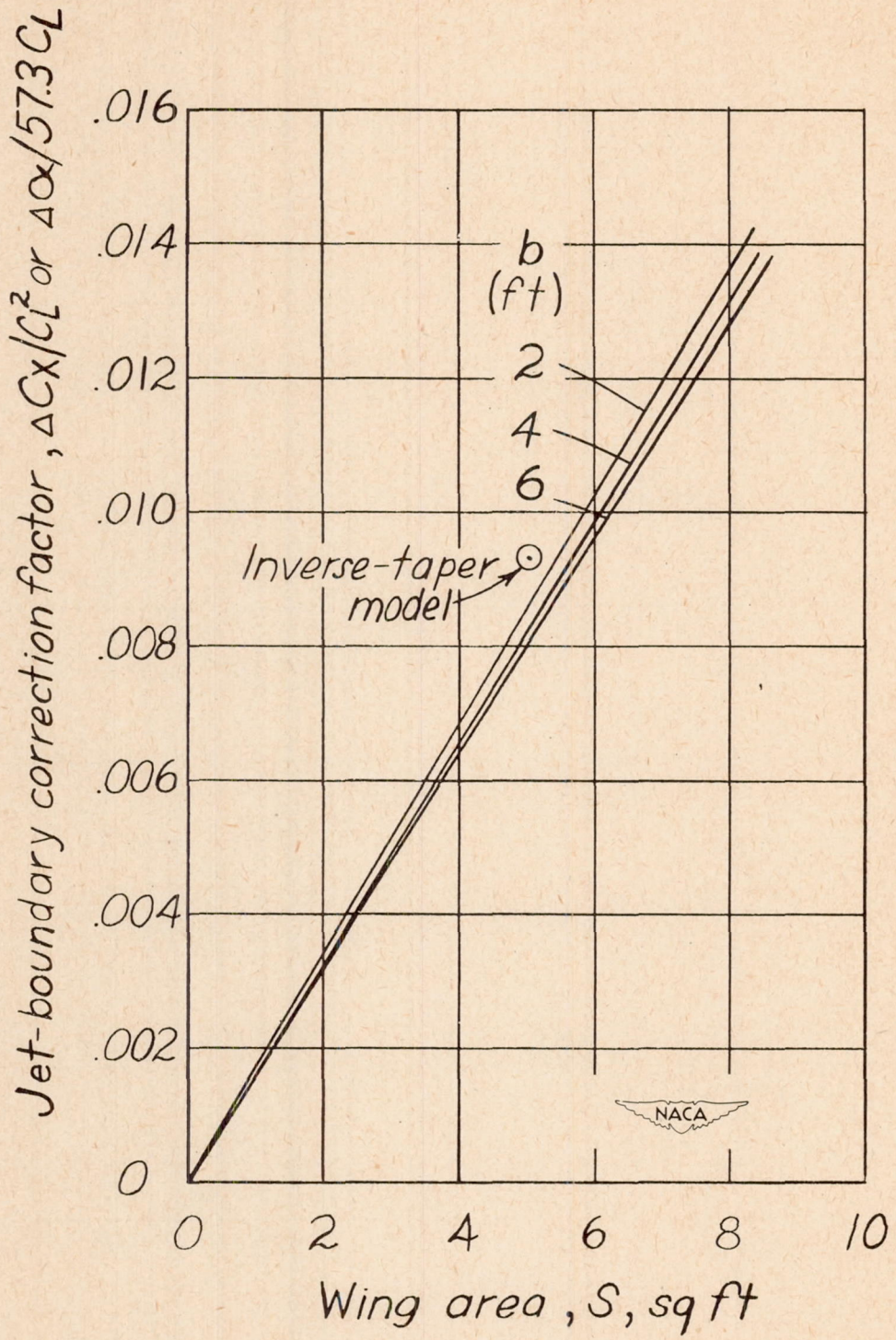

Figure 5.- Jet-boundary correction factors for wings.

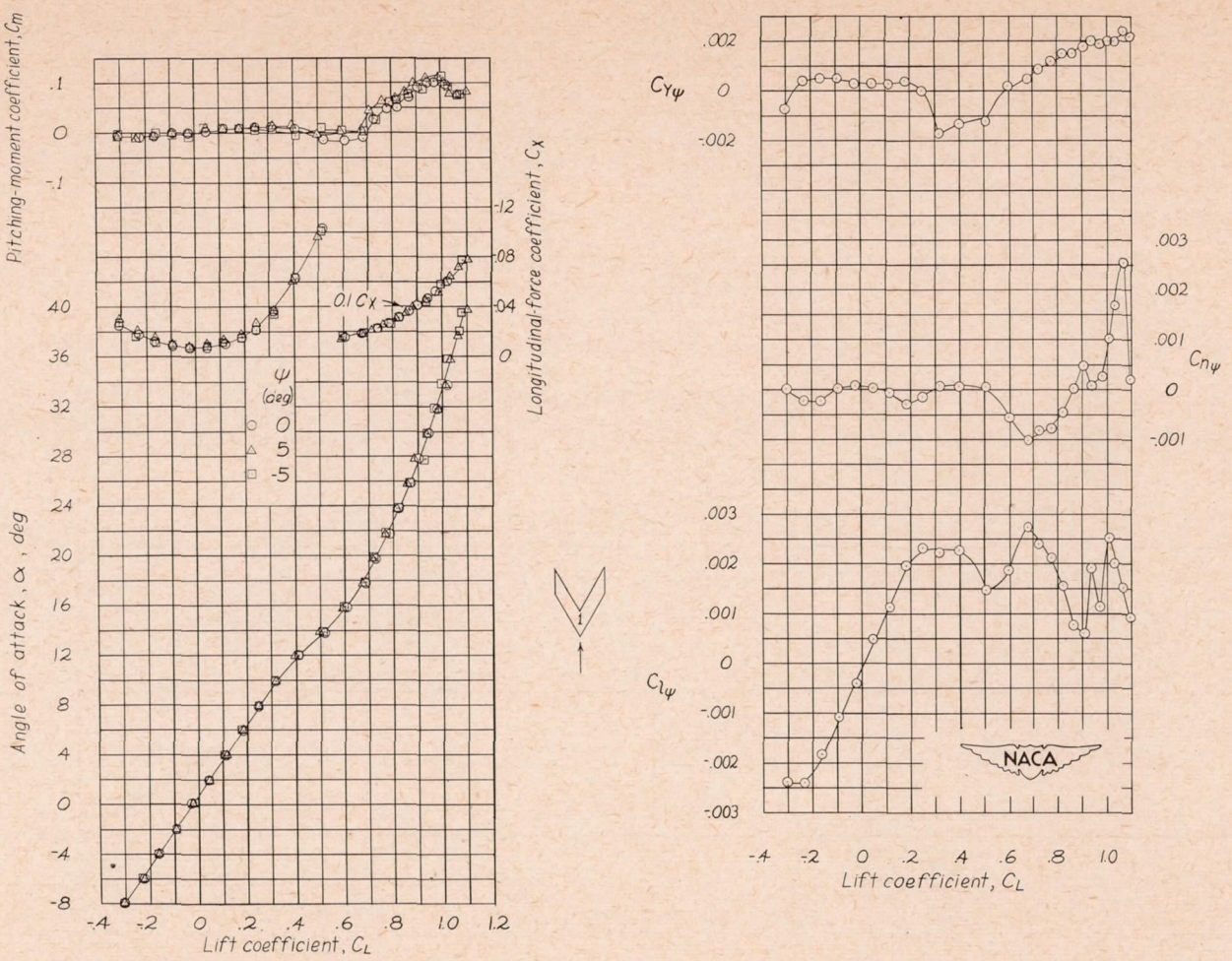

Figure 6.- Aerodynamic characteristics of a sweptback wing. $\Lambda_{c/4} = 60^\circ$; A = 2.6; λ = 1; NACA 0012 airfoil section; model 1.

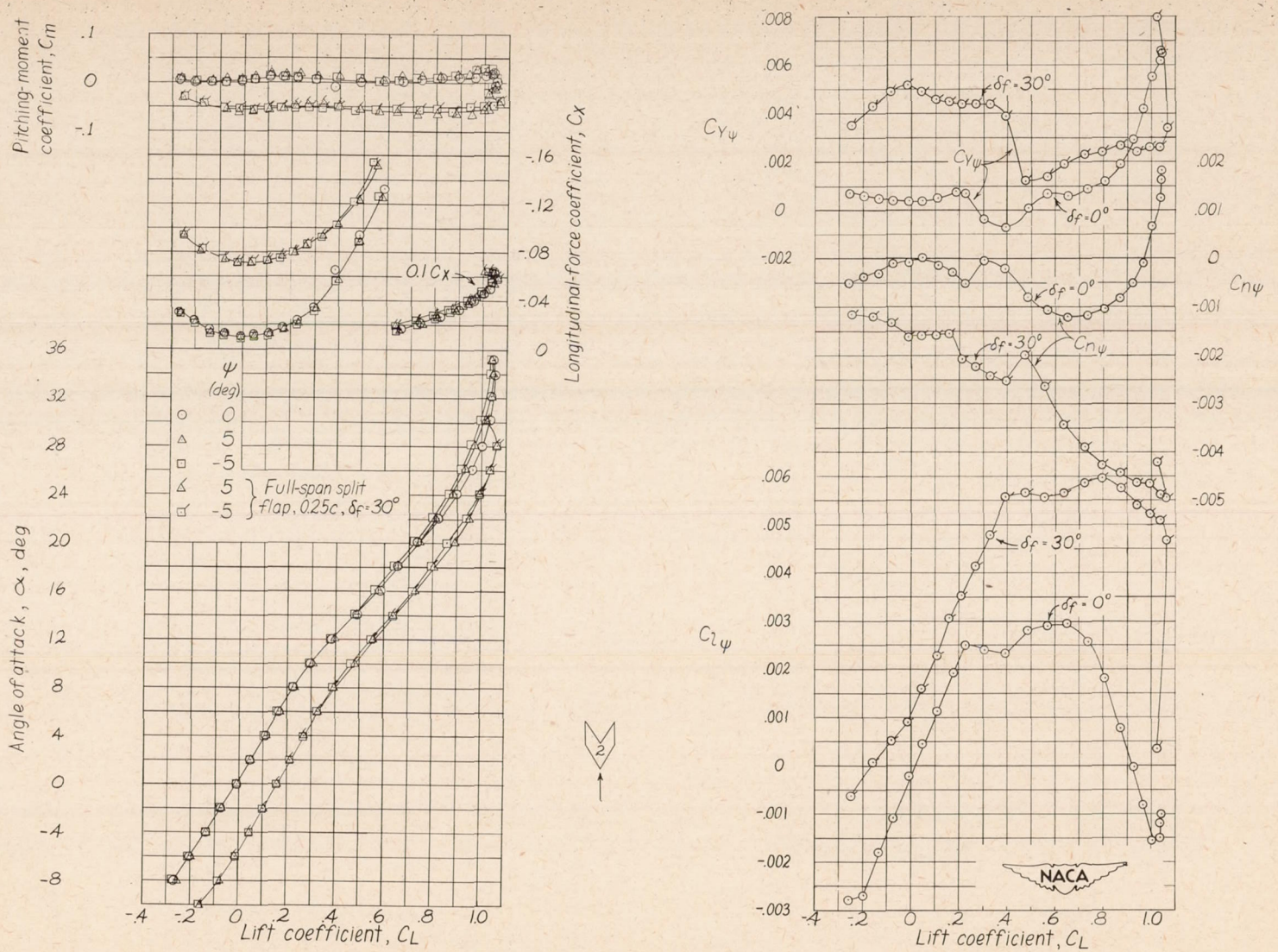

Figure 7.- Aerodynamic characteristics of a sweptback wing. $\Lambda_{c/4} = 60°$; A = 1.5; λ = 1; NACA 0012 airfoil section with full-span 0.25c split flap at trailing edge; model 2.

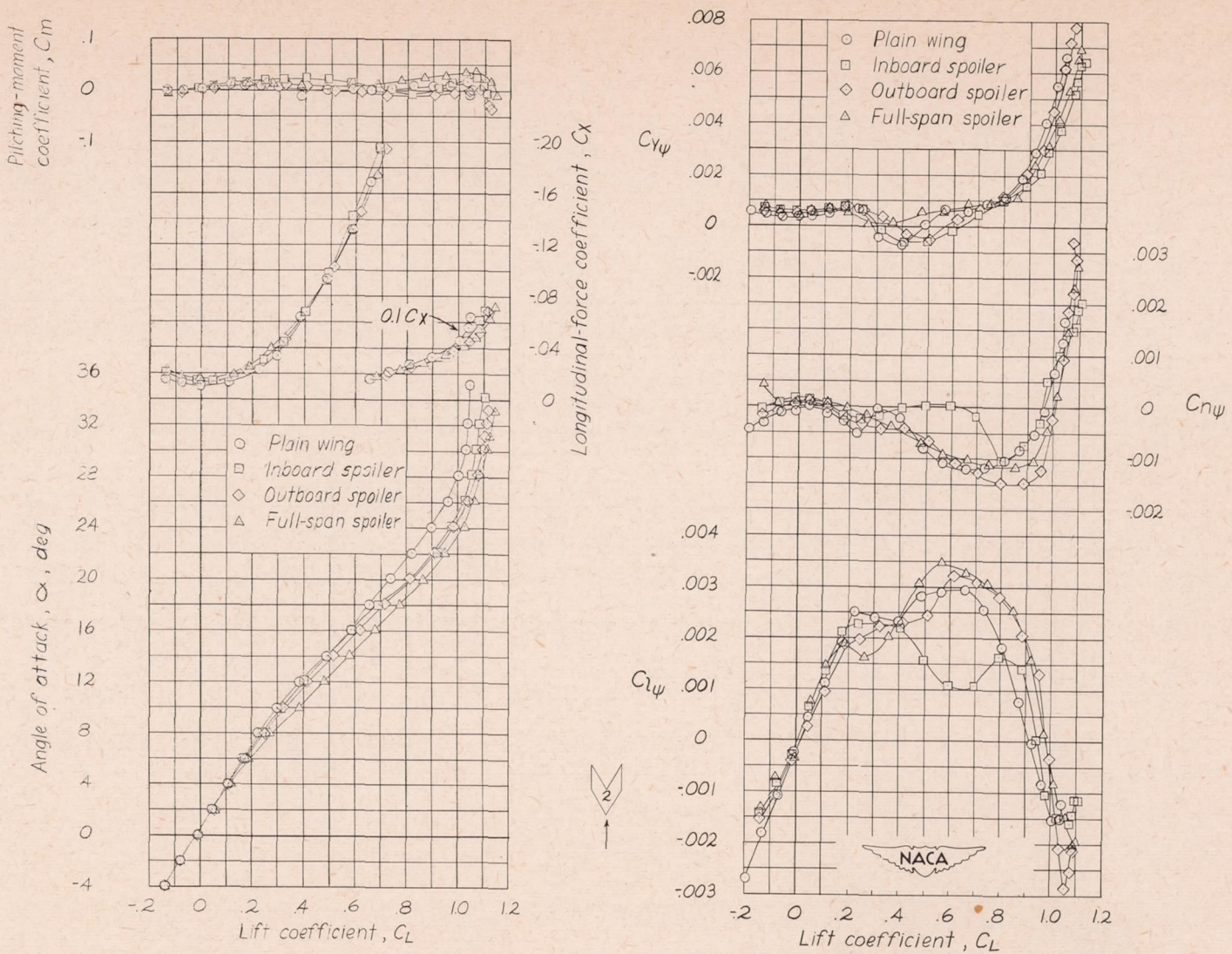

Figure 8.- Aerodynamic characteristics of a sweptback wing. $\Lambda_{c/4} = 60°$; A = 1.5; λ = 1; NACA 0012 airfoil section with 0.025c nose spoilers of various spans; model 2.

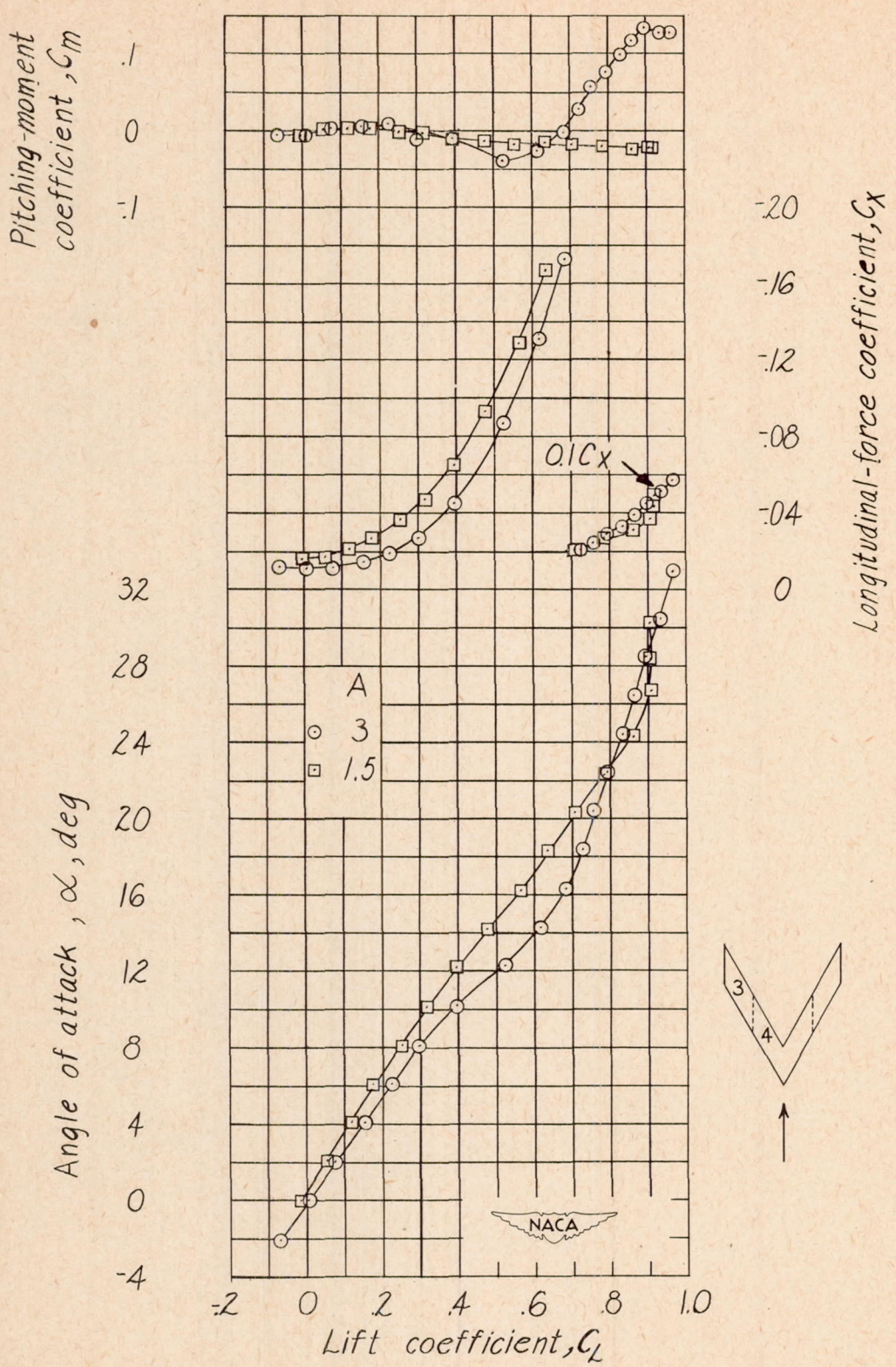

Figure 9.- Aerodynamic characteristics of sweptback wings. $\Lambda_{c/4} = 60°$; A = 3 and 1.5; $\lambda = 1$; NACA 0015 airfoil section; models 3 and 4.

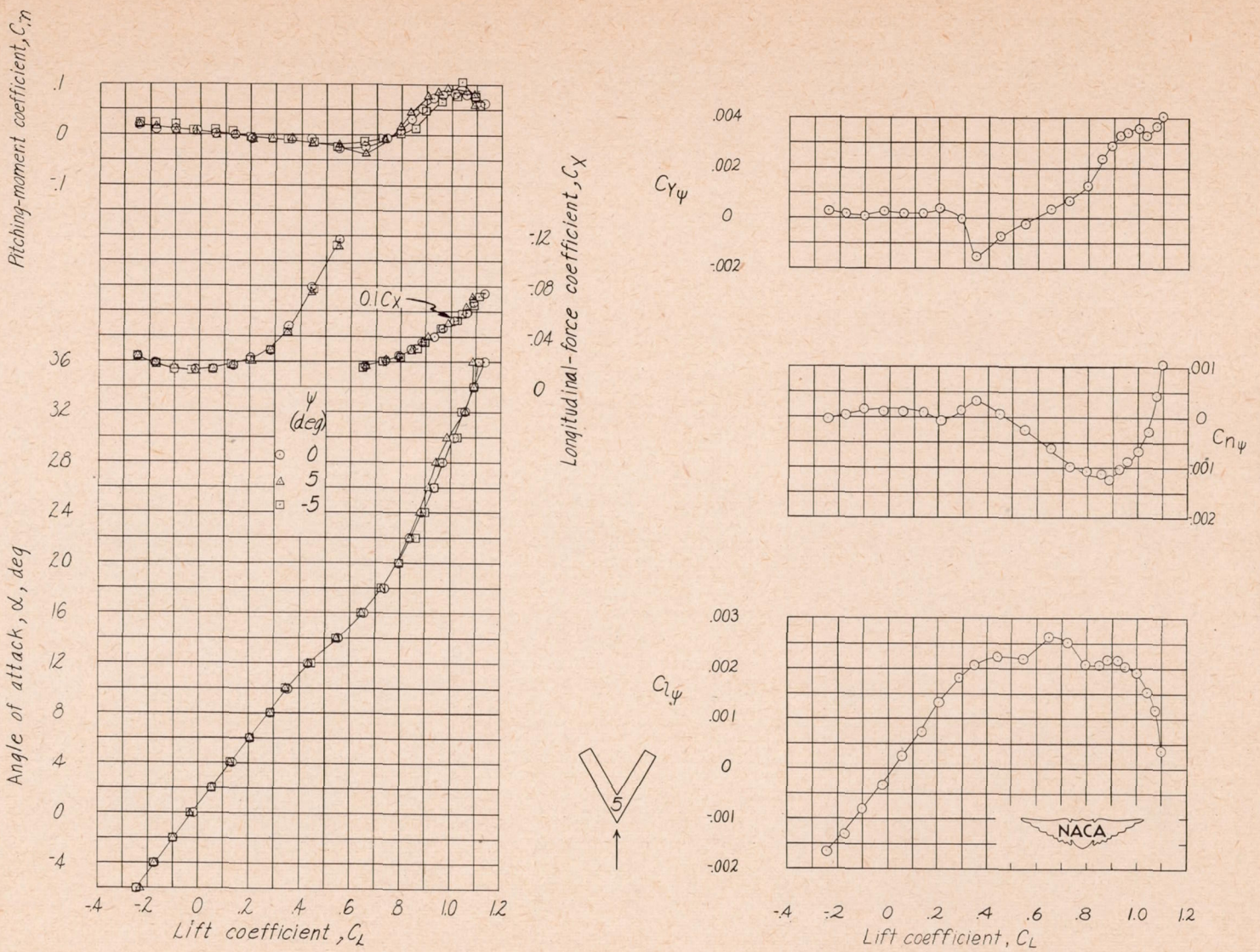

Figure 10.- Aerodynamic characteristics of a sweptback wing. $\Lambda_{c/4} = 60°$; A = 3.1; λ = 1; NACA 0012 airfoil section with tips cut off normal to leading edge; model 5.

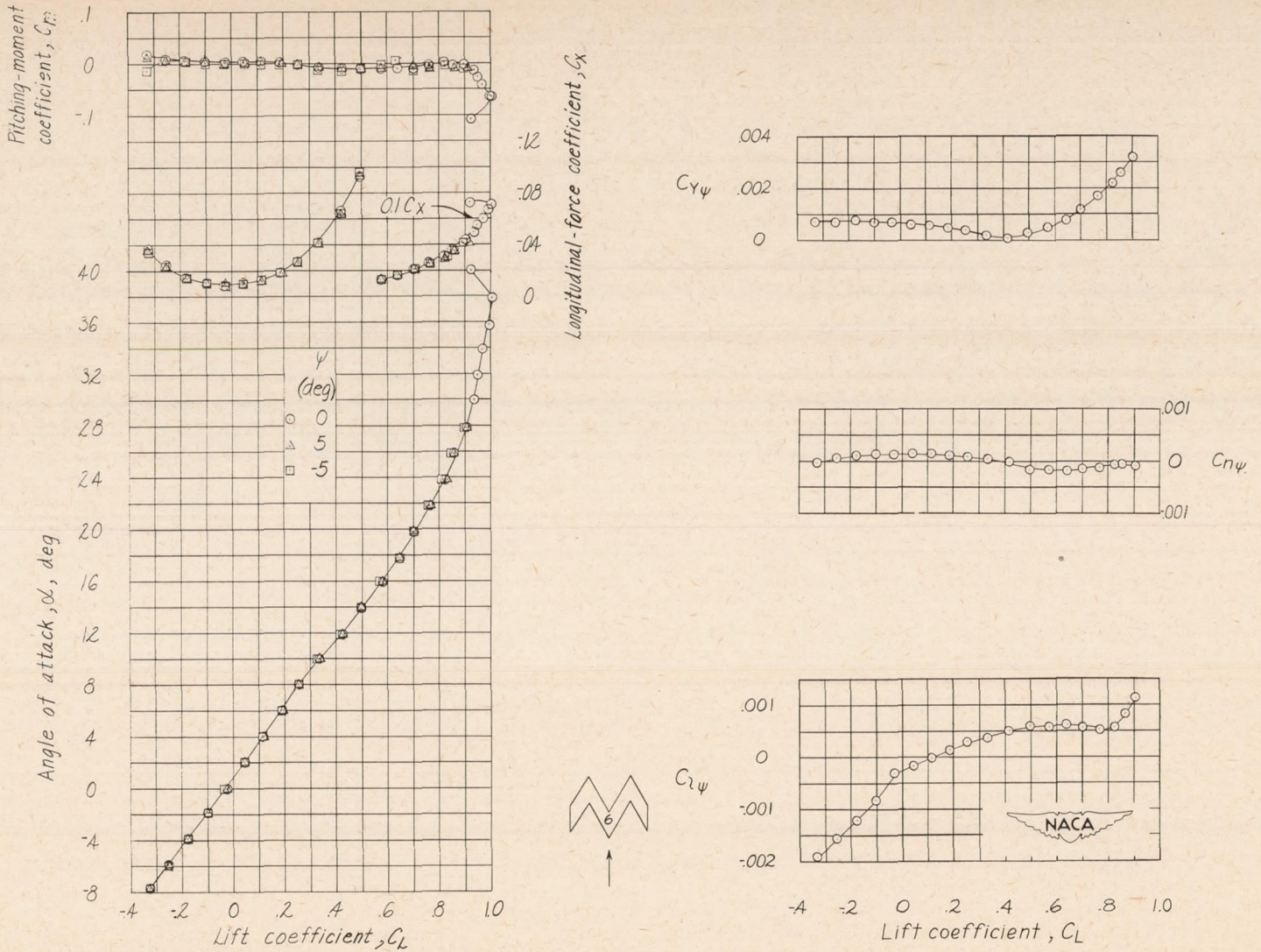

Figure 11.- Aerodynamic characteristics of a swept wing. $\Lambda_{c/4} = \pm 60°$; $A = 2.6$; $\lambda = 1$; inboard $0.6\frac{b}{2}$ swept back 60°; outboard $0.4\frac{b}{2}$ swept forward 60°; NACA 0012 airfoil section; model 6.

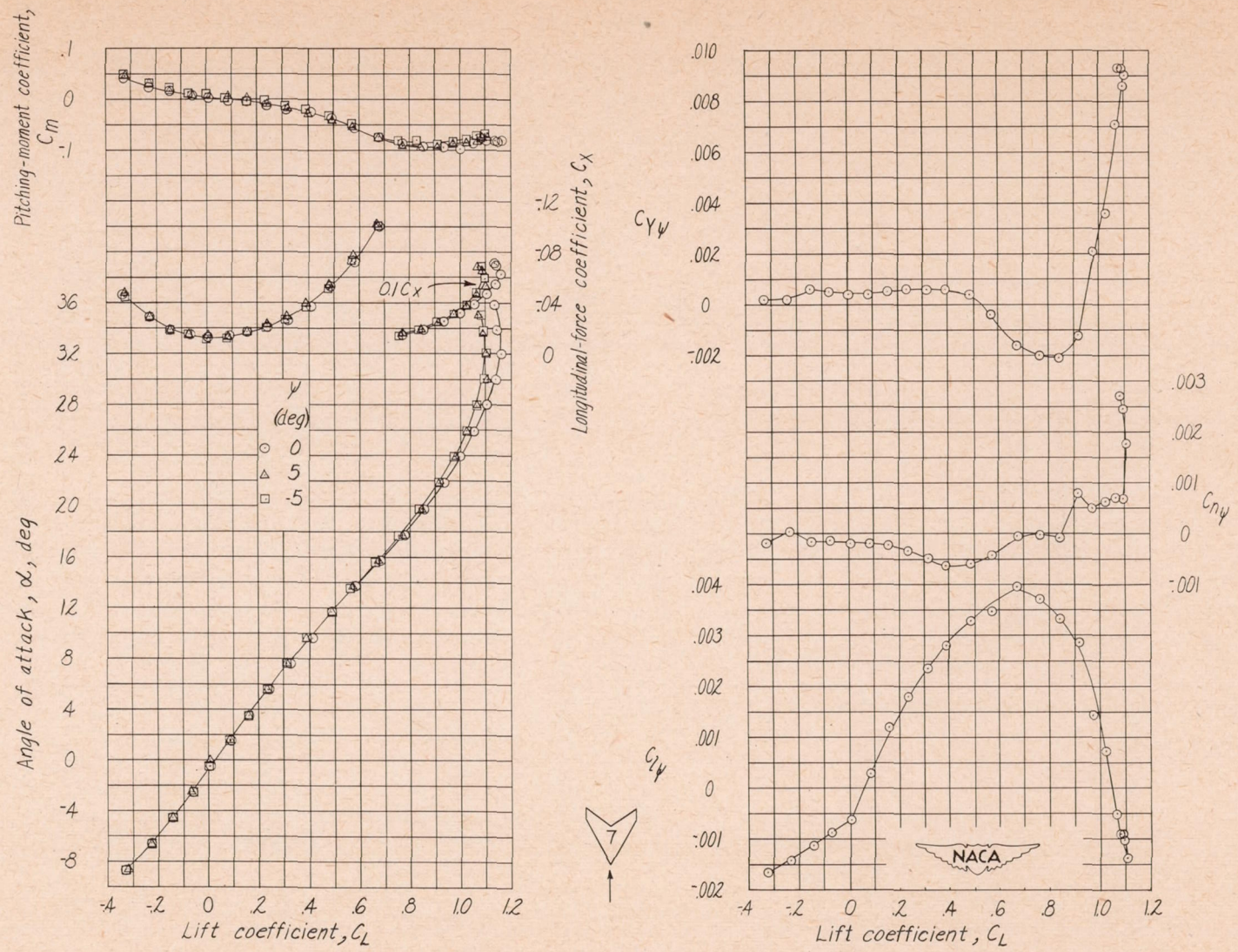

Figure 12.- Aerodynamic characteristics of a sweptback wing. $\Lambda_{c/4} = 56^\circ$; A = 2.1; λ = 2.5; NACA 23012 airfoil section; model 7.

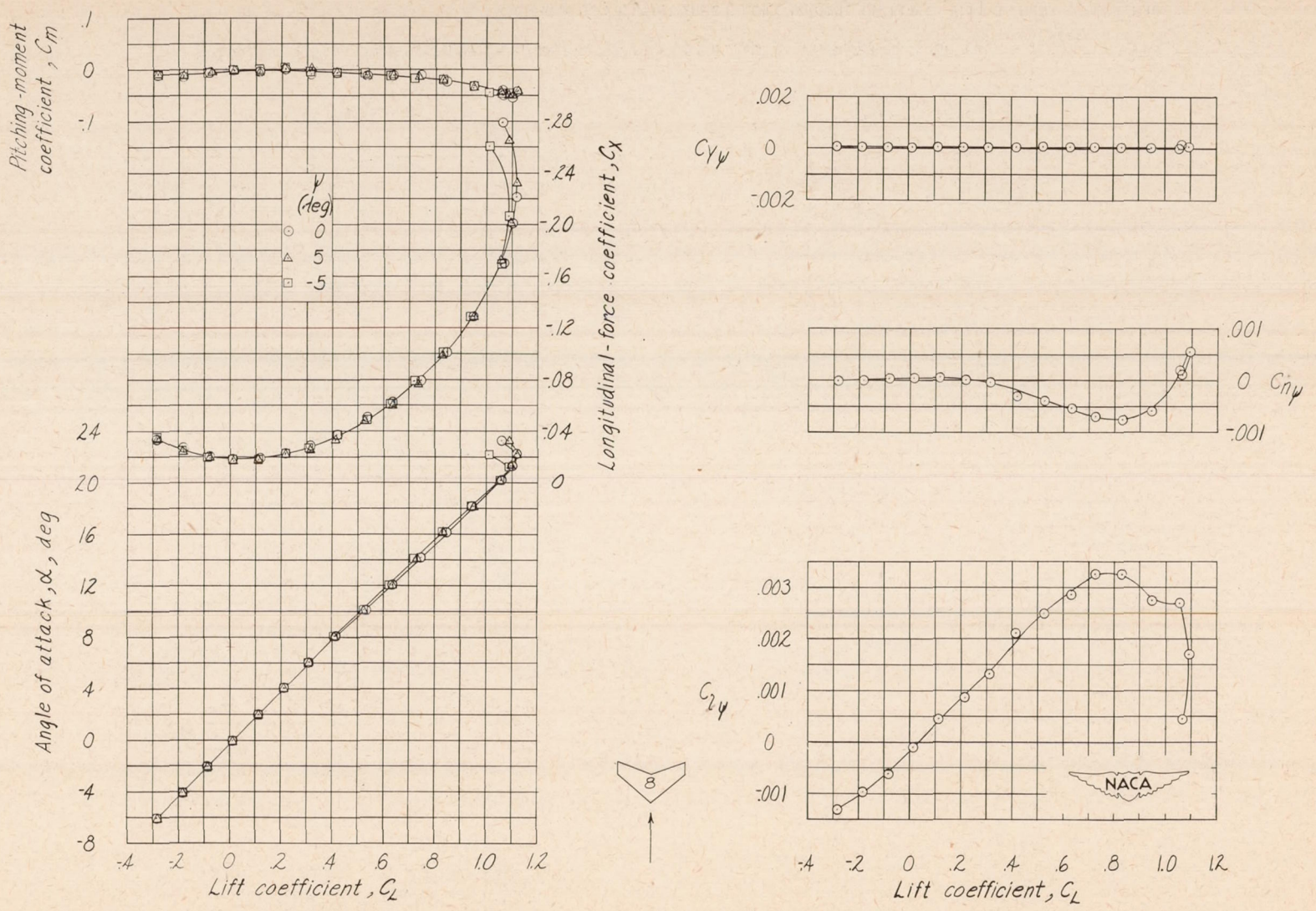

Figure 13.- Aerodynamic characteristics of a sweptback wing. $\Lambda_{c/4} = 37.5°$; A = 3; λ = 2.04; NACA 23012 airfoil section; model 8.

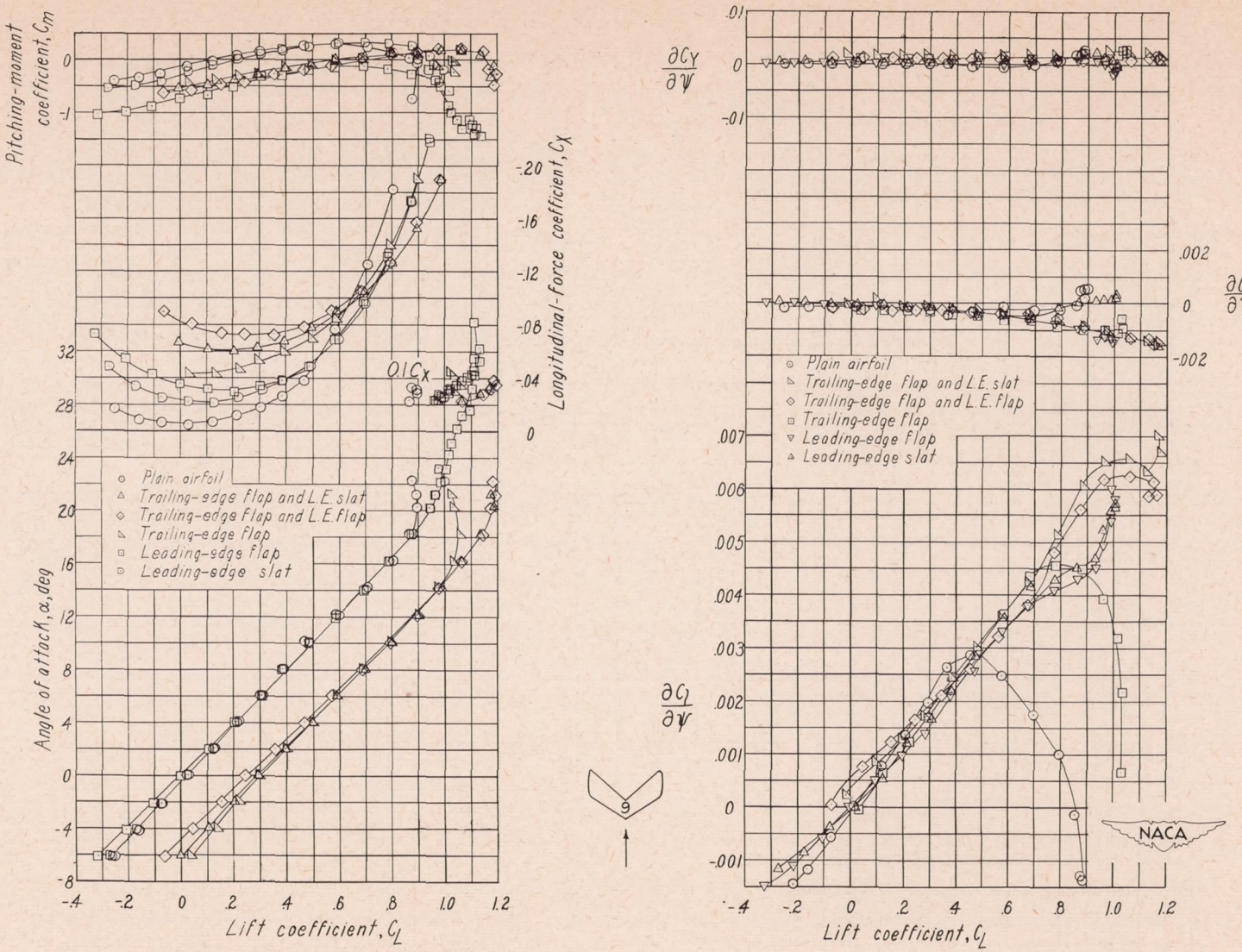

Figure 14.- Aerodynamic characteristics of a sweptback wing. $\Lambda_{c/4} = 37.5^{\circ}$; A = 3; $\lambda = 0.617$; low-drag-type section with faired tips and various high-lift devices; model 9.

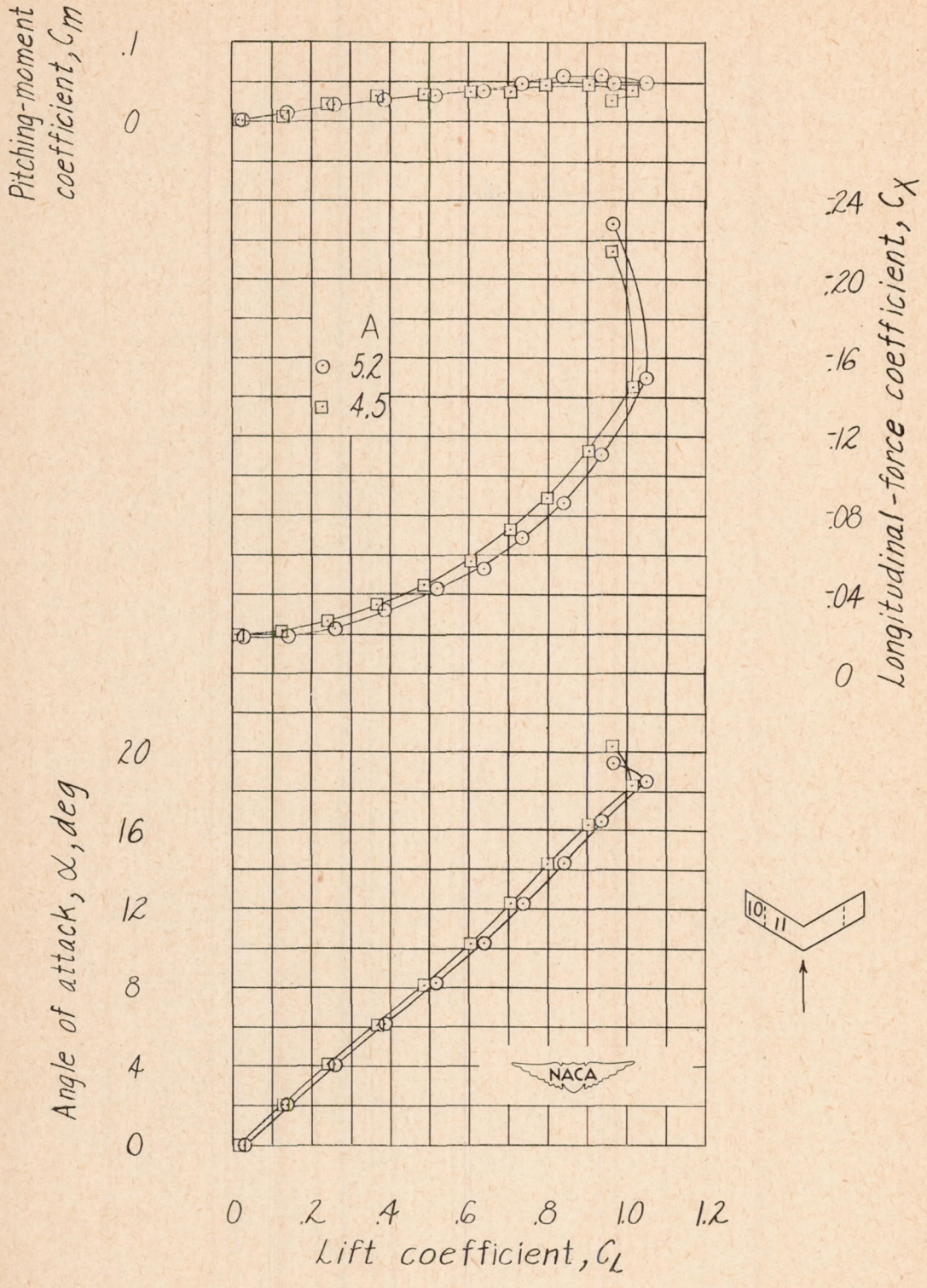

Figure 15.- Aerodynamic characteristics of sweptback wings. $\Lambda_{c/4} = 30^\circ$; A = 5.2 and 4.5; $\lambda = 1$; NACA 0015 airfoil section; models 10 and 11.

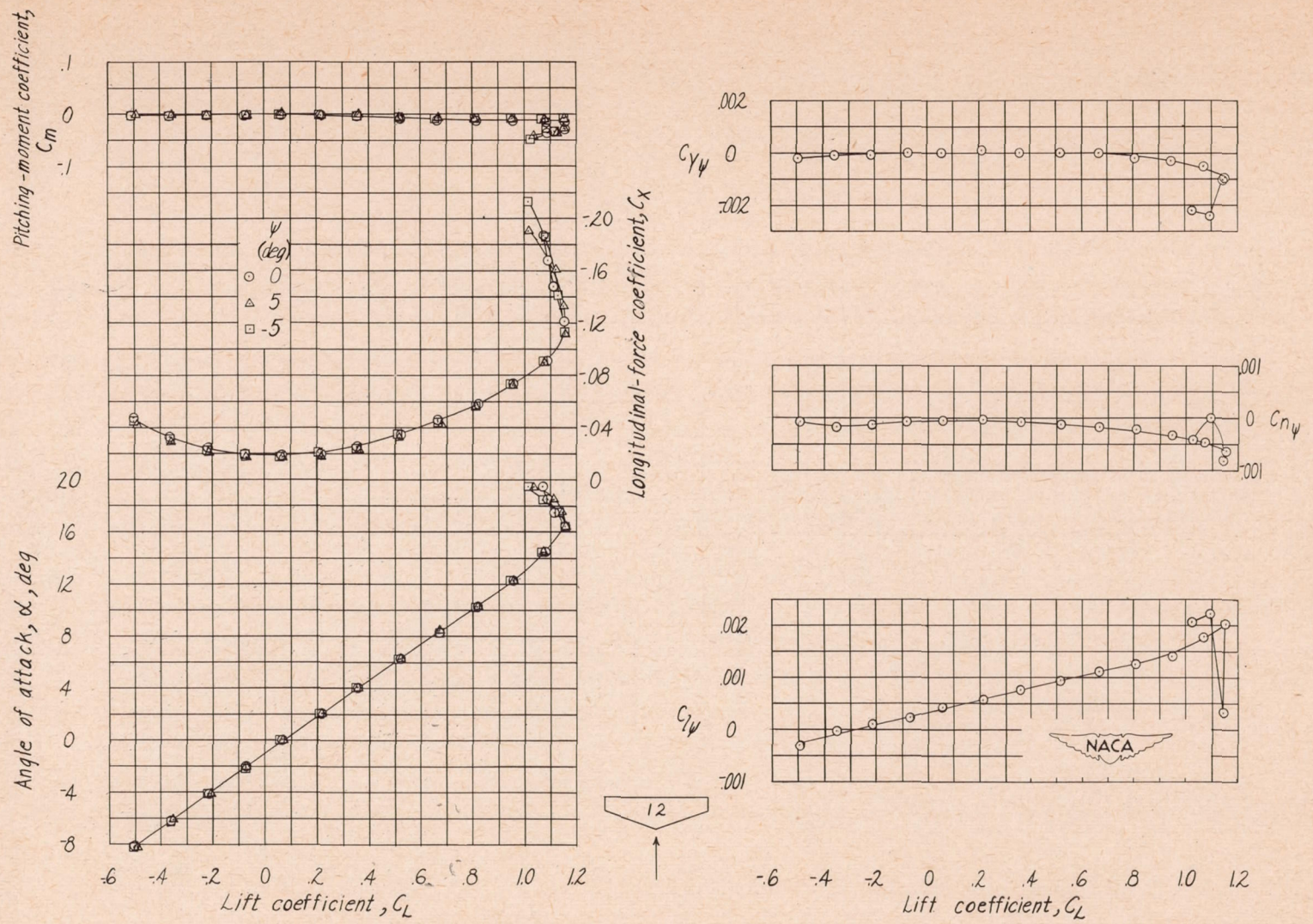

Figure 16.- Aerodynamic characteritics of a sweptback wing. $\Lambda_{c/4} = 14^\circ$; $A = 6$; $\lambda = 3$; NACA 23012 airfoil section; model 12.

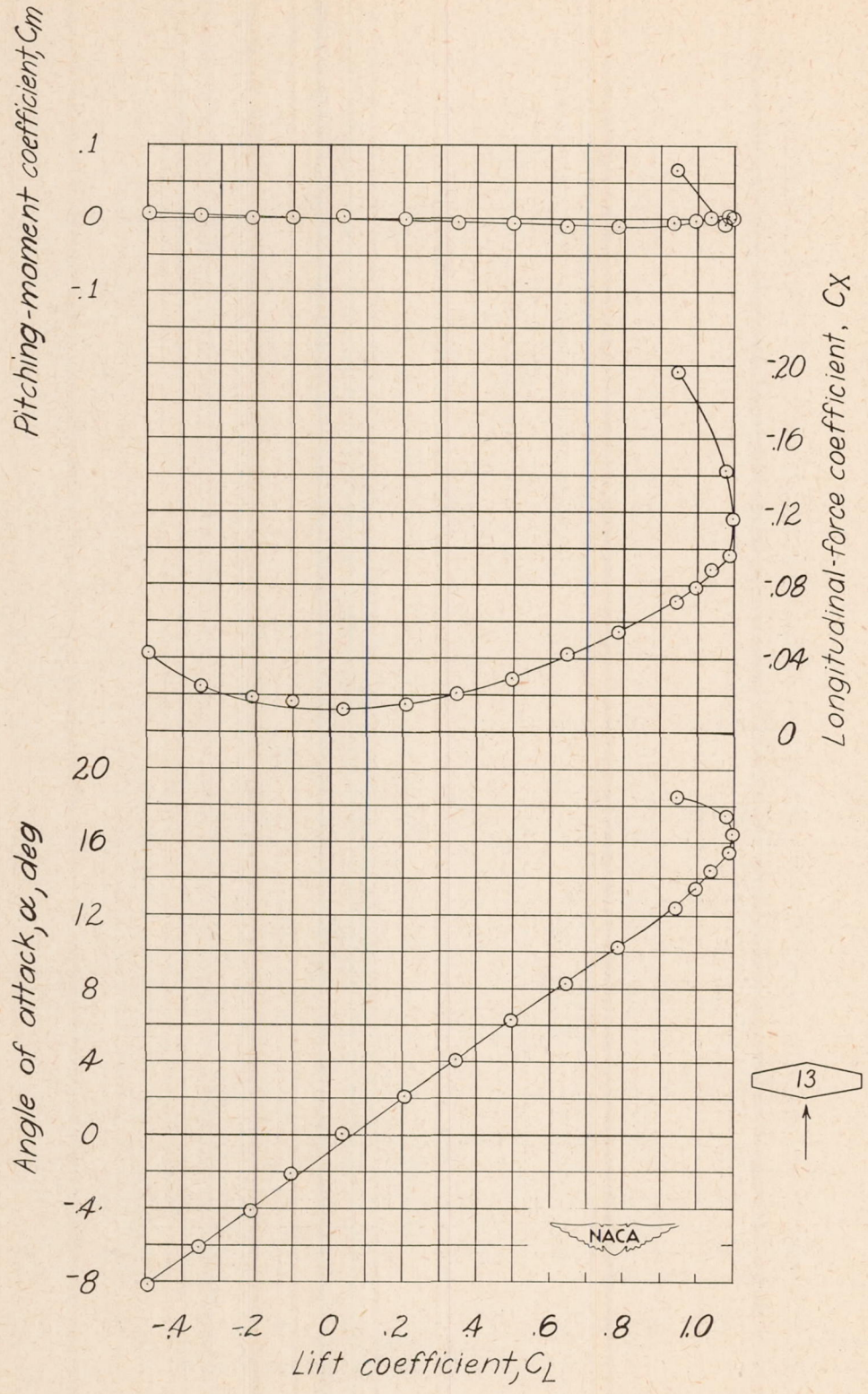

Figure 17.- Aerodynamic characteristics of a sweptback wing. $\Lambda_{c/4} = 6^{\circ}$; A = 6; $\lambda = 5$; NACA 23012 airfoil section; model 13.

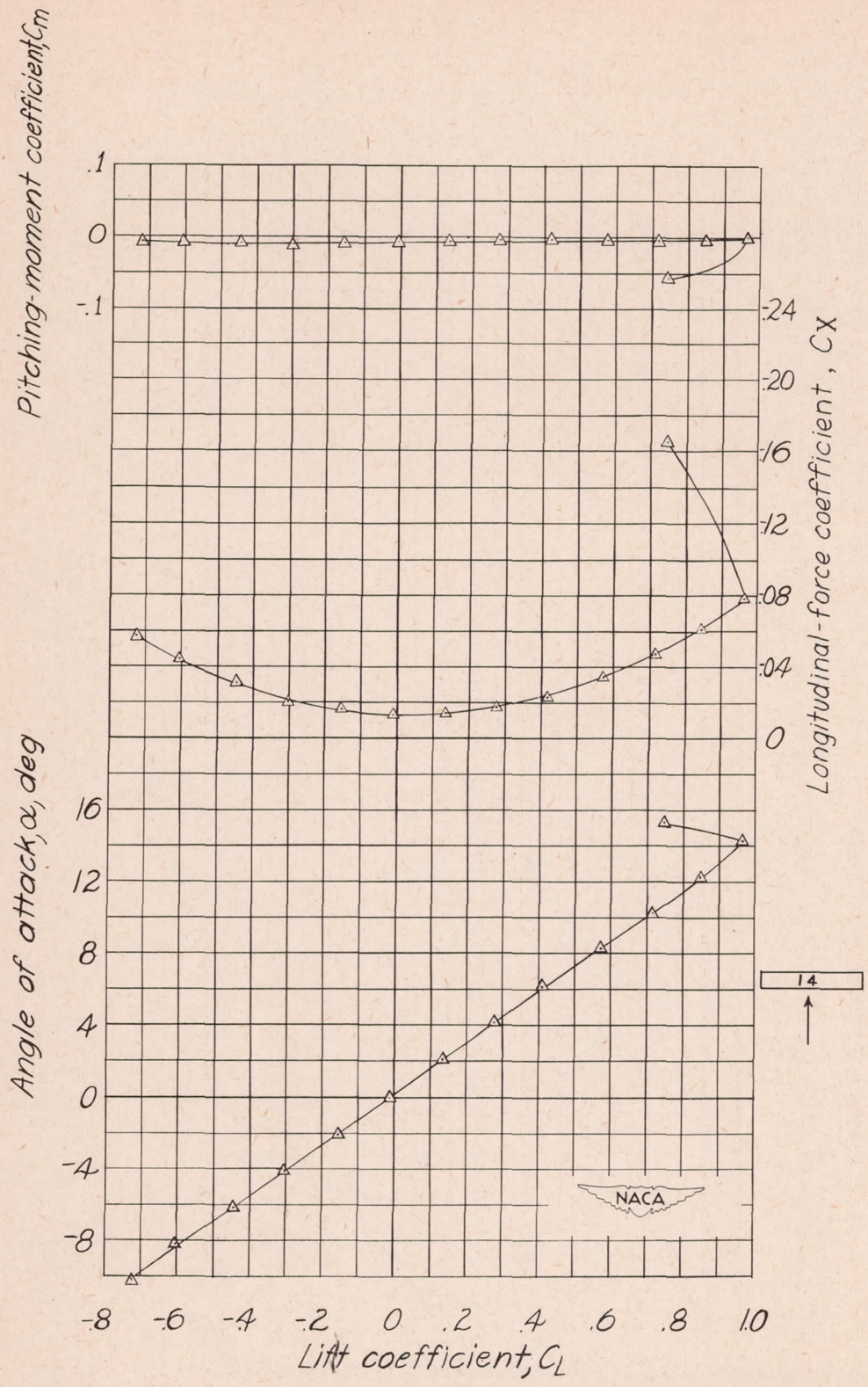

Figure 18.- Aerodynamic characteristics of an unswept wing. $\Lambda_{c/4} = 0^\circ$; $A = 6$; $\lambda = 1$; NACA 0012 airfoil section; model 14.

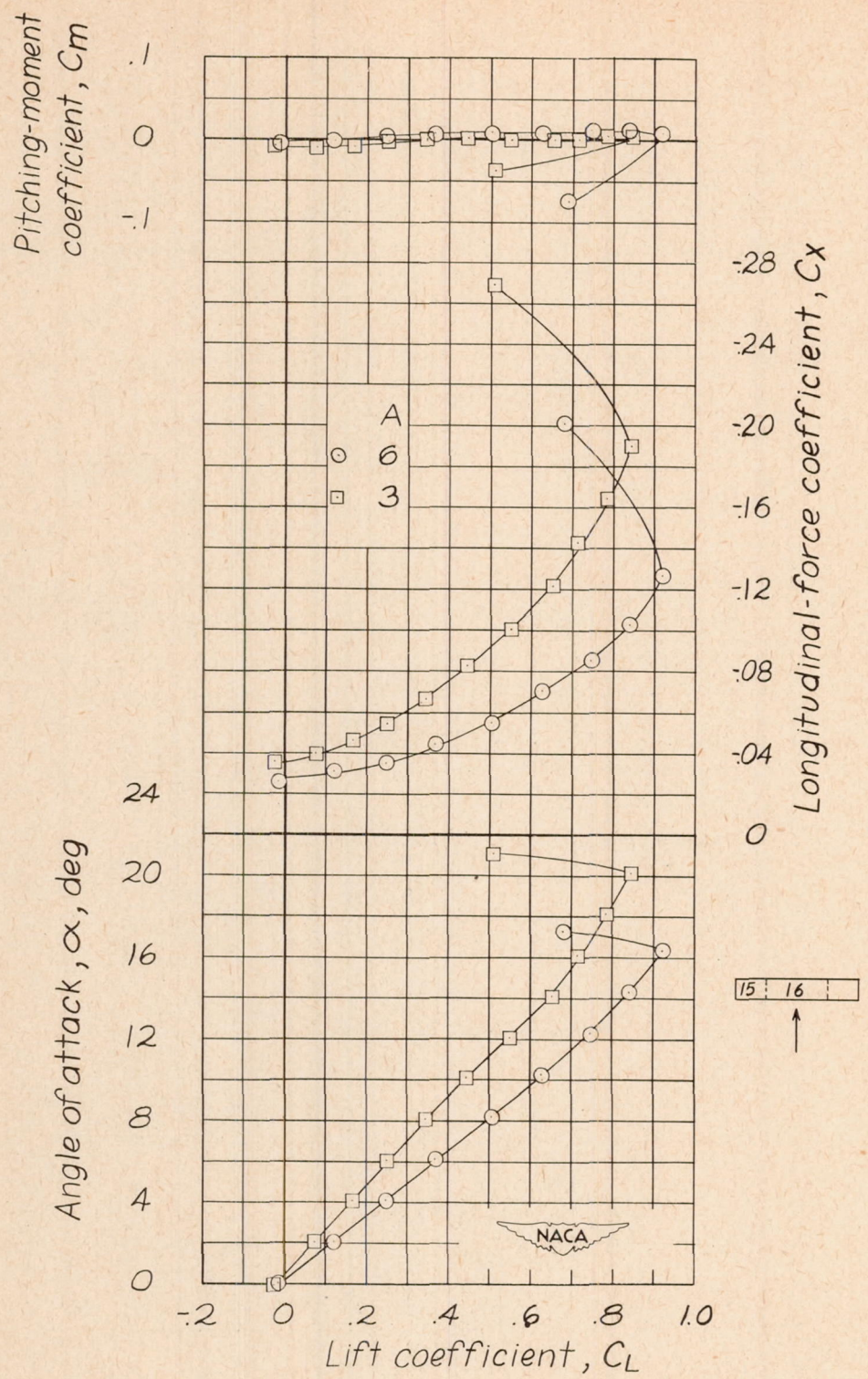

Figure 19.- Aerodynamic characteristics of unswept wings. $A_{c/4} = 0^{\circ}$; A = 6 and 3; $\lambda = 1$; NACA 0015 airfoil section; models 15 and 16.

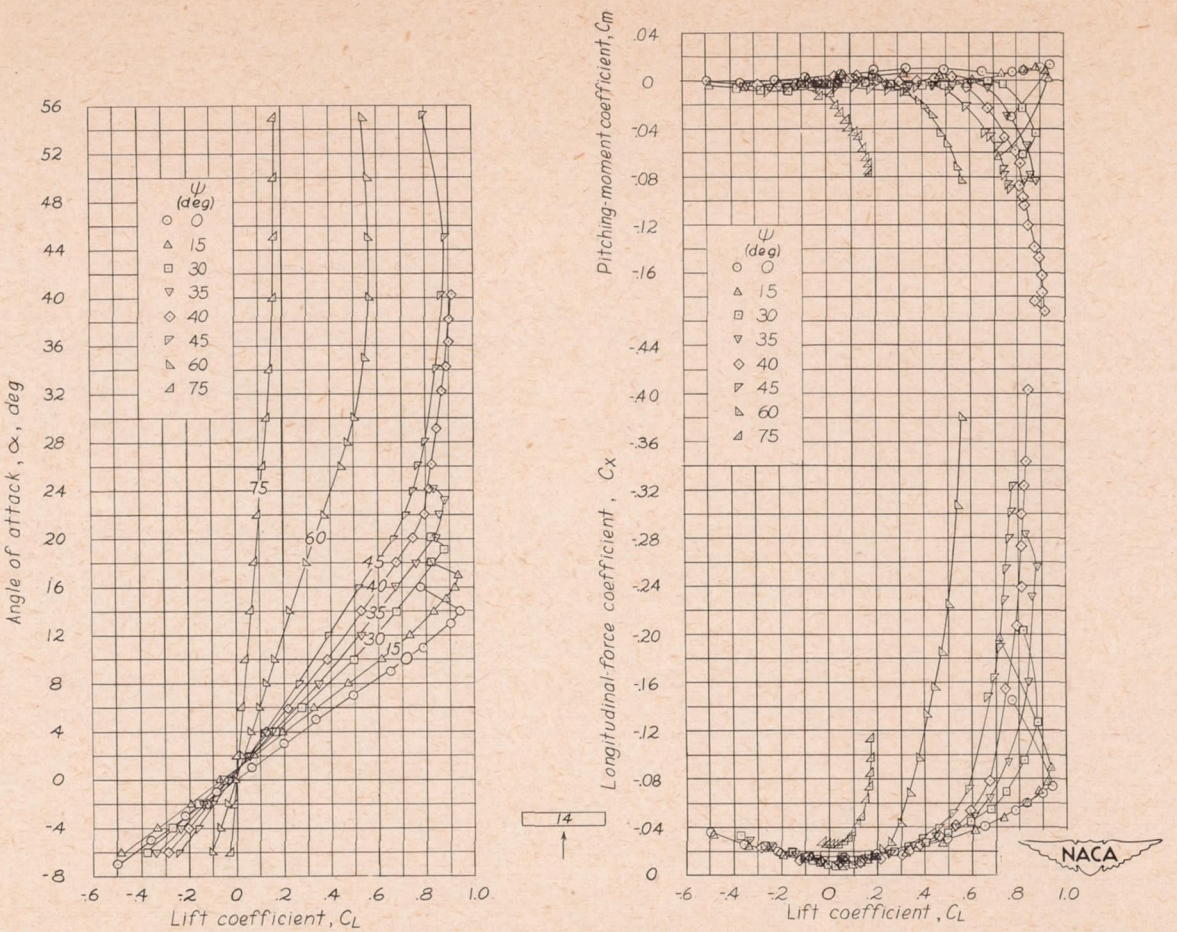

(a) Stability axes.

Figure 20.- Aerodynamic characteristics of an unswept wing at various angles of yaw. $\Lambda_{c/4} = 0^{\circ}$; $A = 6$; $\lambda = 1$; NACA 0012 airfoil section; model 14.

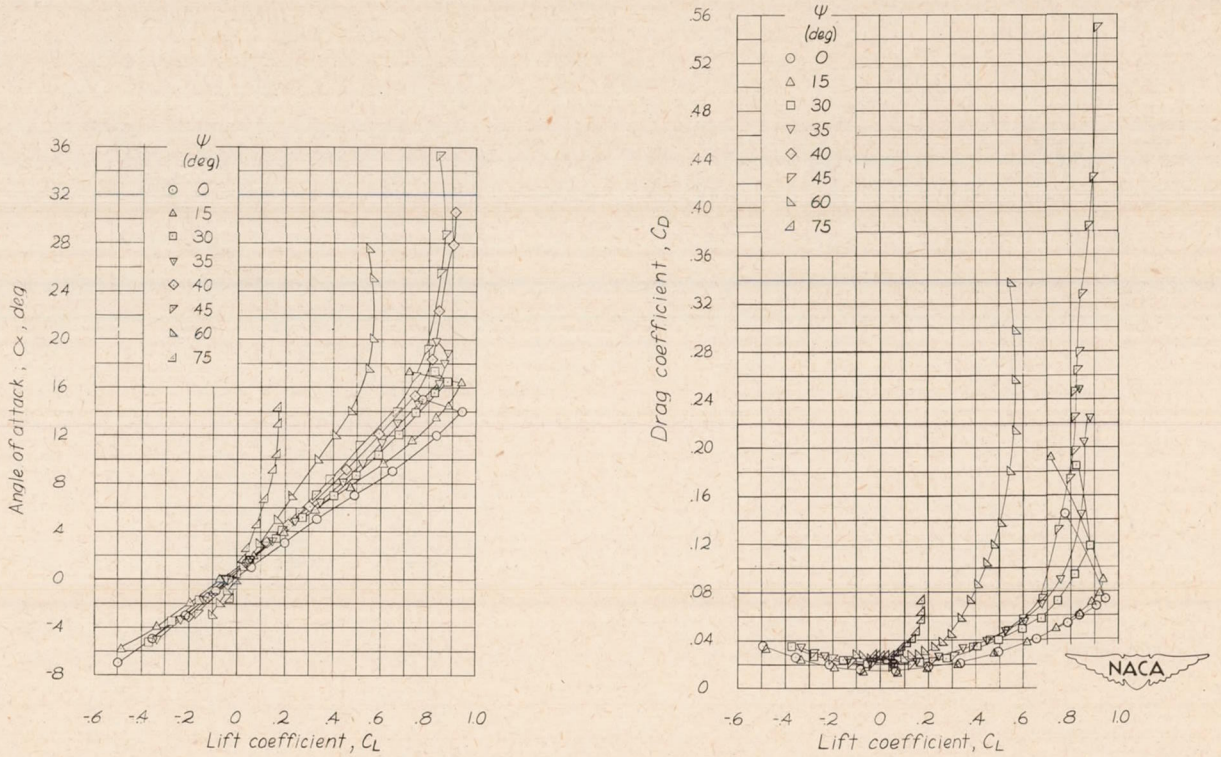

(b) Wind axes.

Figure 20.- Concluded.

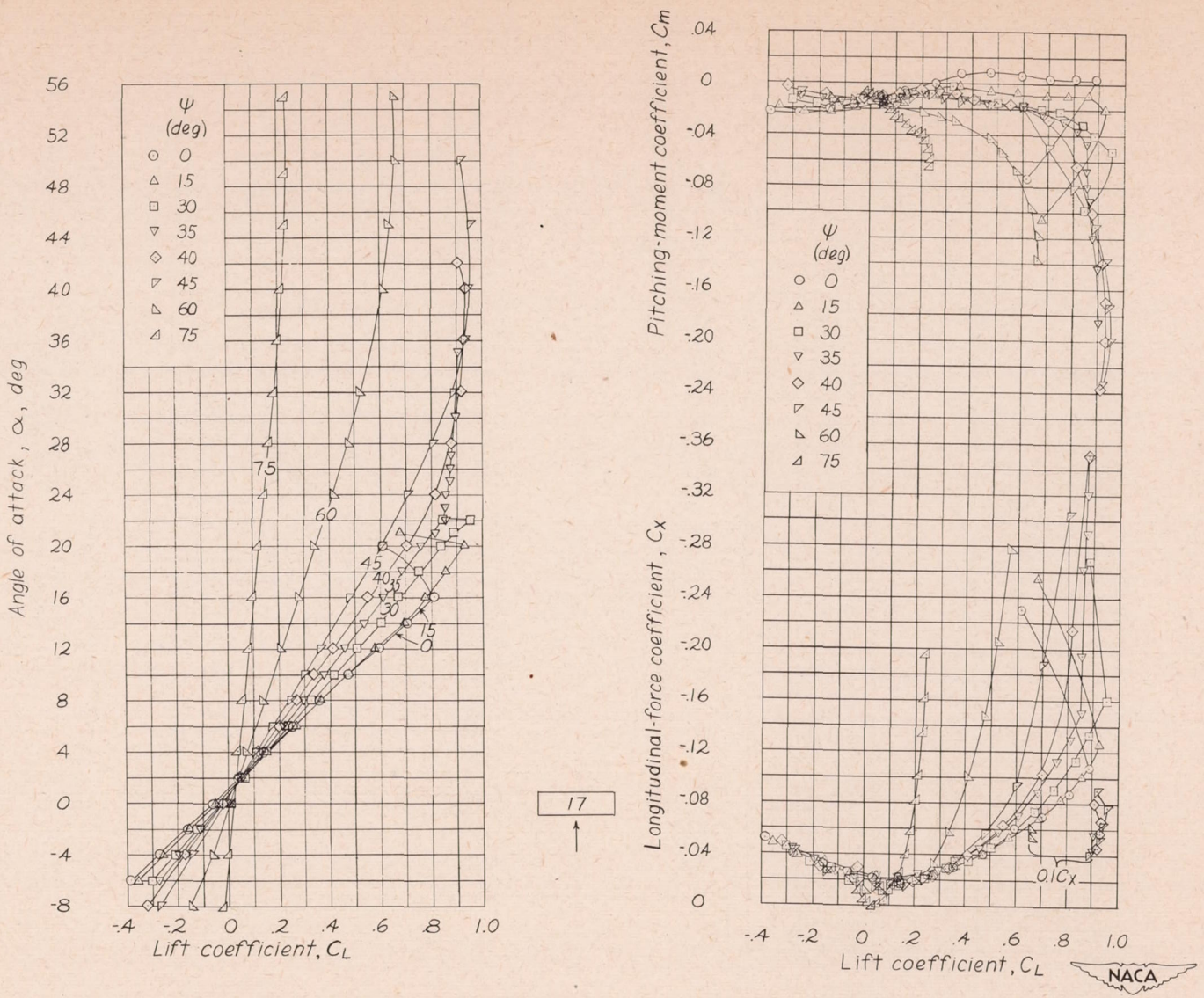

(a) Stability axes.

Figure 21.- Aerodynamic characteristics of an unswept wing at various angles of yaw. $\Lambda_{c/4} = 0^{\circ}$; A = 3; λ = 1; NACA 0012 airfoil section; model 17.

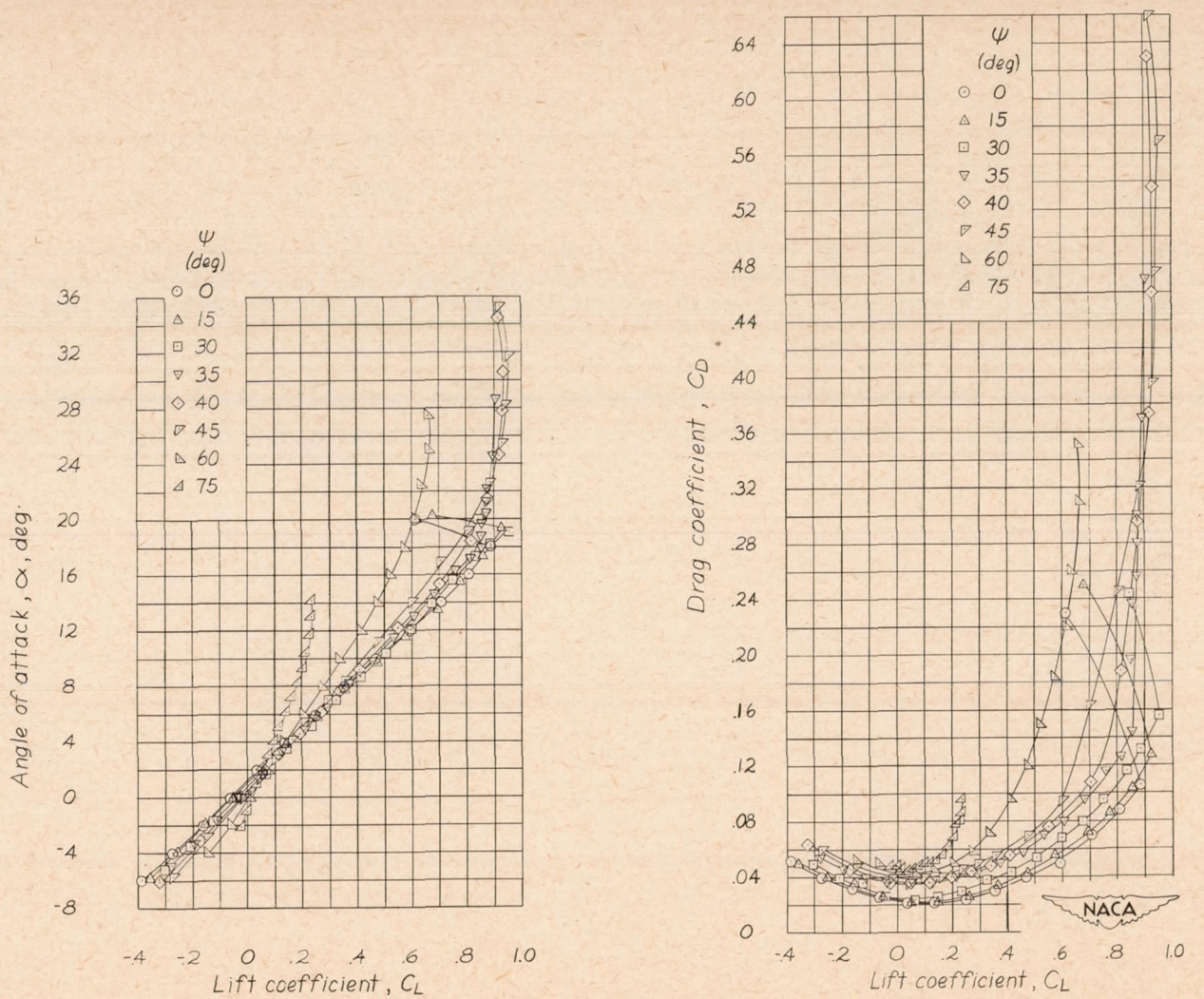

(b) Wind axes.

Figure 21.- Concluded.

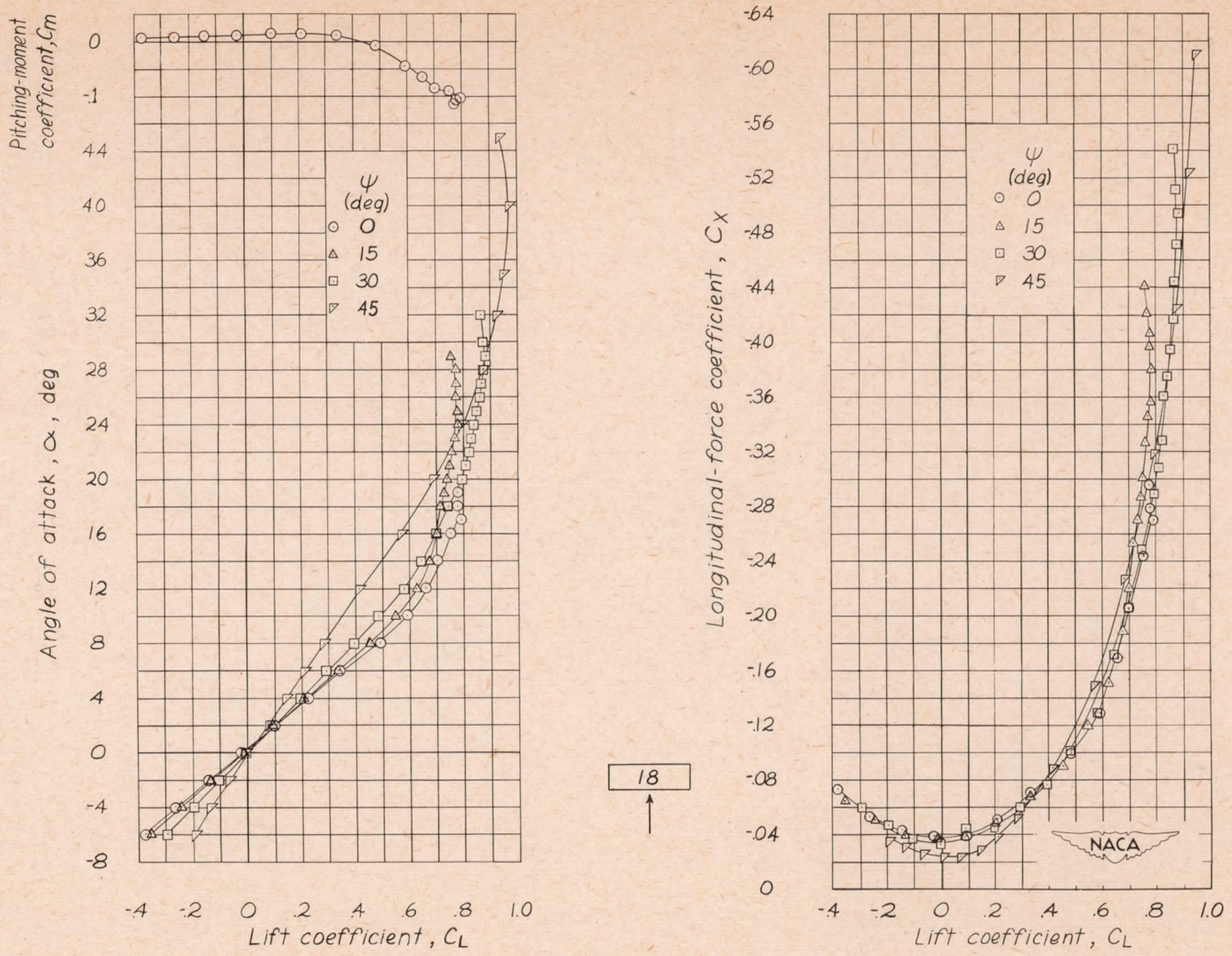

(a) Stability axes.

Figure 22.- Aerodynamic characteristics of an unswept wing at various angles of yaw. $\Lambda_{c/4} = 0^{\circ}$; A = 3; λ = 1; flat-plate section; model 18.

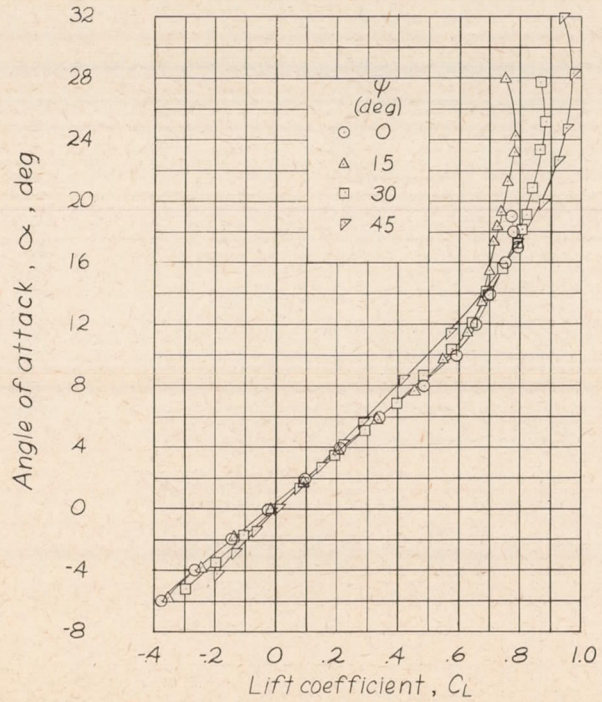

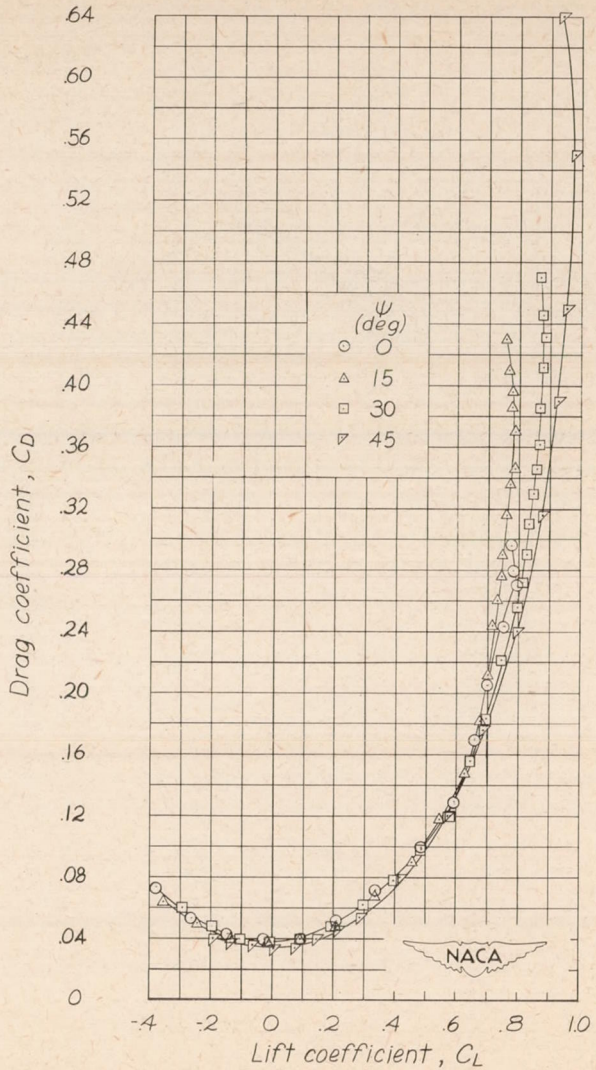

(b) Wind axes.

Figure 22.- Concluded.

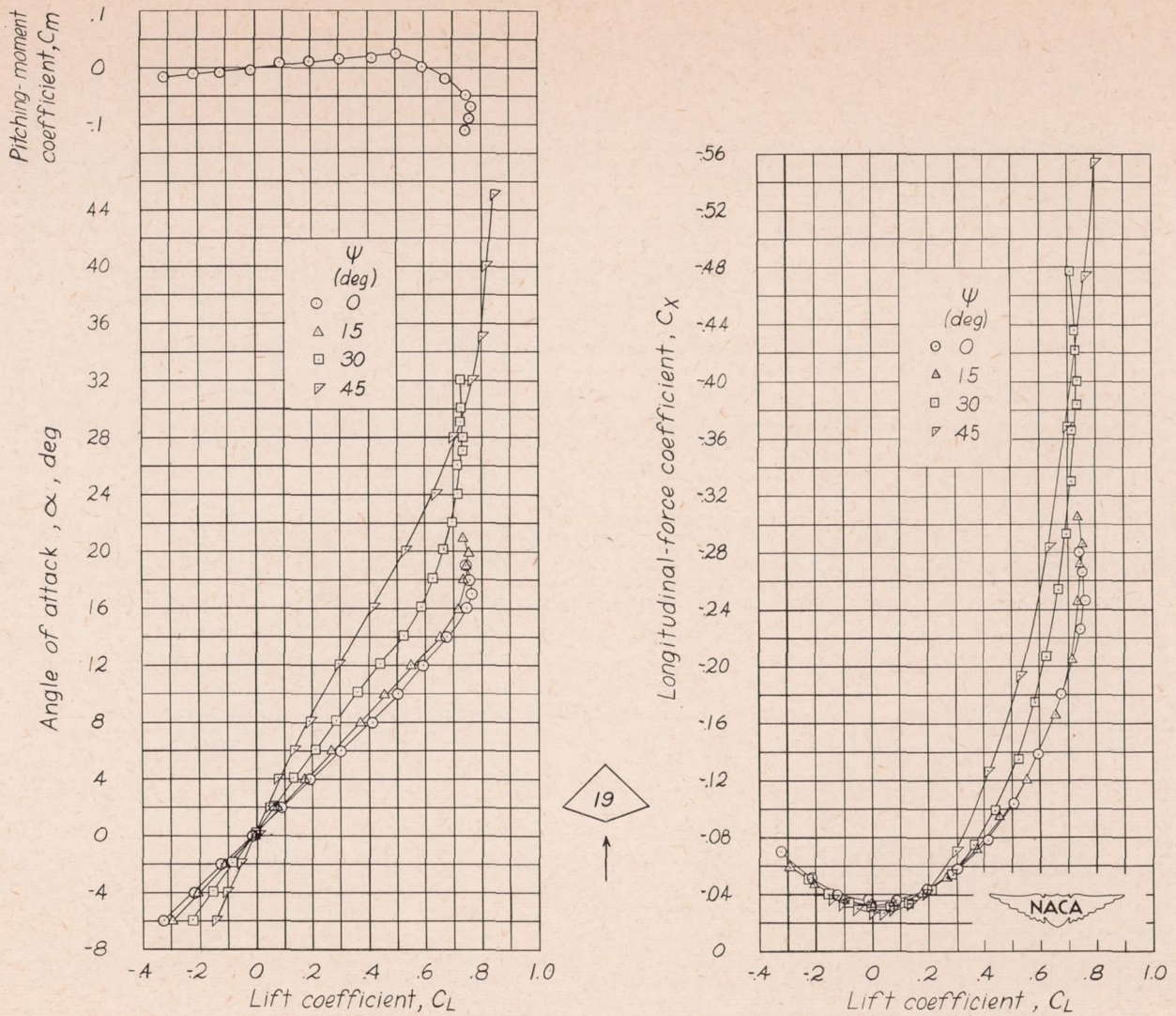

(a) Stability axes.

Figure 23.- Aerodynamic characteristics of an unswept wing at various angles yaw. $\Lambda_{c/4} = 0^\circ$; $A = 3$; $\lambda = \infty$; flat-plate section; model 19.

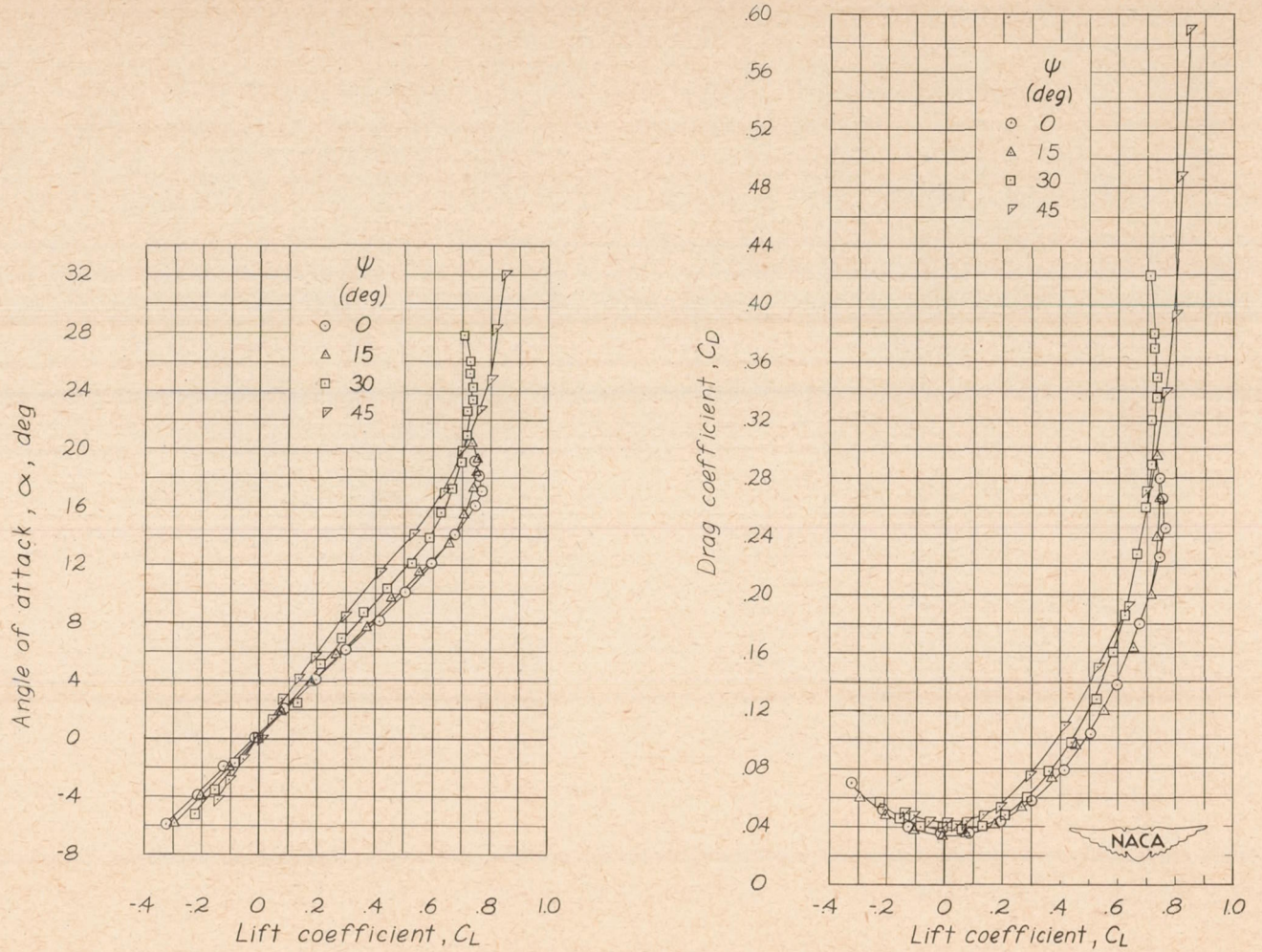

(b) Wind axes.

Figure 23.- Concluded.

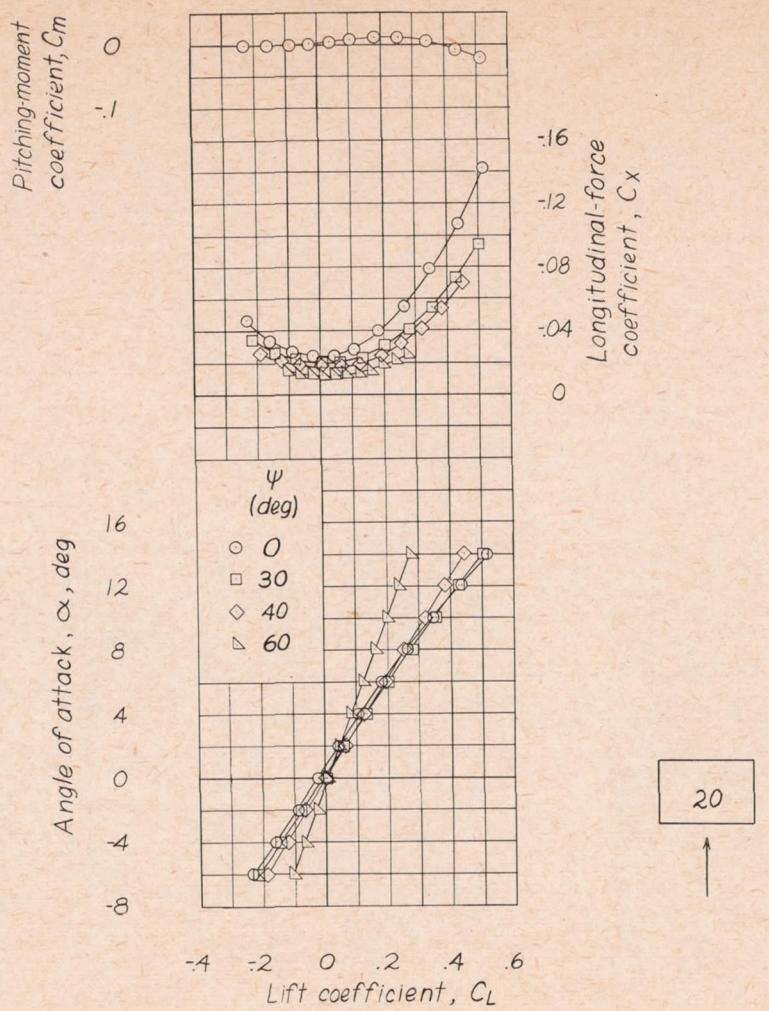

(a) Stability axes.

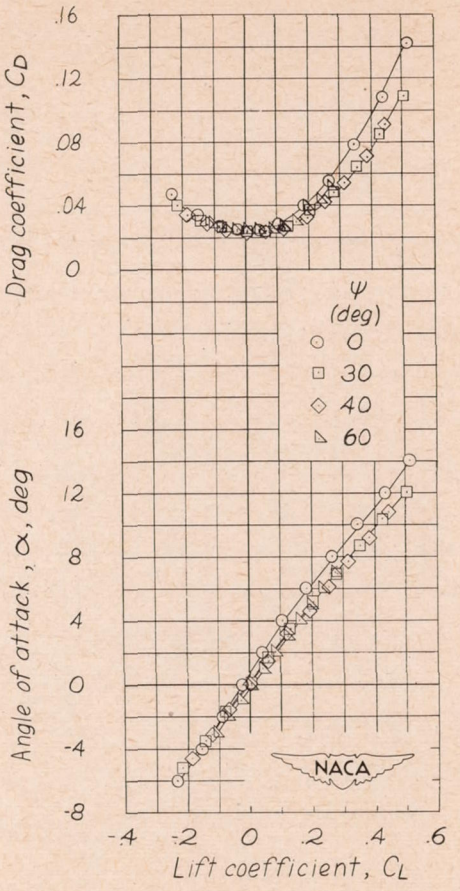

(b) Wind axes.

Figure 24.- Aerodynamic characteristics of an unswept wing at various angles of yaw. $\Lambda_{c/4} = 0^\circ$; A = 1.27; λ = 1; flat-plate section; model 20.

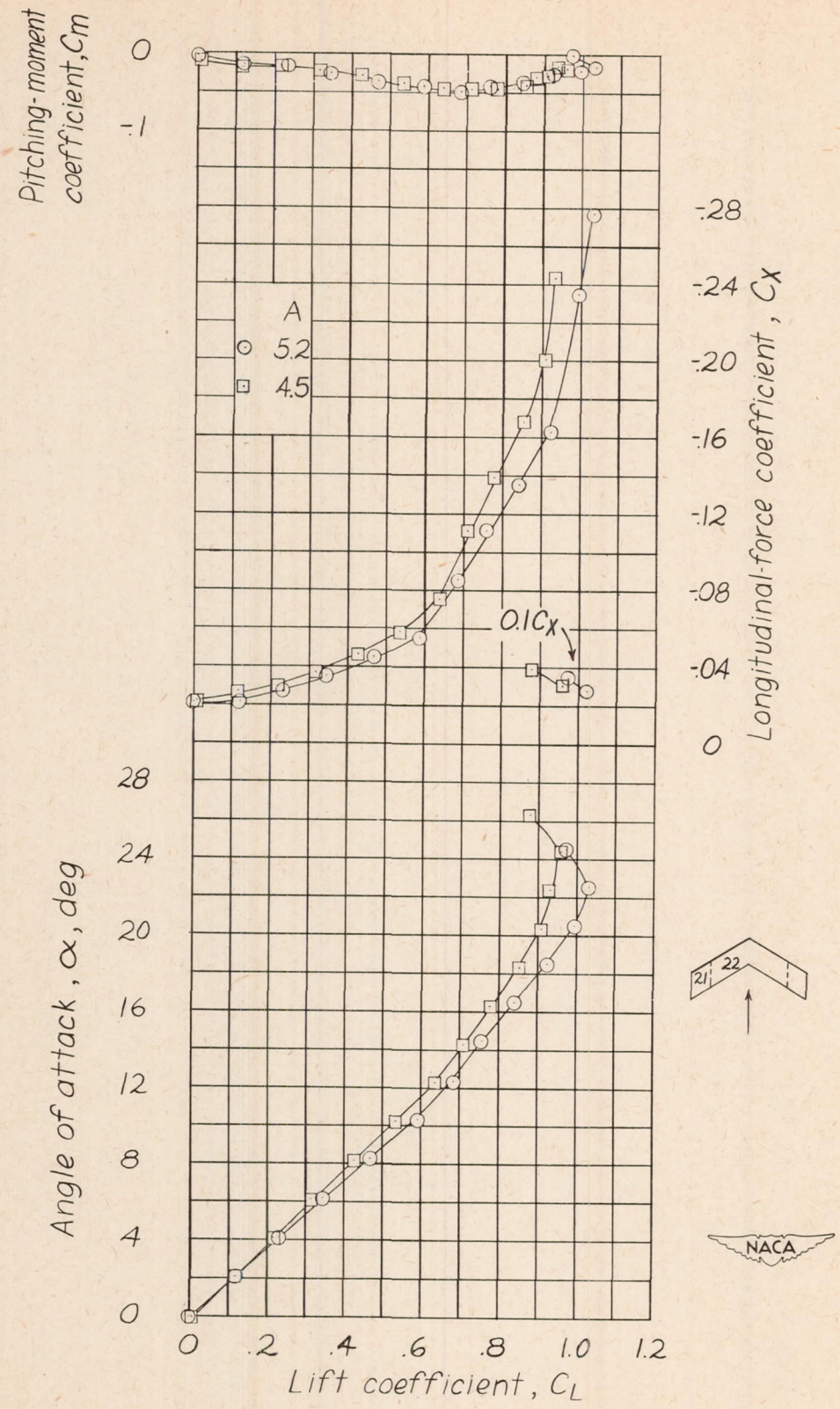

Figure 25.- Aerodynamic characteristics of sweptforward wings. $\Lambda_{c/4} = -30°$; A = 5.2 and 4.5; $\lambda = 1$; NACA 0015 airfoil section; models 21 and 22.

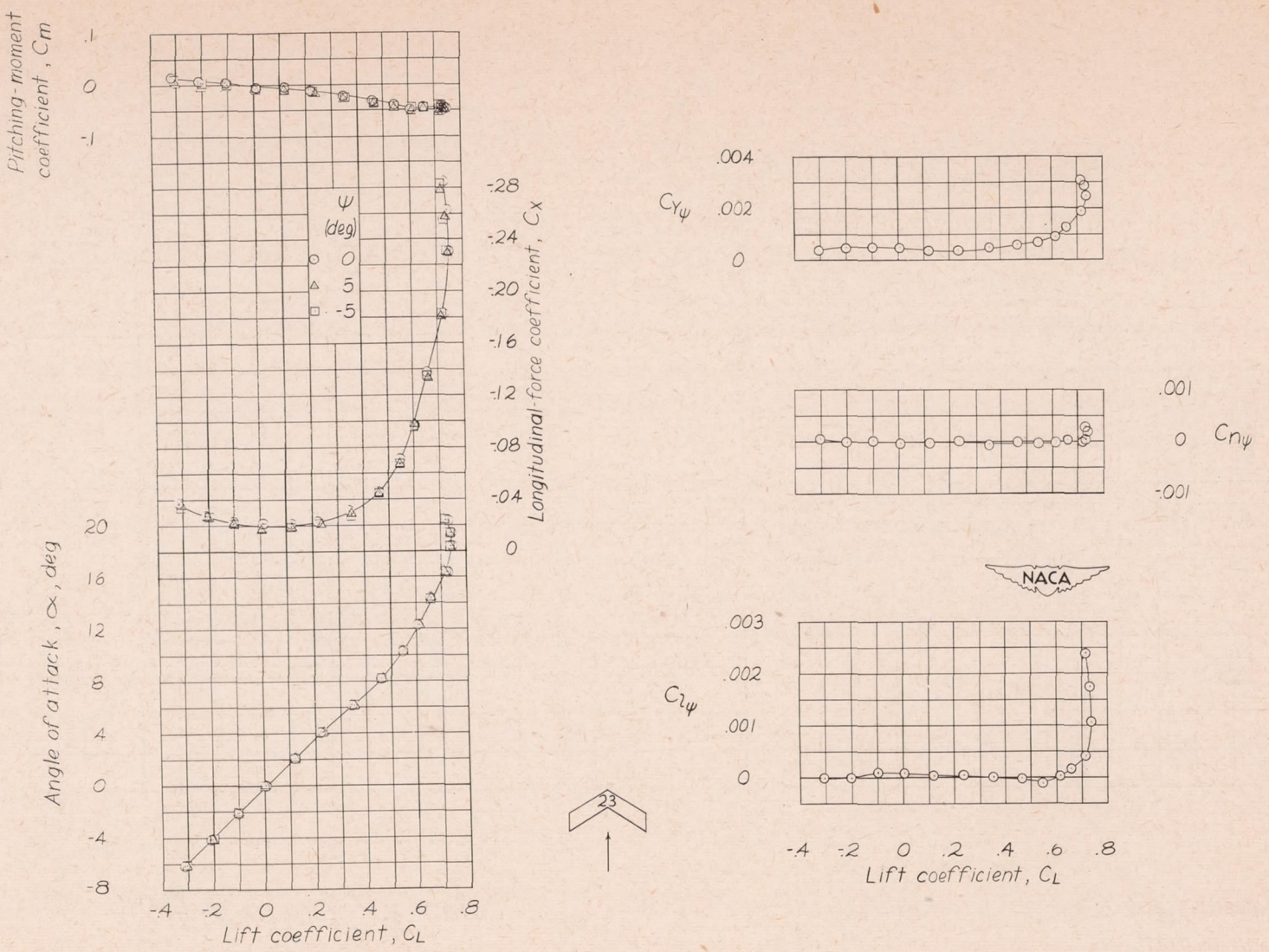

Figure 26.- Aerodynamic characteristics of a sweptforward wing. $\Lambda_{c/4} = -30^{\circ}$; A = 3.6; λ = 1; NACA 0012 airfoil section; model 23.

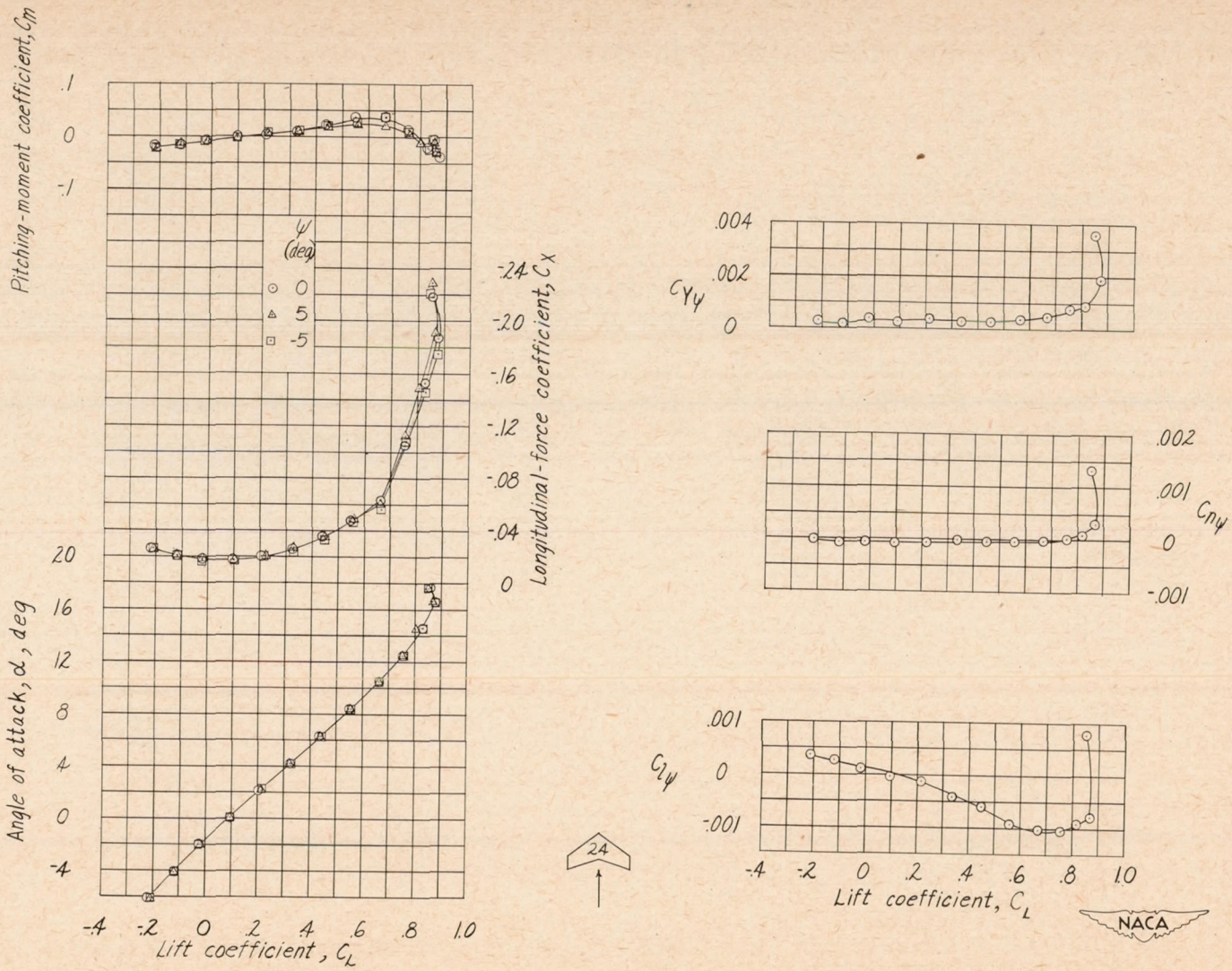

Figure 27.- Aerodynamic characteristics of a sweptforward wing. $\Lambda_{c/4} = -30^\circ$; A = 3.6; λ = 2.85; NACA 23012 airfoil section; model 24.

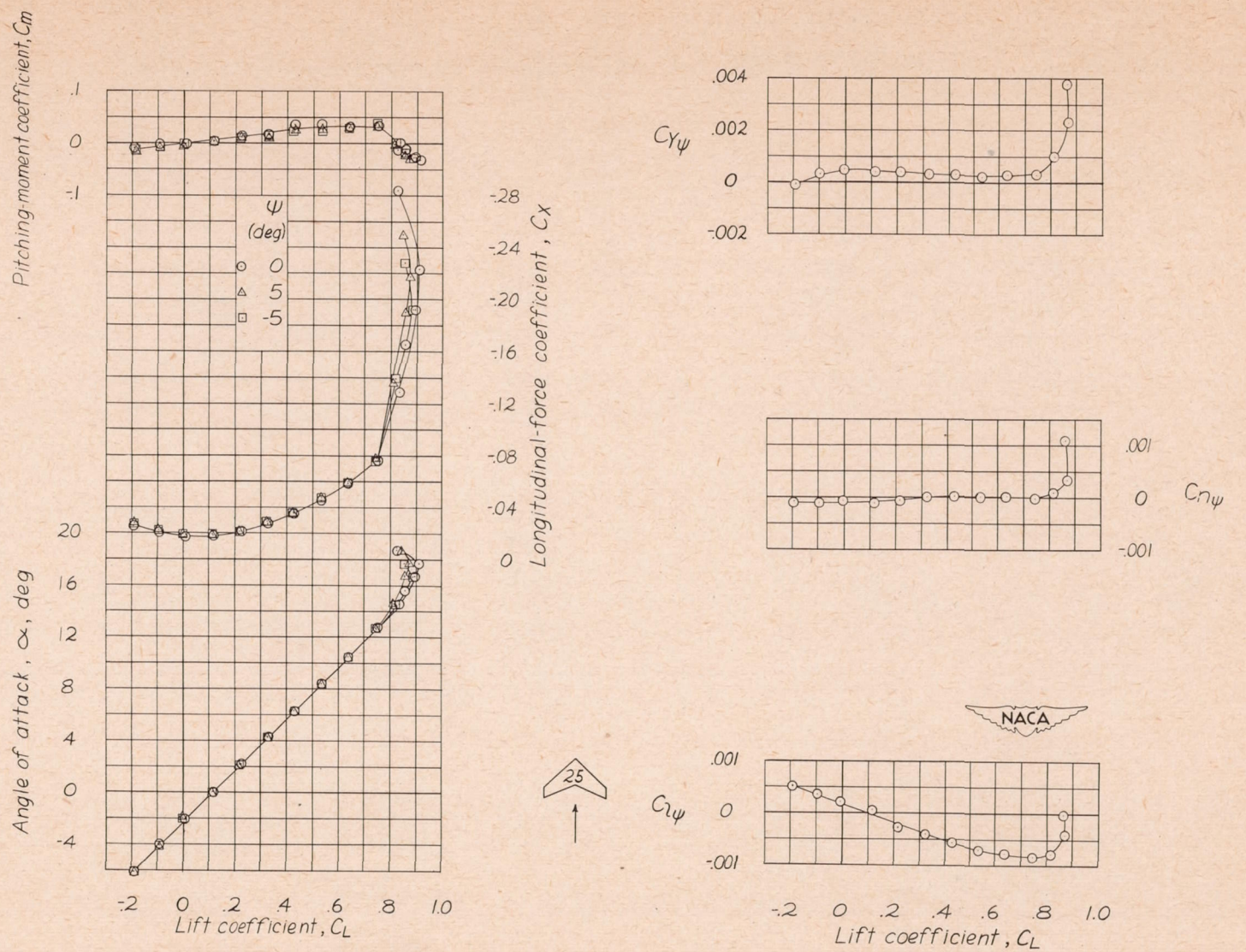

Figure 28.- Aerodynamic characteristics of a sweptforward wing. $\Lambda_{c/4} = -30^\circ$; A = 3.6; λ = 4.24; NACA 23012 airfoil section; model 25.

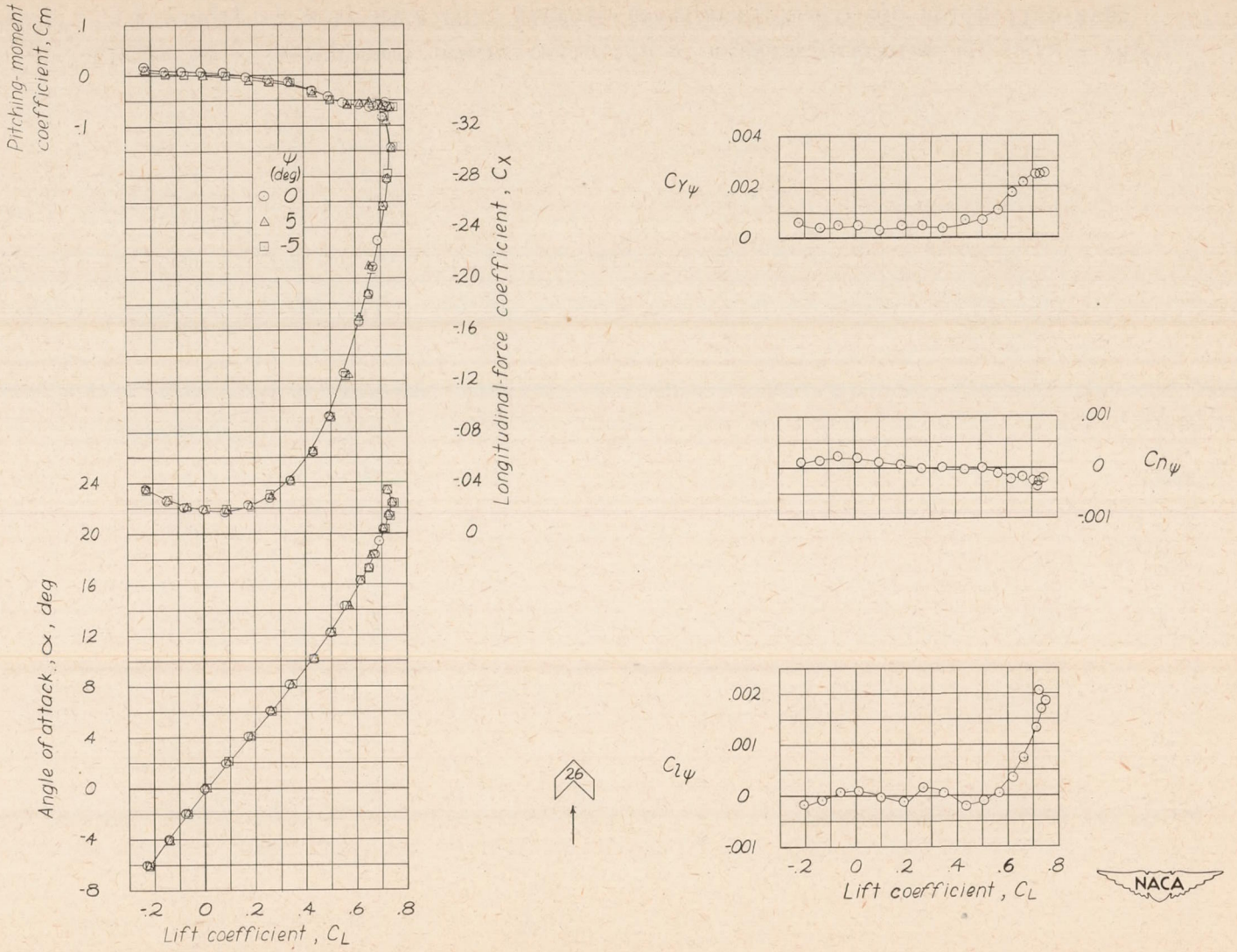

Figure 29.- Aerodynamic characteristics of a sweptforward wing. $\Lambda_{c/4} = -45^\circ$; A = 2.1; λ = 1; NACA 0012 airfoil section; model 26.

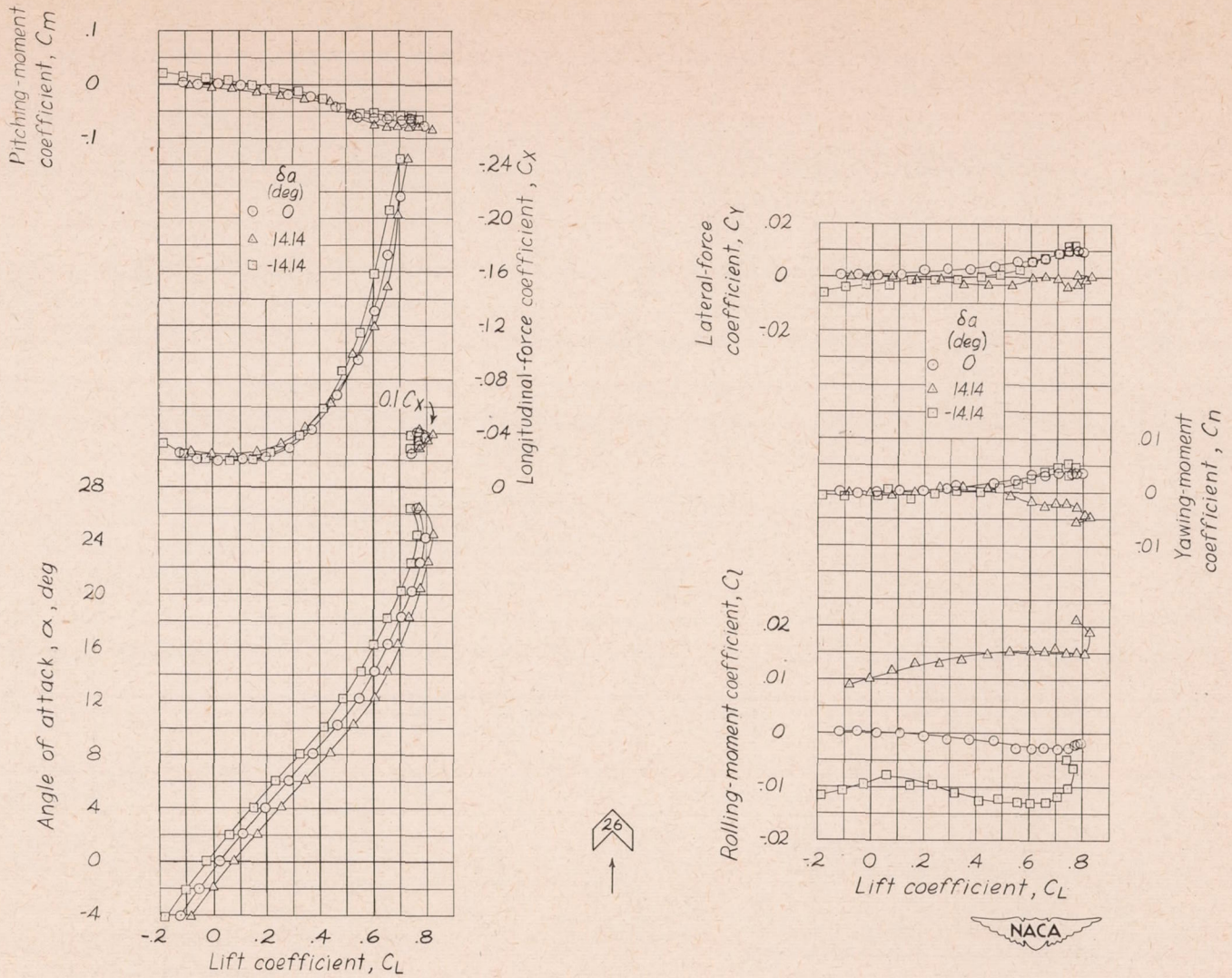

Figure 30.- Aerodynamic characteristics of a sweptforward wing. $\Lambda_{c/4} = -45°$; A = 2.1; λ = 1; NACA 0012 airfoil section with a 0.20c split-flap-type aileron on left wing only; model 26.

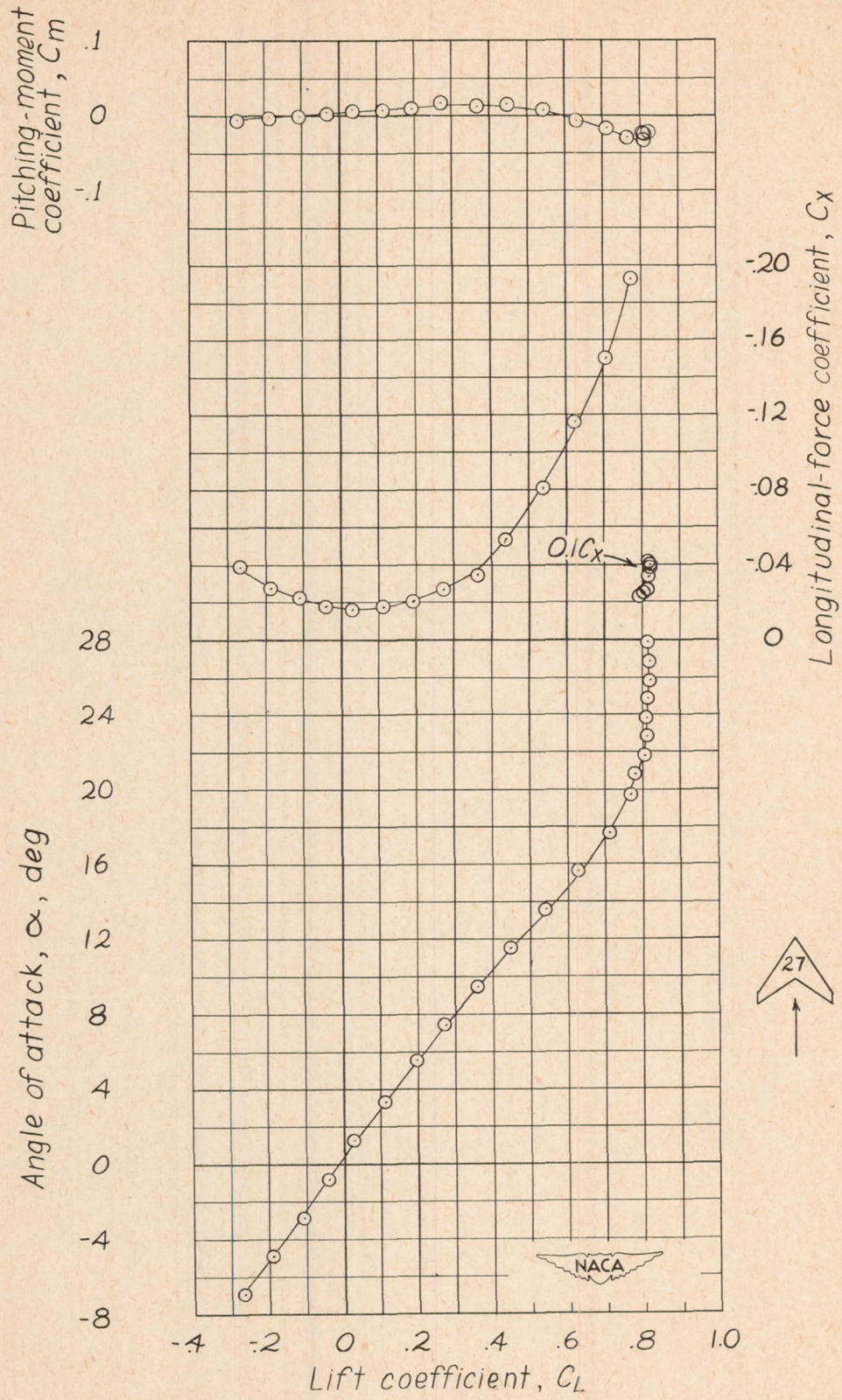

Figure 31.- Aerodynamic characteristics of a sweptforward wing. $\Lambda_{c/4} = -46.6^{\circ}$; A = 2.1; λ = 2.5; NACA 23012 airfoil section; model 27.

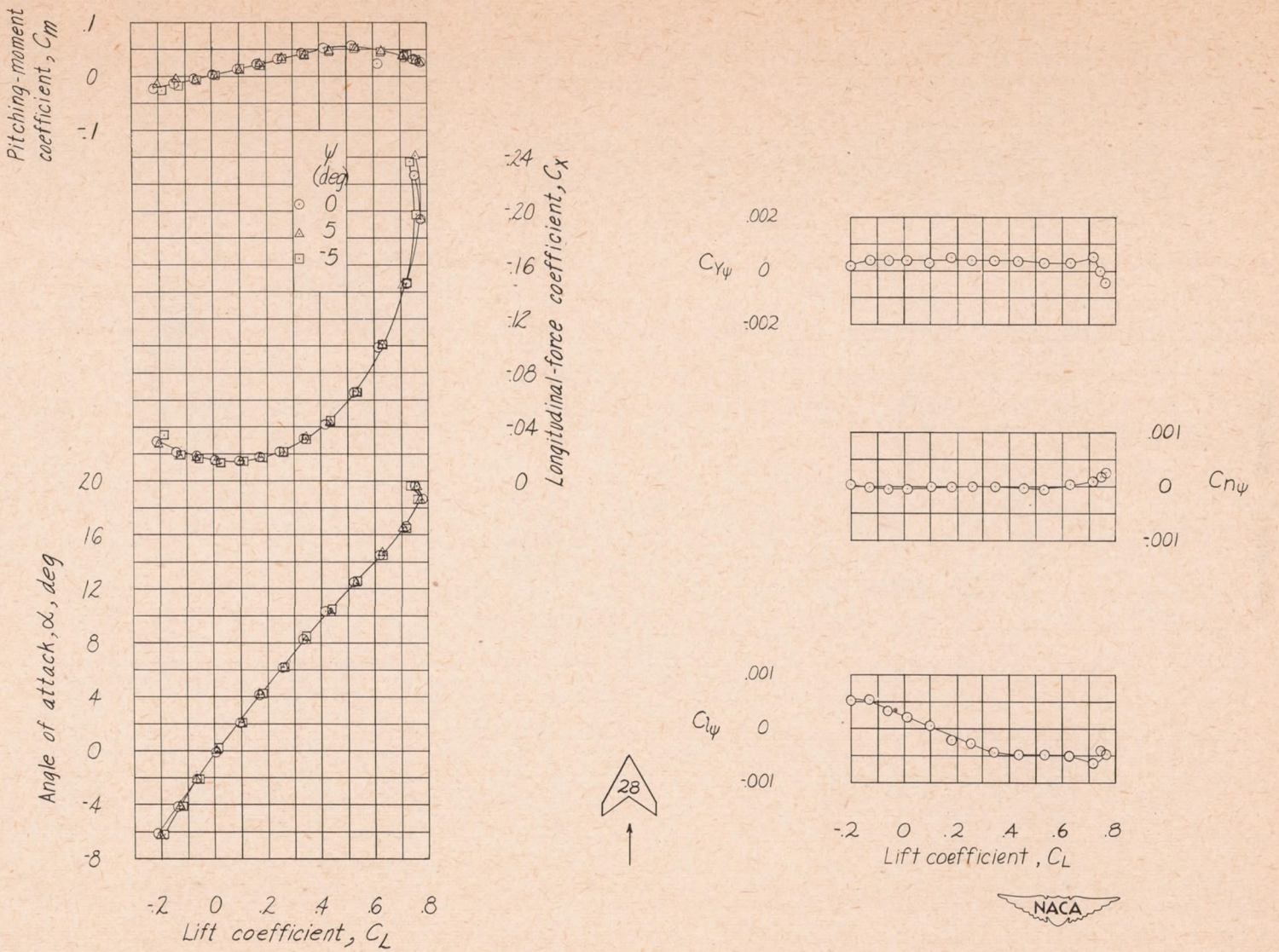

Figure 32.- Aerodynamic characteristics of a sweptforward wing. $\Lambda_{c/4} = -45^\circ$; A = 2.1; λ = 3.88; NACA 23012 airfoil section; model 28.

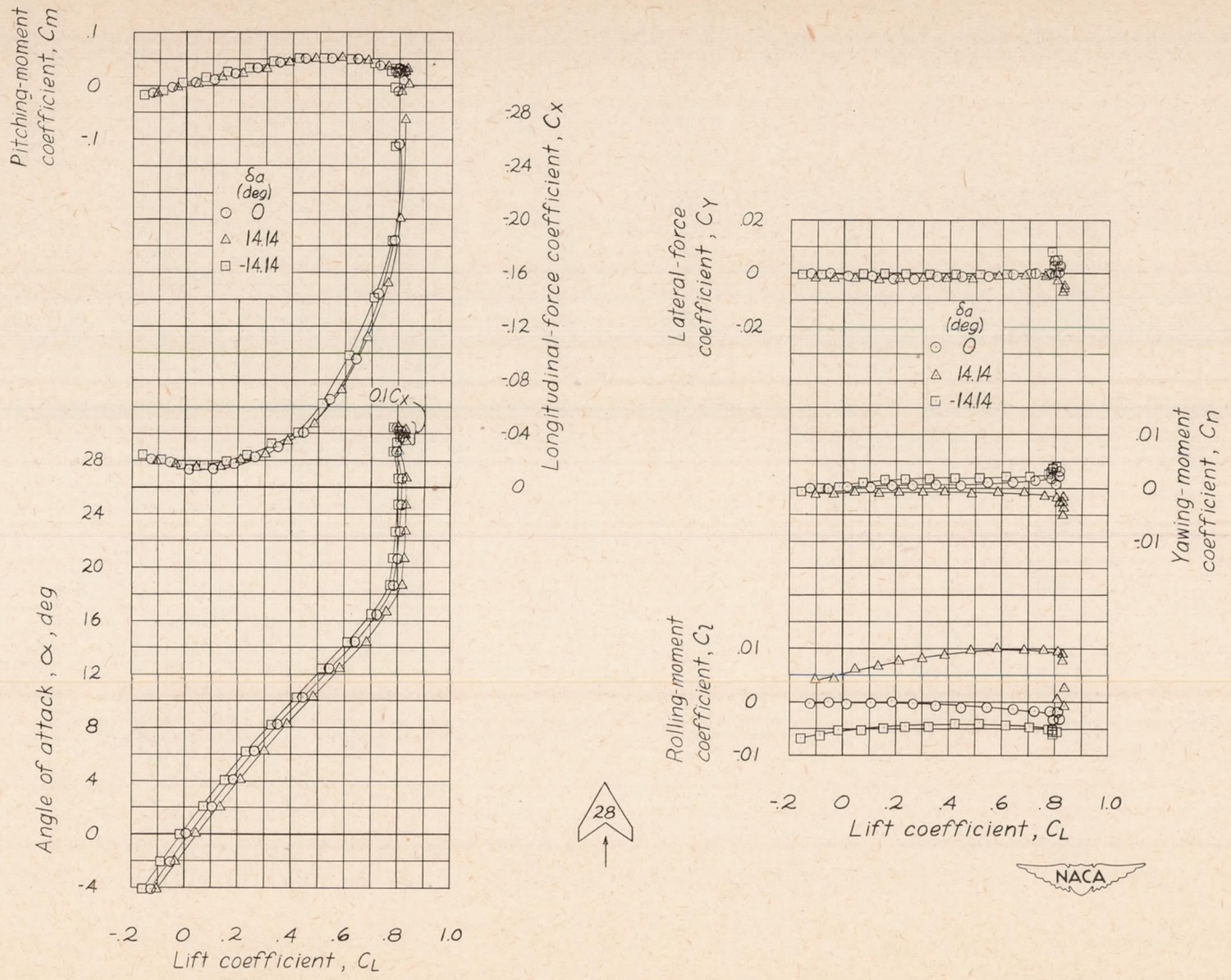

Figure 33.- Aerodynamic characteristics of a sweptforward wing. $\Lambda_{c/4} = -45^{\circ}$; A = 2.1; λ = 3.88; NACA 23012 airfoil section with a 0.20c split-flap-type aileron on left wing only; model 28.

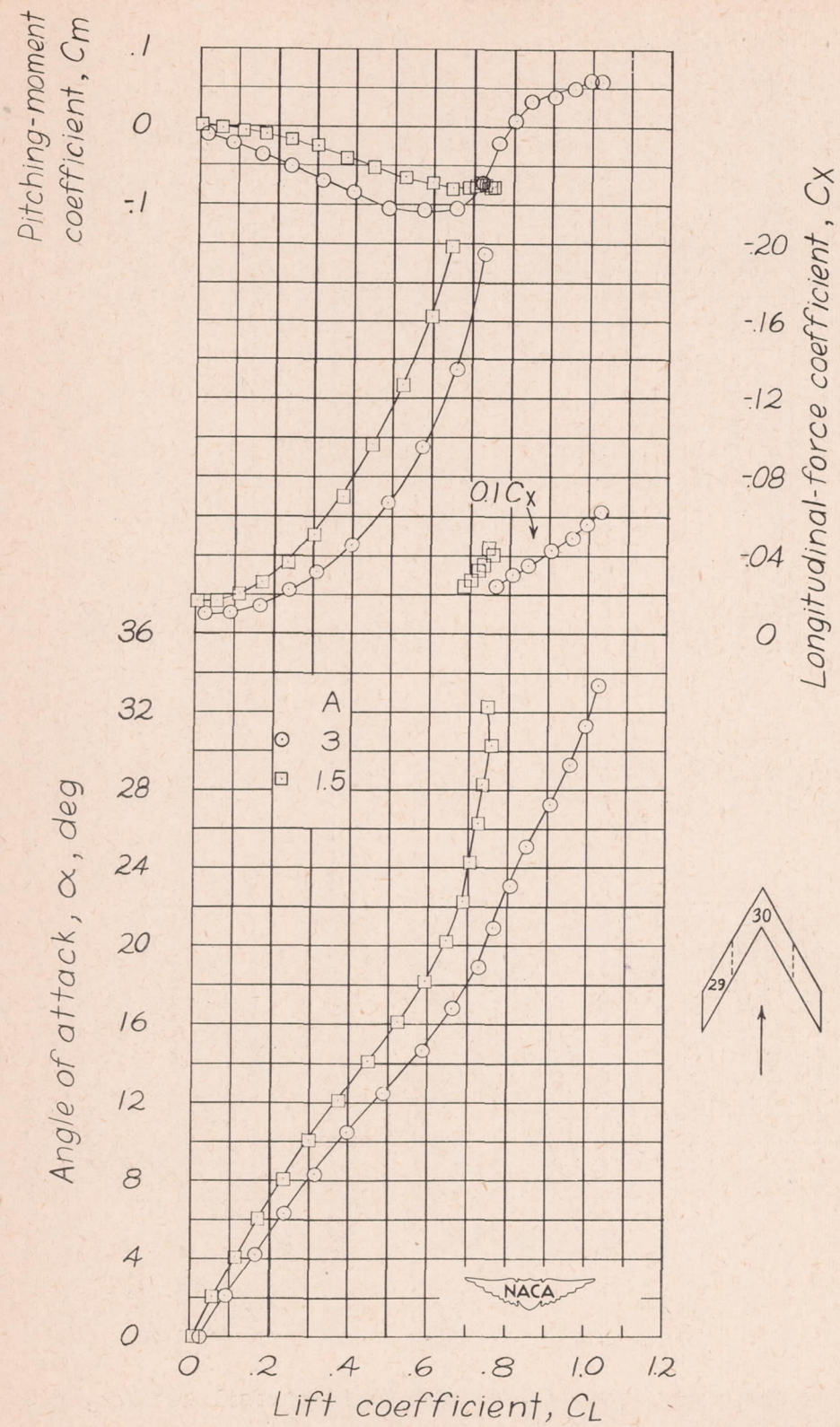

Figure 34.- Aerodynamic characteristics of sweptforward wings. $\Lambda_{c/4} = -60^{\circ}$; A = 3 and 1.5; $\lambda = 1$; NACA 0015 airfoil section; models 29 and 30.

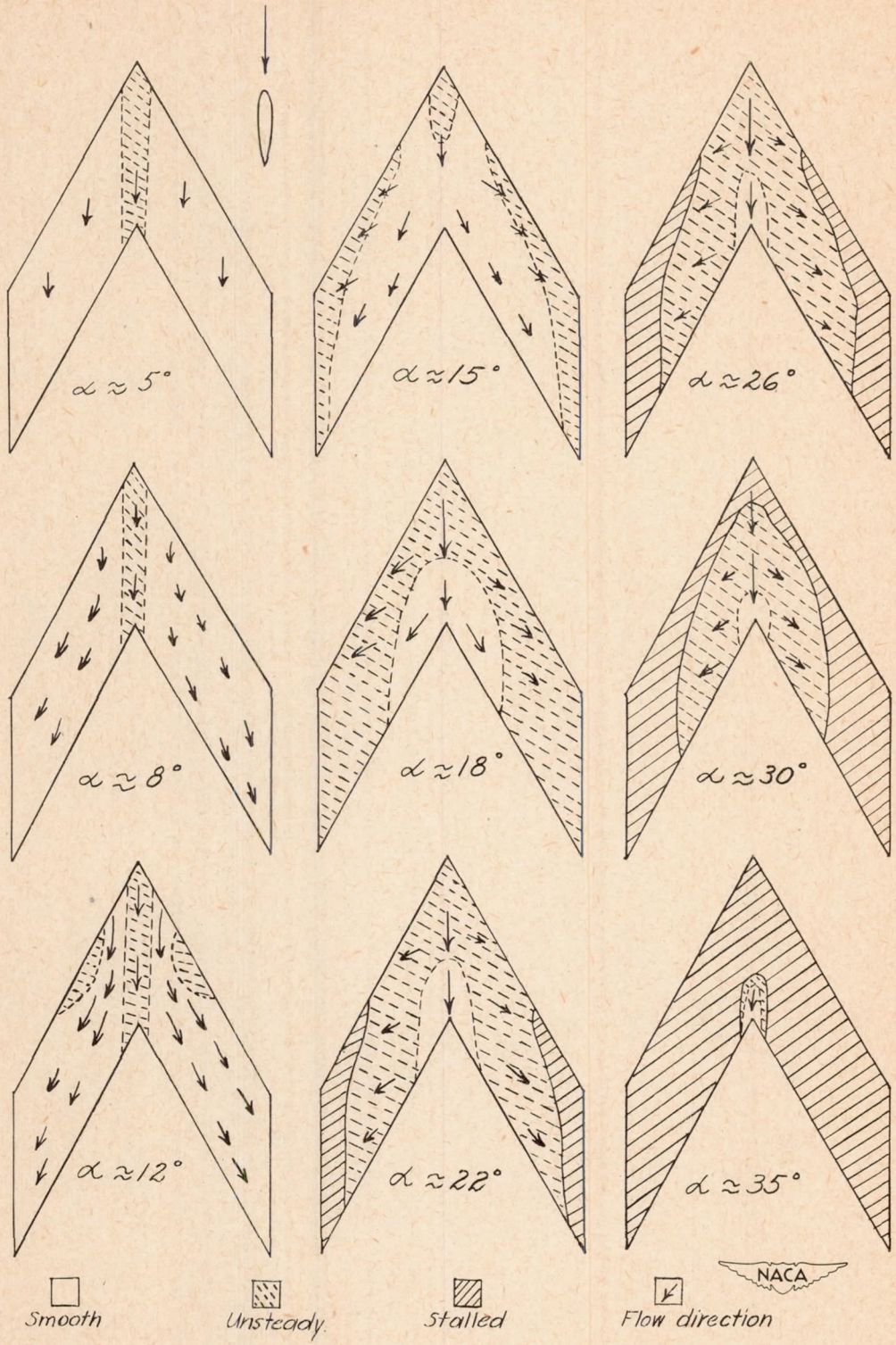

(a) $\Lambda_{c/4} = 60°$; A = 1.5; λ = 1; NACA 0012 airfoil section; model 2.

Figure 35.- Tuft studies of various wing plan forms.

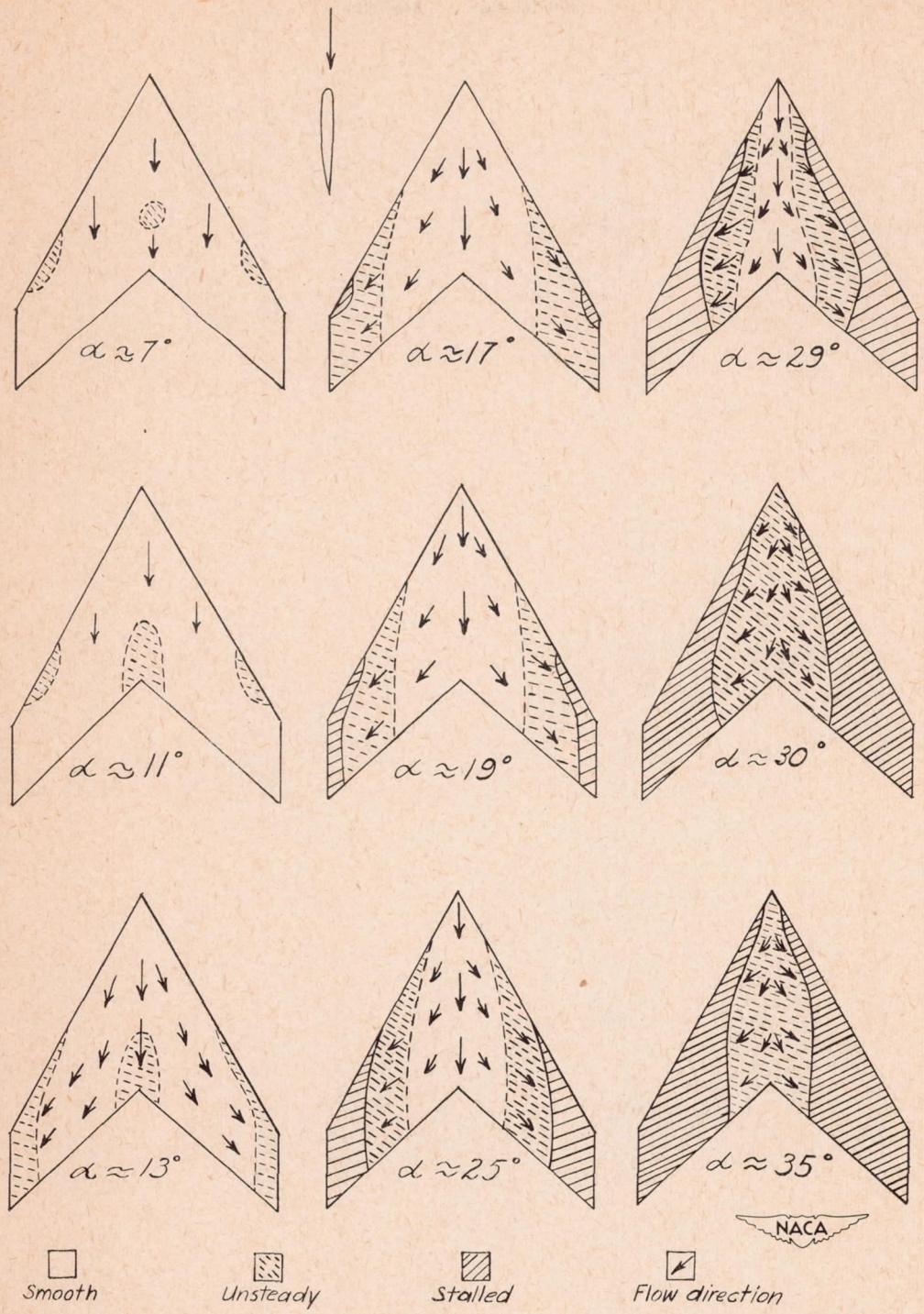

(b) $\Lambda_{c/4} = 56°$; A = 2.1; λ = 2.5; NACA 23012 airfoil section; model 7.

Figure 35.- Continued.

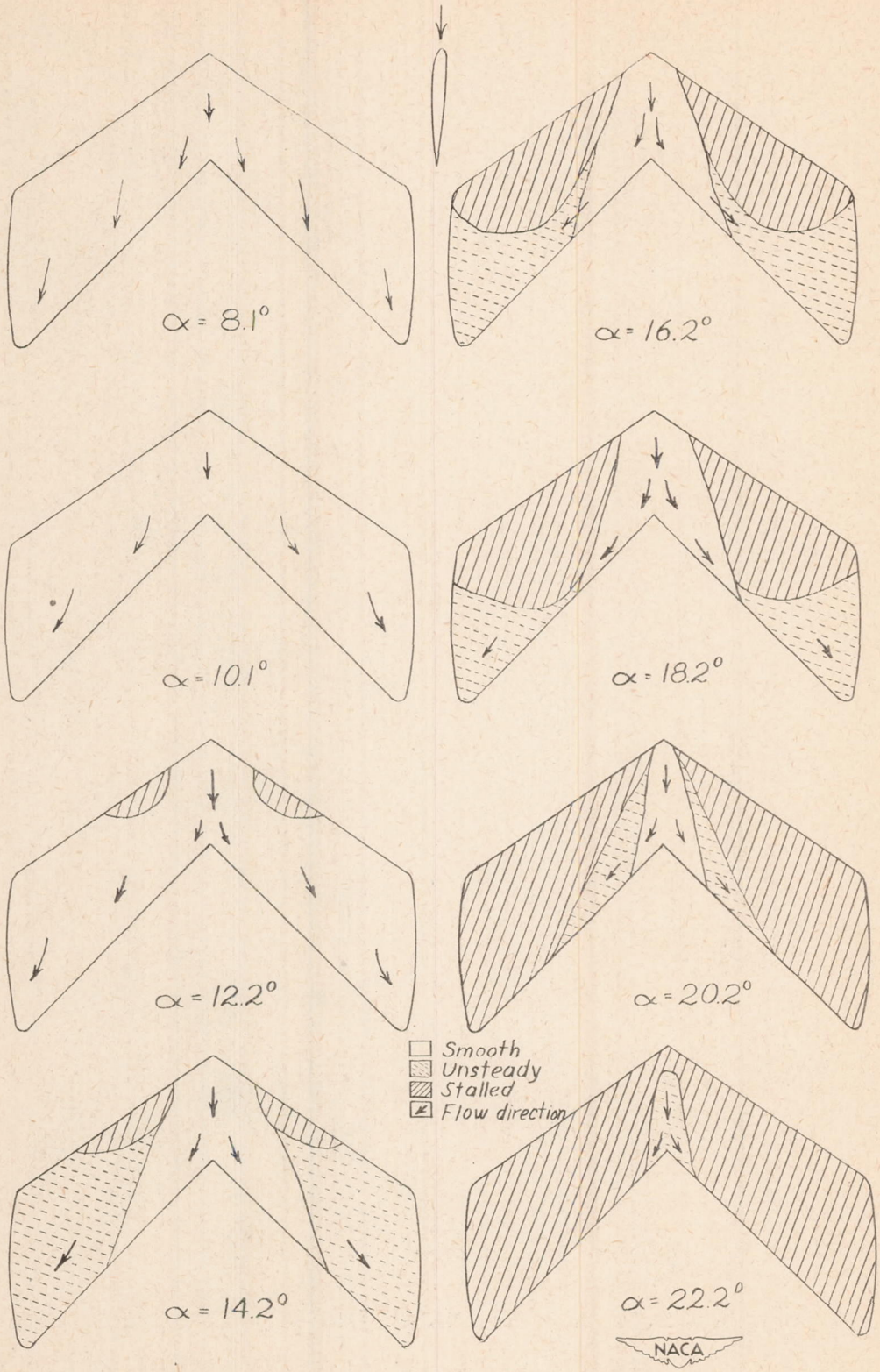

(c) $\Lambda_{c/4} = 37.5°$; A = 3; λ = 0.617; low-drag-type airfoil section; model 9.

Figure 35.- Continued.

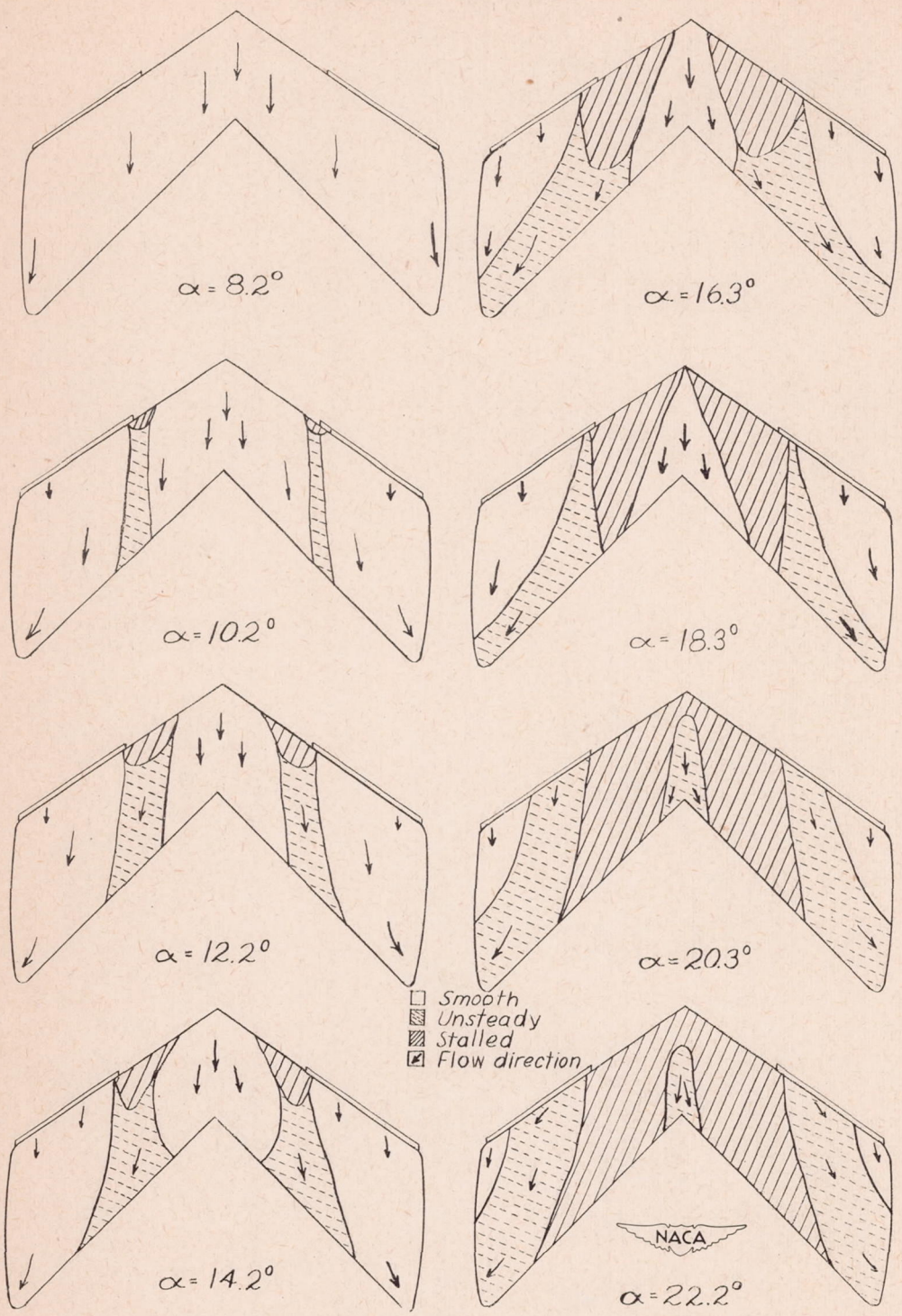

(d) $\Lambda_{c/4} = 37.5°$; A = 3; $\lambda = 0.617$; low-drag-type airfoil section with tip slat; model 9.

Figure 35.- Continued.

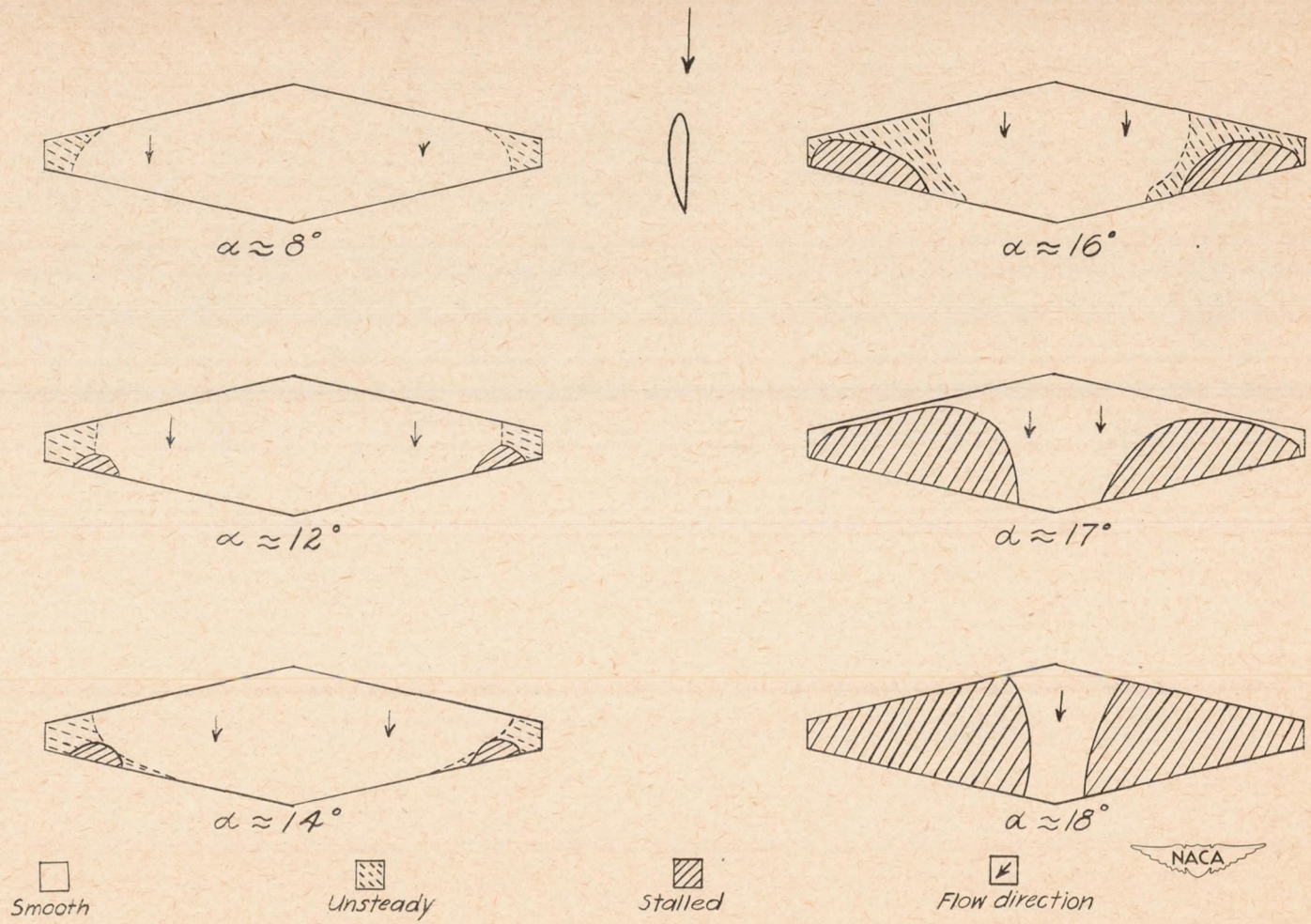

(e) $\Lambda_{c/4} = 6°$; A = 6; λ = 5; NACA 23012 airfoil section; model 13.

Figure 35.- Continued.

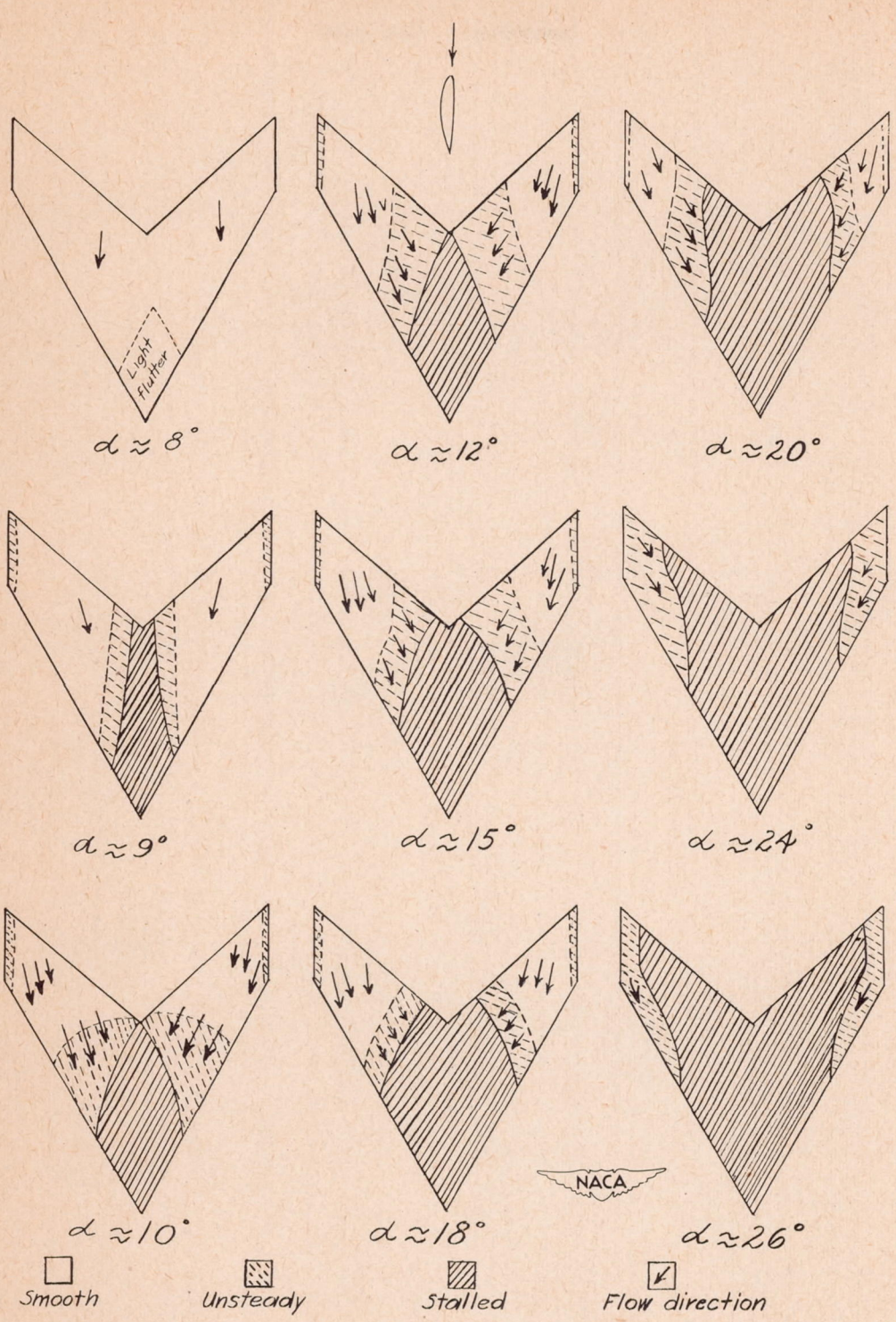

(f) $\Lambda_{c/4} = -46.6°$; A = 2.1; λ = 2.5; NACA 23012 airfoil section; model 27.

Figure 35.- Concluded.

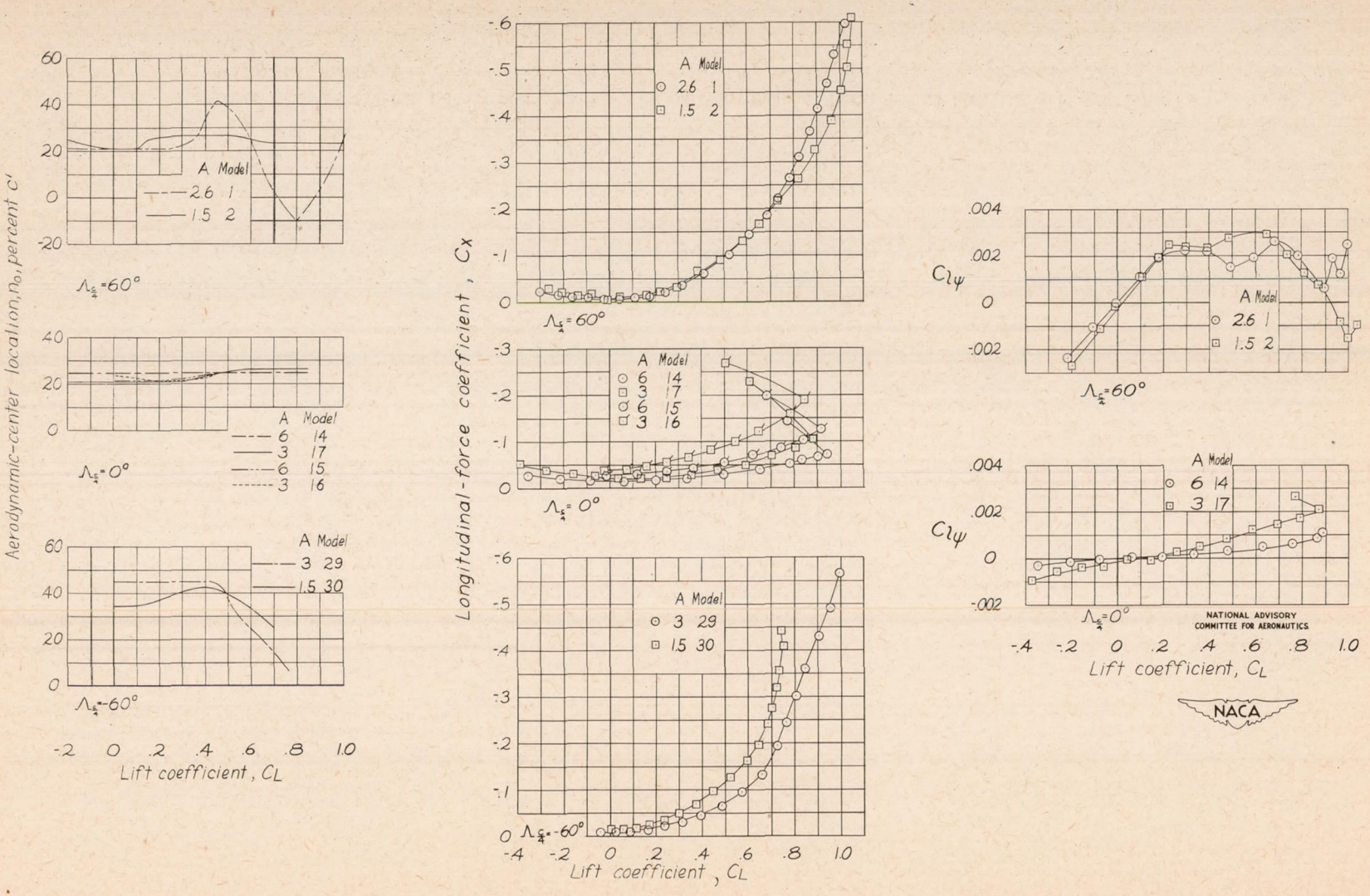

Figure 36.- Effect of aspect ratio on aerodynamic characteristics of various untapered wings. Models 1, 2, 14, 15, 16, 17, 29, and 30.

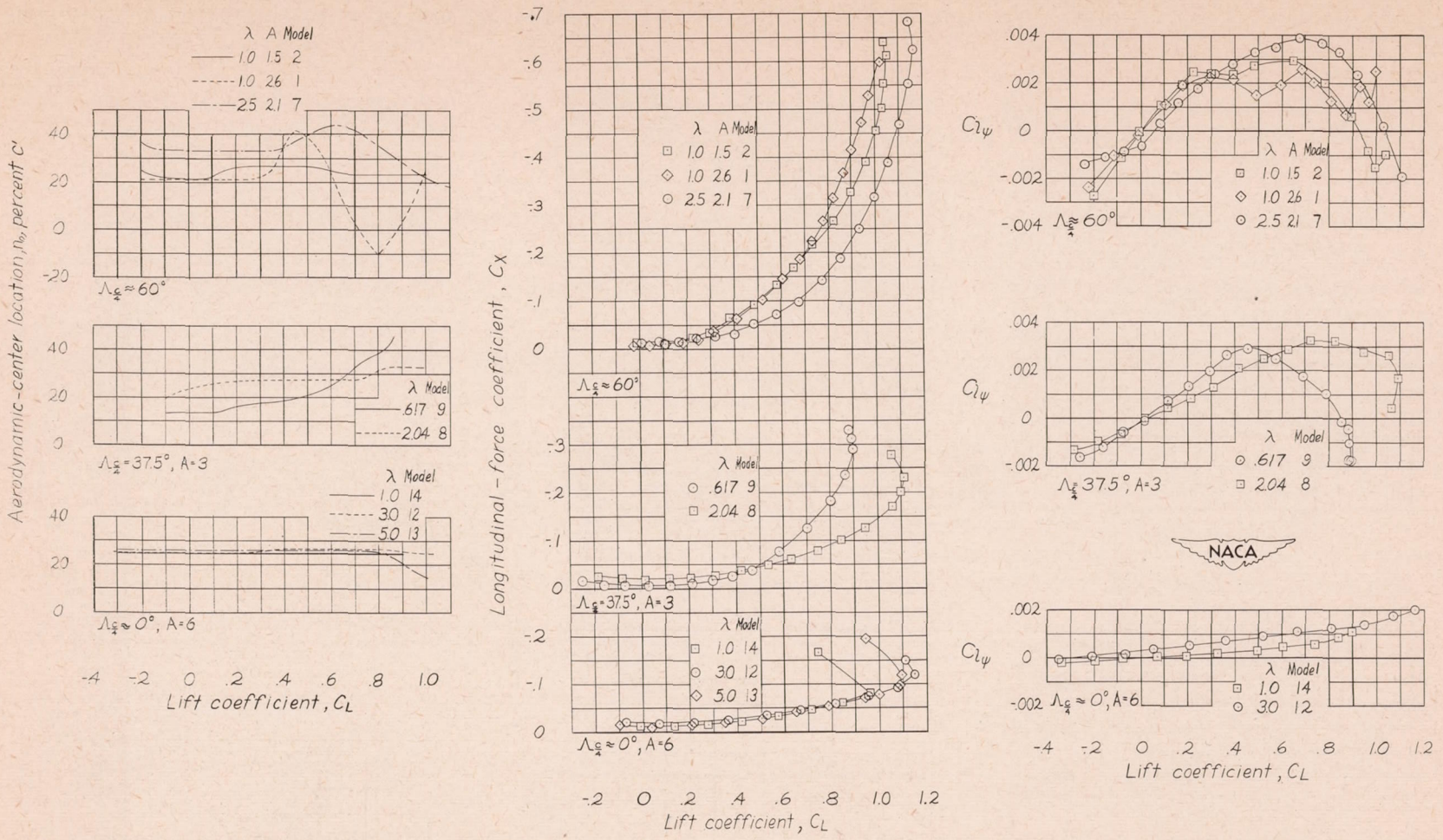

Figure 37.- Effect of taper ratio on aerodynamic characteristics of various wings. Models 1, 2, 7, 8, 9, 12, 13, 14, 18, 19, 23, 24, 25, 26, 27, and 28.

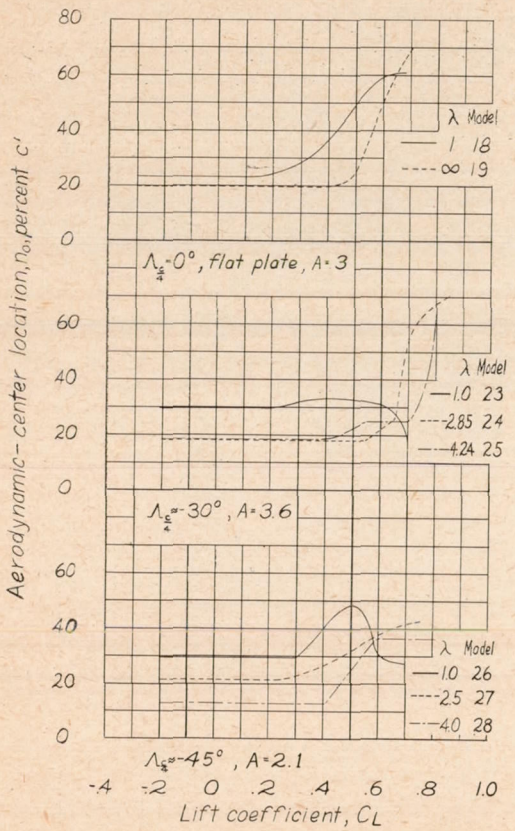

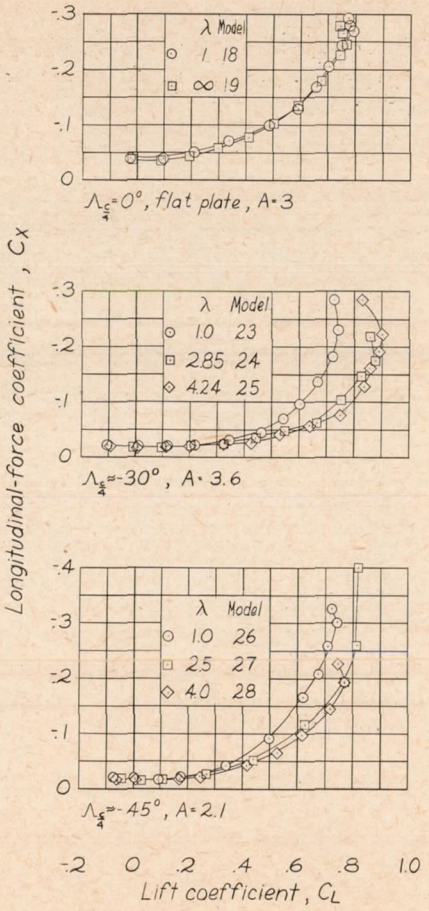

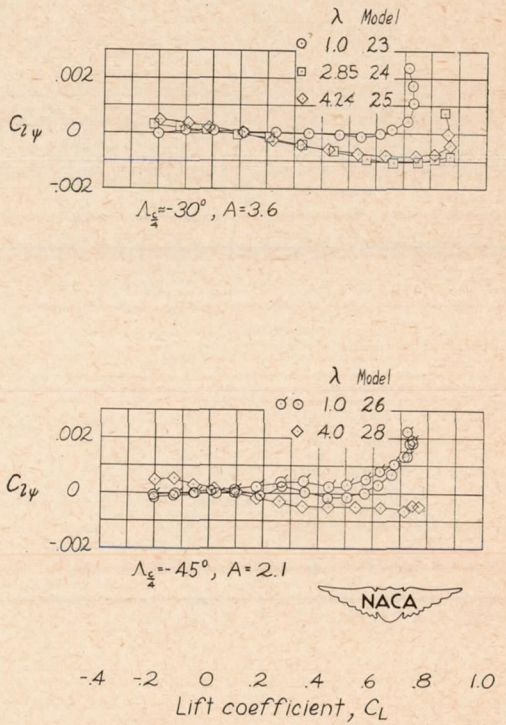

Figure 37.- Concluded.

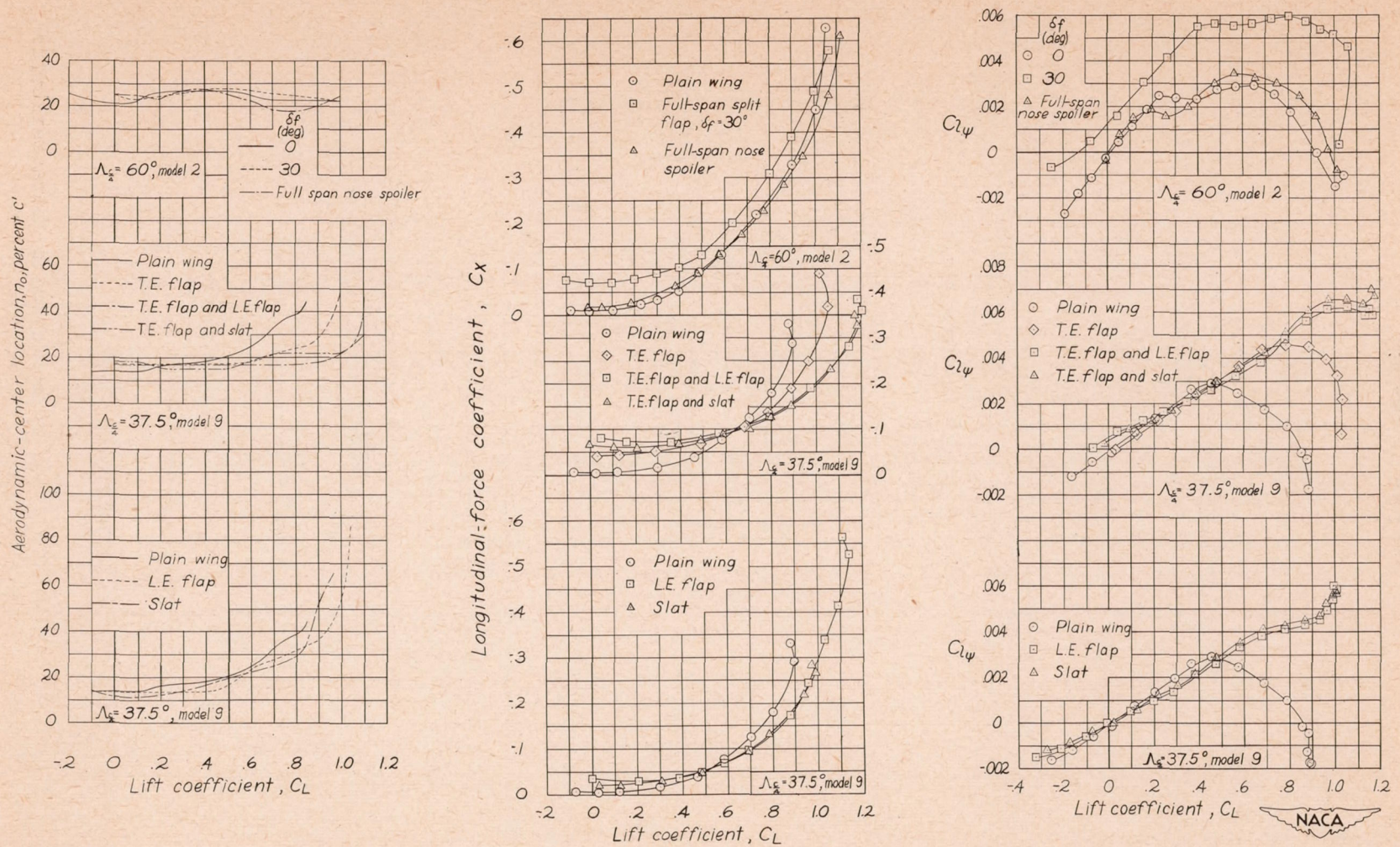

Figure 38.- Effect of high-lift devices on aerodynamic characteristics of sweptback wings. Models 2 and 9.

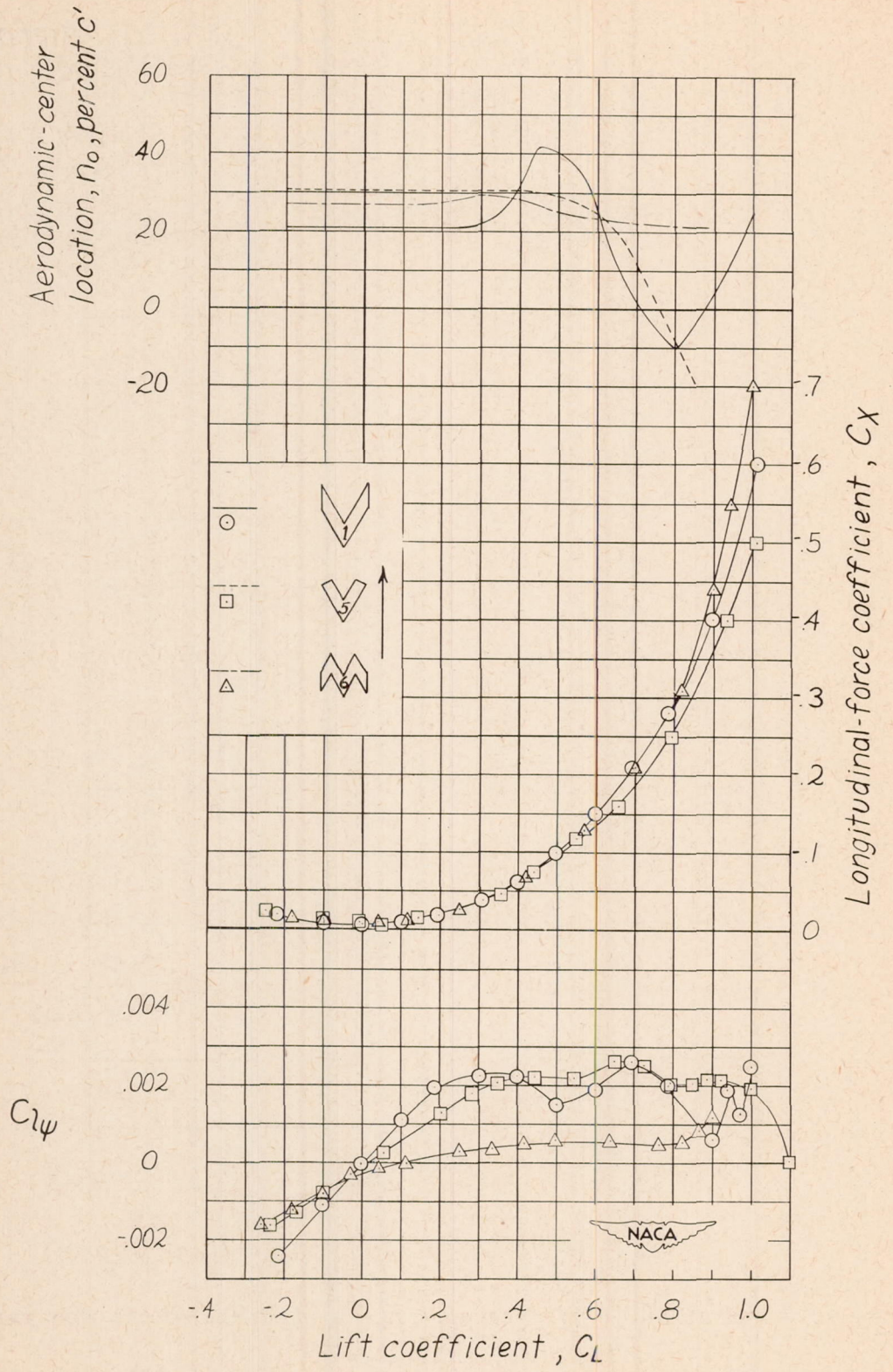

Figure 39.- Effect of tip modification on aerodynamic characteristics of swept wings. Models 1, 5, and 6.

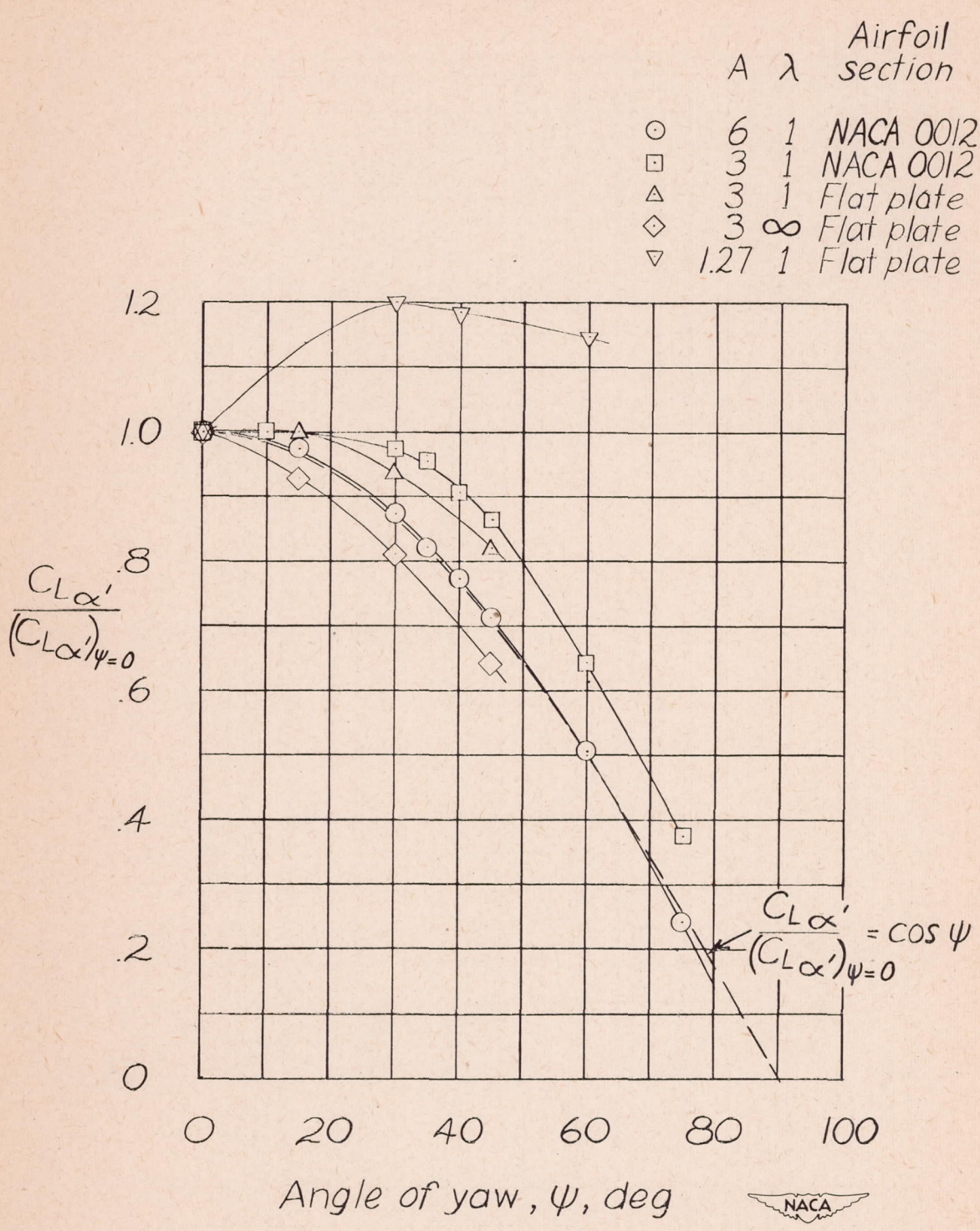

Figure 40.- Variation of lift-curve slope with angle of yaw for various wings.

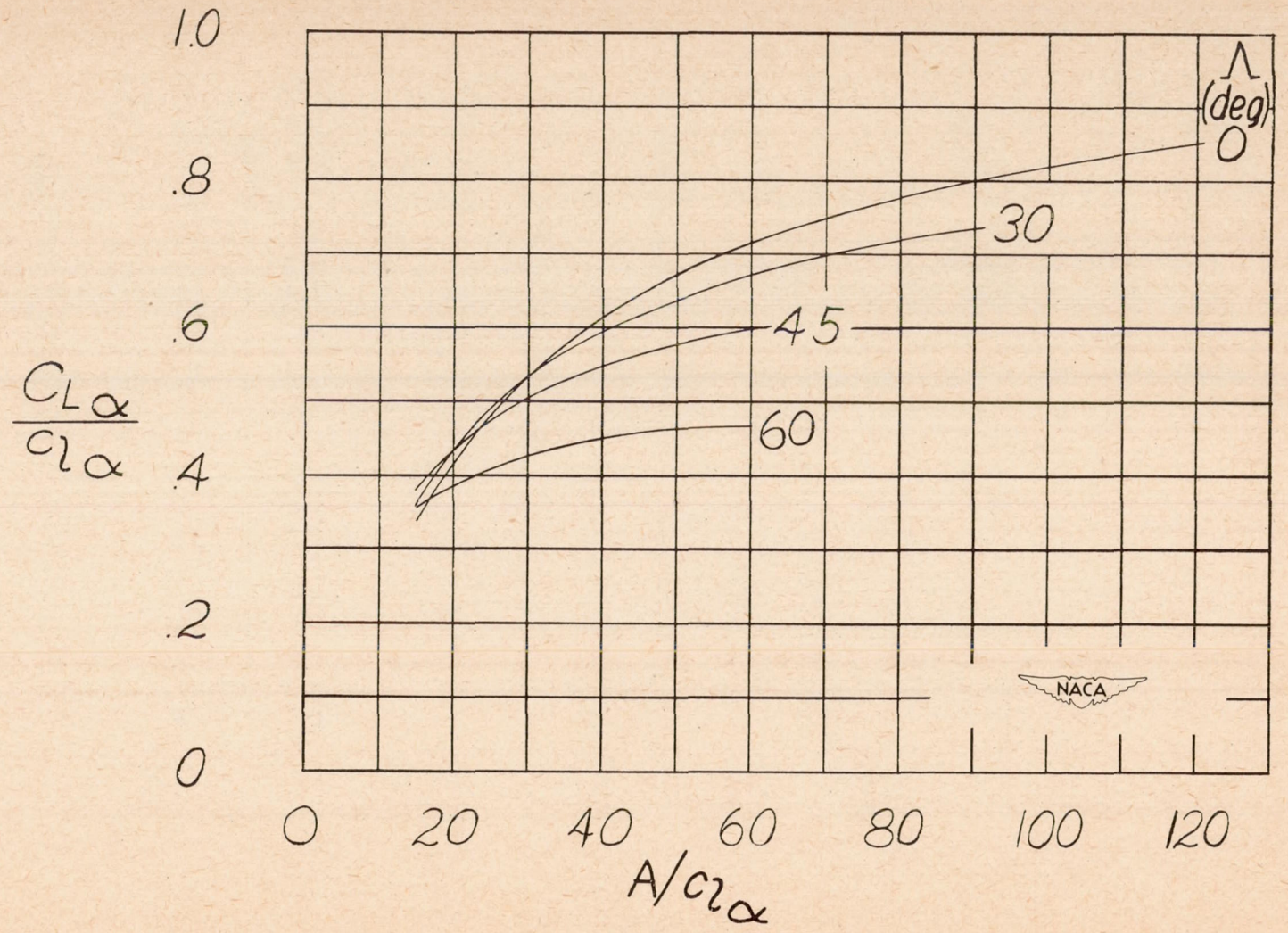

Figure 41.- Theoretical variation of lift-curve slope with aspect ratio and sweep angle.

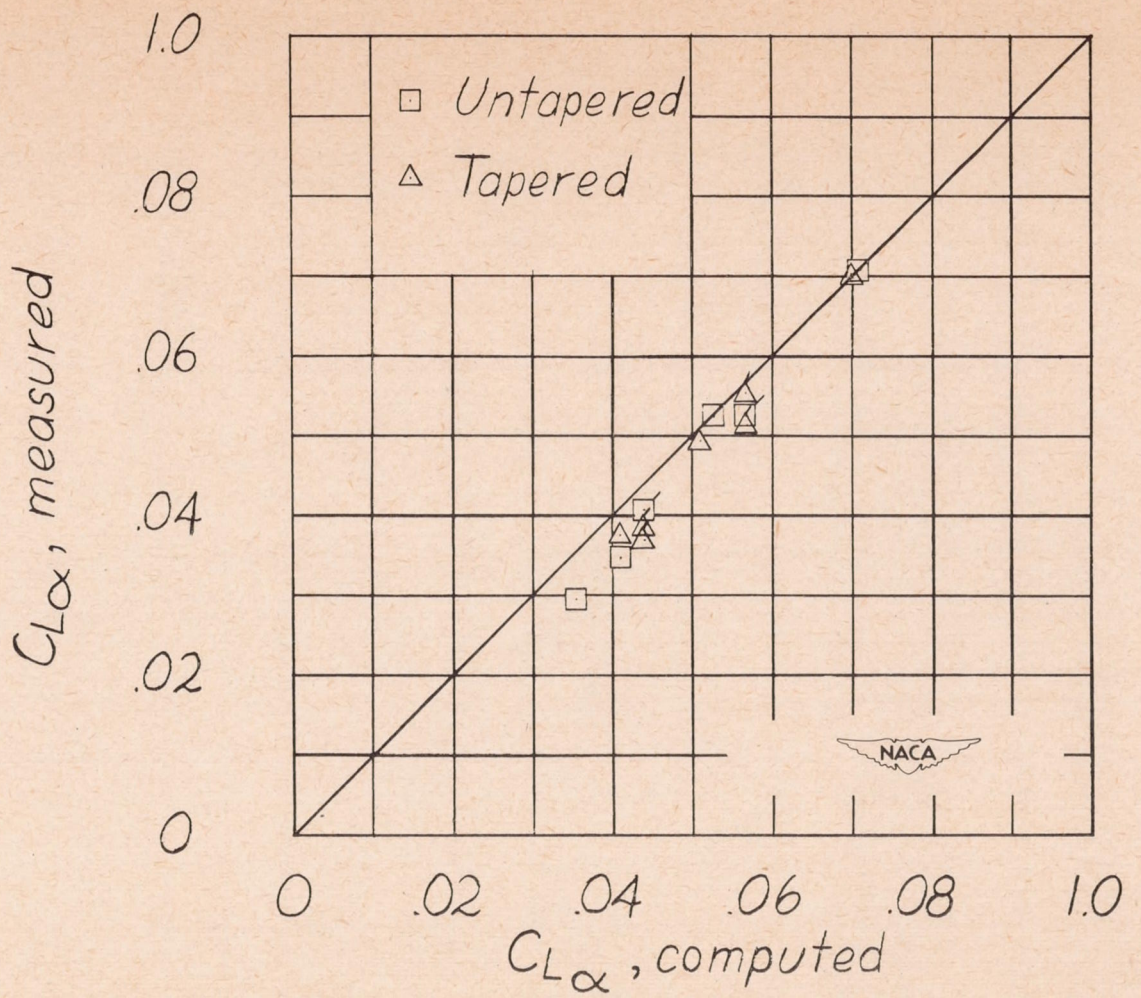

Figure 42.- Comparison of measured and computed values of C_{L_α}. Flagged symbols denote sweptforward wings.

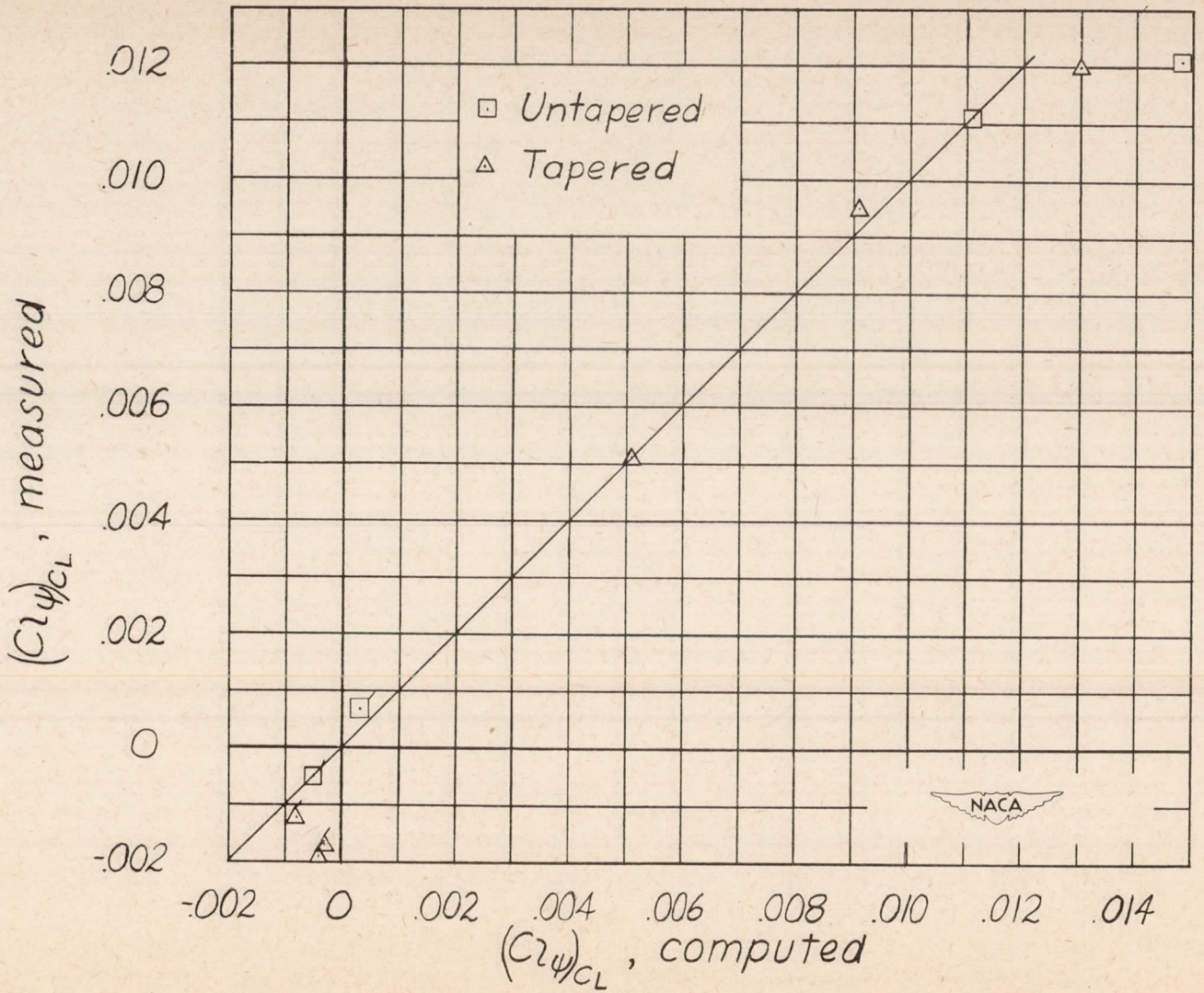

Figure 43.- Comparison of measured and computed values of $\left(C_{l_\psi}\right)_{C_L}$. Flagged symbols denote sweptforward wings.

NACA-Langley - 12-13-51 - 1000